**GPO PRICE** $ _____

**CFSTI PRICE(S)** $ _____

Hard copy (HC) _____

Microfiche (MF) _____

ff 653 July 65

FINAL REPORT

FOR

A DAY-NIGHT HIGH RESOLUTION INFRARED

RADIOMETER EMPLOYING TWO-STAGE RADIANT COOLING

PART I

TWO-STAGE RADIANT COOLER

Contract No. NAS 5-10113
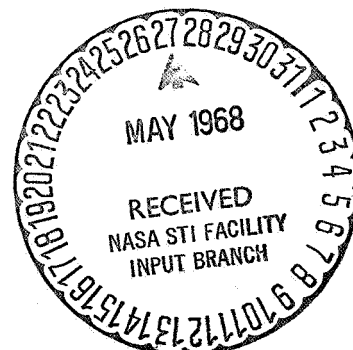
Prepared by

ITT Industrial Laboratories

Fort Wayne, Indiana 46803

For

National Aeronautics and Space Administration

Goddard Space Flight Center

Greenbelt, Maryland 20771

ITTIL No. 1055

11 December, 1967

FINAL REPORT

FOR A

DAY-NIGHT HIGH RESOLUTION INFRARED

RADIOMETER EMPLOYING TWO-STAGE RADIANT COOLING

PART I

TWO-STAGE RADIANT COOLER

Contract No. NAS 5-10113

Prepared by

ITT Industrial Laboratories

Fort Wayne, Indiana 46803

For

National Aeronautics and Space Administration

Goddard Space Flight Center

Greenbelt, Maryland 20771

Contributors

R. V. Annable, J. F. Lodder, R. A. Harber, H. A. Leiter

Approved by

K. L. DeBrosse, Manager
Space & Applied Science Dept.

Dr. C. W. Steeger, Director
Product Development

Dr. R. T. Watson, President
ITT Industrial Laboratories

# ABSTRACT

This part of the final project report covers Phase I, preliminary design study, and Phase II, two-stage radiant cooler. It describes the design, thermal analysis, and testing of a two-stage radiant cooler for use in a 10.5 to 12.5 micron high resolution day-night radiometer. The general design of a two-stage radiant cooler for use on an earth-oriented spacecraft in a sun-synchronous orbit is given. Specific application is made to double- and single-ended coolers in a Nimbus-type orbit. The performance of a double-ended radiant cooler was determined by space chamber experiments simulating orbital operation. The experiments demonstrated that a second-stage temperature below 80 degrees K can be realized under realistic thermal and mechanical conditions.

Part II of the final project report covers Phase III, the integration of the two-stage radiant cooler into a working breadboard model of a day-night radiometer.

## TABLE OF CONTENTS

TABLE OF CONTENTS (Continued)

# LIST OF ILLUSTRATIONS

# LIST OF TABLES

LIST OF TABLES (Continued)

# 1.0 GENERAL DESIGN

A two-stage radiant cooler is a long-life device for generating and maintaining very low spacecraft temperatures without moving parts, power consumption, or stored coolants. A radiant cooler can be designed for use on an earth-oriented spacecraft in a sun-synchronous (near-polar) orbit. A second-stage temperature below 80 degrees K permits the use of fast, sensitive infrared detectors out to wavelengths of 15 microns. Specifically, it allows day and night radiometric mapping of the earth and its cloud cover at high resolution in the 10.5 to 12.5 micron band.

The general design of a two-stage radiant cooler is shown in Figure 1. If the structure is continued as a mirror image below the plane of the patches, a double-ended cooler (Section 2.1) is obtained. Otherwise, a single-ended cooler (Section 2.2) is obtained by thermally insulating the rear patch areas from their respective cones.

The first-stage cone is thermally isolated from the outer surface by multilayer insulation. The mechanical members which support the cone conduct a power much less than the total emitted by the cone and its attached cone end. The outer-surface may be a box with a low $\alpha/\epsilon$ ratio and therefore with a temperature below that of the main spacecraft structure (Section 1.7.2). The box reduces the amount of multilayer insulation needed and permits greater mechanical support of the cone.

The significant thermal loads on the first-stage cone consist of earth infrared, earth reflected sunlight (earthshine) and possibly (depending on the orbit) direct sunlight. In some designs, it may be advantageous to replace some or all of the earth and solar inputs with infrared radiation from low emissivity earth and sun shields (Section 1.7).

The temperature of the first-stage cone is controlled by the addition of a cone end of low $\alpha/\epsilon$ ratio. This cone end is thermally tied to the cone but is not visible from the radiant patches. Such a cone end offsets the high $\alpha/\epsilon$ ratio of the low emissivity cone walls and thereby keeps the cone temperature within bounds in the presence of direct and reflected sunlight.

The outward sloping, specularly reflecting, low emissivity cone walls determine the field-of-view of the patch. The field-of-view is limited in the first stage by the earth and spacecraft structures such as solar panels and adjacent instruments; it is made as large as possible to reduce the radiative coupling between the cone and patch. The cone geometry (angles and relative dimensions) is determined by maximizing the patch area in a cone of given length (or the equivalent, minimizing the cone length for a patch of given area) subject to the above

1

EARTH INFRARED
EARTHSHINE

EARTH SHIELD

SECOND STAGE
CONE

SECOND STAGE
PATCH

FIRST STAGE
CONE

FIRST STAGE
PATCH

FIRST STAGE
CONE END

DIRECT
SUNLIGHT

SUNSHIELD

OUTER
SURFACE

MULTILAYER
INSULATION
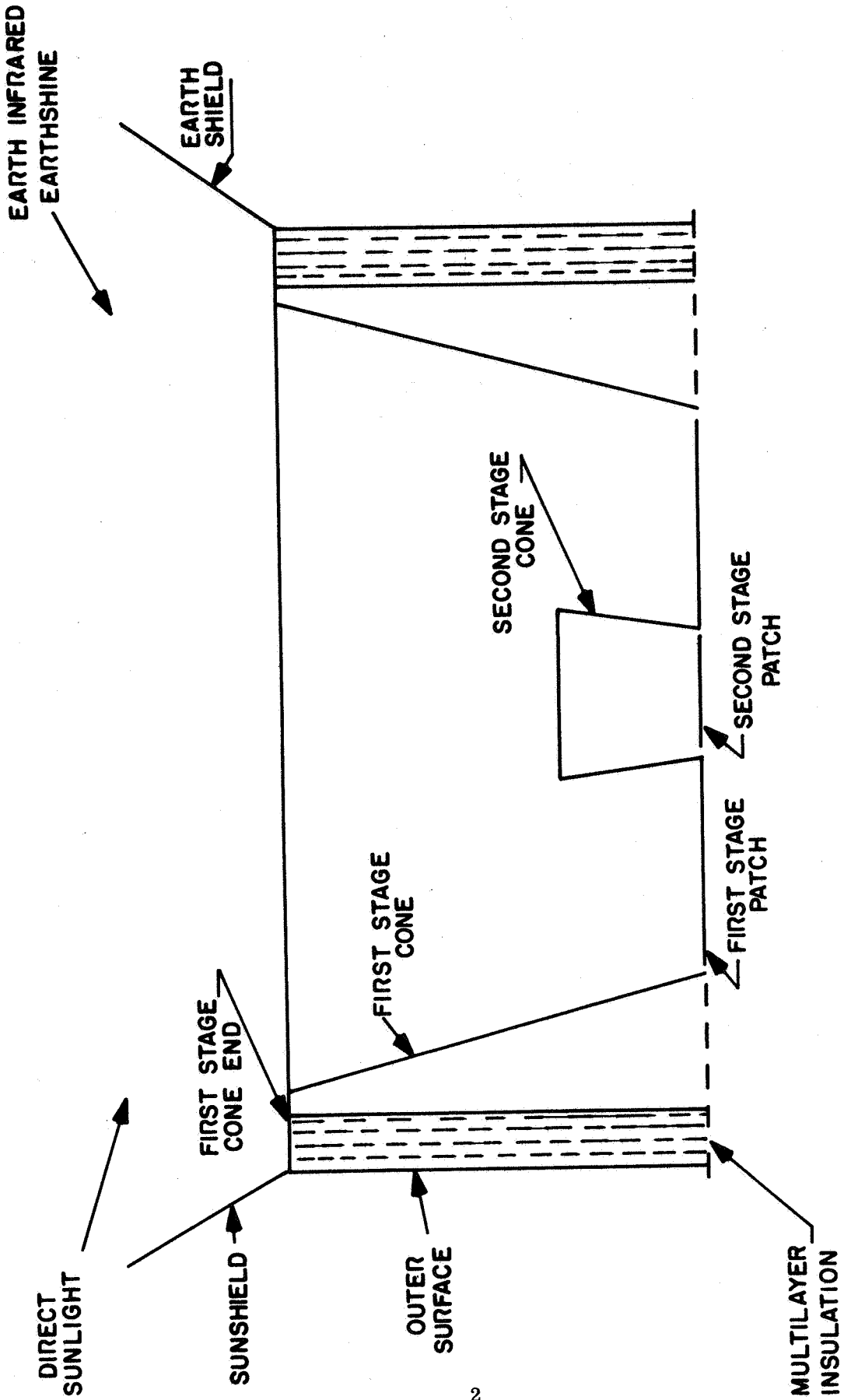
Figure 1 Generalized Two-Stage Radiant Cooler

2

limit on the patch field-of-view (Section 1. 2). The size of the cooler is set by the requirement that non-scaling thermal inputs (from the electrical and optical connections) to each patch are small compared with the total power radiated by that patch.

The first-stage patch is thermally coupled to the first-stage cone and to cold space. The patch is held in position by a caging mechanism during powered launch and by a low conductivity support during orbital flight. As a result, the thermal coupling between the patch and cone is essentially radiative and can be determined from the cone wall emissivity and the cooler geometry (Section 1. 3).

The second-stage cone is designed so that the second-stage patch views only the cone and cold space. The field-of-view of the second-stage patch is limited by the first-stage cone. Because the second-stage patch is not caged during launch and because the temperature range is lower, thermal coupling between the patch and cone is a combination of conductive and radiative.

## 1. 1    Basic Design

The design philosophy for the two-stage radiant cooler gives procedures for setting the actual sizes of the radiant patches and for determining the geometry (angles and relative dimensions) of each stage. By subjecting these procedures to design constraints of non-scaling thermal inputs, maximum patch look angles, and relative size of stages, a procedure is obtained for carrying out the basic design of the cooler.

### 1. 1. 1    Design Philosophy

The design philosophy for the radiant cooler covers two areas, the size of the radiant patches and the geometry of the stages. Design in the first area is based mostly on thermal considerations, while that in the second is largely mechanical in nature.

The size of the two-stage radiant cooler should be large enough that non-scaling thermal inputs to each stage are small compared to the total power radiated by that stage. In the best design these thermal loads which do not scale down with a decrease in patch size are reduced to conduction by way of electrical leads and radiation by way of the opening from the optics to the detector.

In the two-stage cooler, the important non-scaling inputs are in the second (cooler) stage, which determines the size of the cooler, for the most part, since its size sets the scale of the first (warmer) stage. Non-scaling inputs in the second stage are conductive coupling through the electrical leads and radiative coupling through the optical opening to the detector. The electrical leads cannot

be reduced in cross-section or increased in length beyond a certain point because of the increasing electrical resistance and, in the case of long wires, the difficulty of mechanical support. By the insertion of the spectral filter in the first-stage patch the use of a small detector opening, and the proper placement of baffles, the radiative coupling between the relay optics and the detector can be made very small. Radiative coupling between stages via the optical opening is negligible in such an arrangement. In the first stage, the important non-scaling thermal input is probably the radiative coupling through the optical opening.

The design philosophy with respect to size is therefore to have the scale large enough that the non-scaling thermal inputs to a given stage are a small fraction of the power radiated by that stage. This permits some flexibility in optical and electrical design and simplifies the thermal design of the cooler by keeping it largely independent of electrical and optical requirements.

In addition to the size, the relative dimensions and angles of each stage must be determined. This is accomplished by minimizing the ratio of cone length (distance from a patch of zero thickness along the patch normal to the end of the cone) to patch size in the vertical and horizontal planes of the cooler, subject to the constraints that there are maximum patch look angles in each plane (Section 1.2). The vertical plane is the plane through the center of the earth and the center of the patch, in which the maximum look angle is set by the tangent to the earth's surface. The horizontal plane is perpendicular to the vertical plane, goes through the center of the patch, and is parallel to a plane tangent to the earth's surface at the subpoint of the satellite. This procedure provides the required patch area within the minimum cone length, which minimizes the volume occupied by the cooler and aids in sound vibration design. In the second stage, it has the added advantage of minimizing the surface area of the second-stage cone, which is a source of radiative thermal load to the first stage. Minimizing the cone length to patch width ratio in the vertical and horizontal planes subject to maximum look angles in these planes determines the cone angles in each plane and the aspect ratio of the radiant patch.

## 1.1.2   Design Constraints

The above design philosophy has meaning only in the presence of constraints on the design of the cooler. Setting the sizes of the cooling patches, i.e., their radiant power levels, is necessary because of non-scaling thermal inputs. Minimizing the cone length to patch width ratio is necessary only when the patch must have a restricted angular view to avoid coupling to external radiant sources; otherwise, no cone at all is required.

In the first stage, the maximum patch look angle in the vertical plane is set in one direction by the earth and in the opposite direction by the satellite.

4

The cooler is symmetrical about the patch normal in the vertical plane with the maximum look angle set by the requirement that the patch not view the earth. In the horizontal direction, the maximum look angle is larger, but is eventually limited by the spacecraft and adjacent instruments.

The maximum look angle of the second stage is set in both planes by the requirement that its patch have no view or only a very small view of the cone of the first stage, which is an external radiant source to the second stage. As a result, the maximum look angles are smaller in the second stage than in the first.

The scale factor between the two stages might be set by the non-scaling thermal inputs in each stage. In reality, however, a third type of design constraint usually sets the relative size. The radiant power of the second stage should be a small fraction of the radiant power of the first stage, so it does not affect the thermal performance of the first stage. In addition, the cone for the second stage is a source of radiative thermal input to the first stage but does not add significantly to the radiant power of the first stage. The second stage should be large enough to overcome its non-scaling thermal inputs, but not so large that its cone loads down the first stage, thereby increasing its temperature and that of the second stage. These are not very precise constraints, but they do tend to set the range of the scale factor between stages.

## 1.1.3  Basic Dimensions and Angles

The combination of design philosophy and design constraints gives a procedure for designing the basic radiant cooler. The non-scaling thermal loads on the second stage set the size or range of sizes on its patch area. The cone for the second stage is then designed to have the minimum length which will limit the view factor (fraction of radiant emission) from the second-stage patch to the first-stage cone to a small value. Unfortunately this cannot be done precisely without knowing the size and design of the first stage. A first approximation can be made, however, by determining the geometry of the first stage. This is accomplished by minimizing the cone length to patch dimension ratio in the vertical and horizontal planes subject to the maximum look angles in these planes. This procedure determines the vertical and horizontal cone angles and the patch aspect ratio of the first stage (i.e., its geometry). This same geometry then serves as a first approximation to the geometry of the second stage and therefore gives a preliminary design for the second stage.

The size of the second stage plus the constraints on relative stage size then set the approximate scale for the first stage. It is then necessary to calculate the view factor between the second-stage patch and the first-stage cone and to increase the length of the second-stage cone until the view factor is reduced to an

5

acceptable value. It may then be desirable to alter the geometry of the second stage a little to see if its cone length can be reduced for the same patch area while maintaining the small view factor.

The basic dimensions and angles of two specific cooler designs are given in Sections 2.1.1 and 2.2.1.

## 1.2    Optimization of Cooler Geometry

The optimization of the cooler geometry determines the relative dimensions and the angles in the vertical and horizontal planes of each stage. The optimization is carried out by minimizing the ratio of cone length (distance from a radiant patch of zero thickness along the patch normal to the cone mouth) to patch half width in the vertical and horizontal planes, subject to the constraint that the patch must have a given maximum look angle. This procedure places a given patch area in a cooler of minimum length or, conversely, a maximum patch area in a cone of given length. It determines the cone angles in each plane and the aspect ratio of the rectangular radiant patch.

The geometry of a radiant cooler stage through a vertical or horizontal plane is shown in Figure 2. This may also be considered a section of a truncated right circular cooler. The cone length $\ell$ of the stage is given by

$$\ell \;=\; (r_2 - r_1) \cos \theta \tag{1}$$

where

$$r_2 \;=\; \text{distance along cone surface from apex to mouth}$$

$$r_1 \;=\; \text{distance along cone surface from apex to patch}$$

$$\theta \;=\; \text{half angle of cone}$$

The total length of a double-ended two-stage cooler, from cone mouth to cone mouth, is $2\ell$. The half width of the patch in the plane is given by

$$c \;=\; r_1 \sin \theta \tag{2}$$

And the ratio of cone length to patch half width is

$$\frac{\ell}{c} \;=\; \frac{1 - \dfrac{r_1}{r_2}}{\dfrac{r_1}{r_2}} \; \cot \theta \tag{3}$$
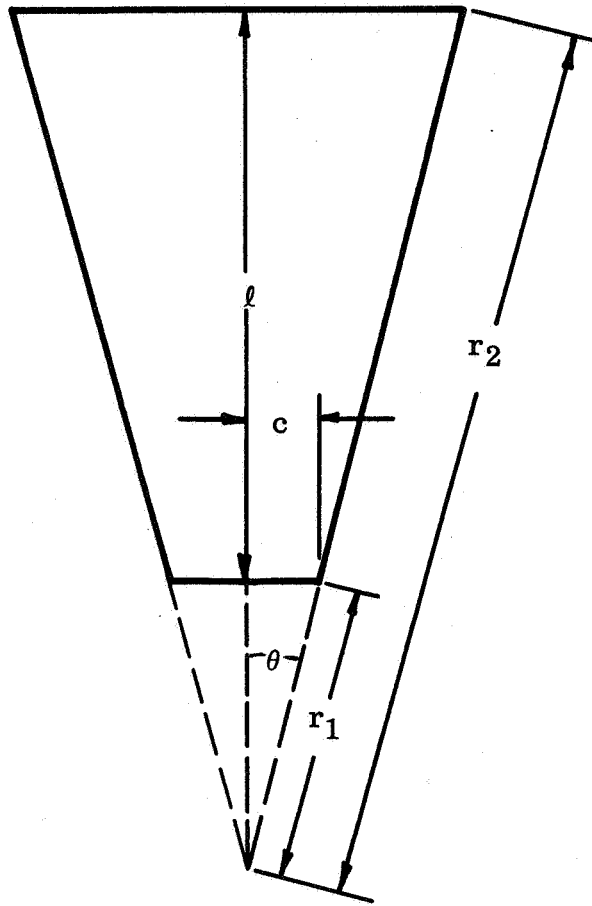
Figure 2    Radiant Cooler Geometry

Now the maximum look angle, $\phi$, for a spherical patch is given by (see Figure 3)

$$\sin (\phi - \theta) = \frac{r_1}{r_2} \tag{4}$$

This relation is a good approximation for a flat patch when $\theta$ is small and a safe value of any $\theta$, since $\phi$ for a flat patch is always less than or equal to $\phi$ for a spherical patch in a cone of the same geometry (same $\theta$ and $r_1/r_2$). The angle $\phi$ is the maximum angle to the patch normal (axis of the cone) at which radiation from the patch leaves the cone mouth and the maximum angle to the cone axis of an external object that can be seen from the patch area. The effect of the cone is therefore to act as a crude collimator or directional antenna for patch radiation and as a set of blinders to an observer on the radiant patch.

Thus for a given maximum look angle

$$\frac{\ell}{c} = \frac{1 - \sin (\phi - \theta)}{\sin (\phi - \theta)} \cot \theta \tag{5}$$

The cone length to patch half width ratio for fixed $\phi$ is then only a function of the cone half-angle $\theta$.

To minimize $\ell/c$.

$$\frac{d(\ell/c)}{d\theta} = 0 = \cot \theta \cdot \cos (\phi - \theta)$$

$$-\csc^2 \theta \ [1 - \sin (\phi - \theta)] \cdot \sin (\phi - \theta) \tag{6}$$

For small cone angles we may use the approximation $\cos \theta = 1$, in which case (6) can be solved for $\sin \theta$. The result is

$$\sin \theta = \frac{-\cos \phi (1 - \sin \phi) + (1 - \sin \phi)^{1/2}}{\cos^2 \phi + \sin \phi} \tag{7}$$

This formula can be used to determine a first approximation to the optimum cone half angle, which can be used as the starting value in equation (5) to determine a more accurate result.

Once the optimum value of the cone half angle has been calculated, the ratio $r_1/r_2$ is set by equation (4) for the given maximum look angle. This sets the geometry, but not the scale, of the cooler. The ratio of minimum $\ell/c$ values in the horizontal and vertical planes yields the optimum aspect ratio of the radiant patch.
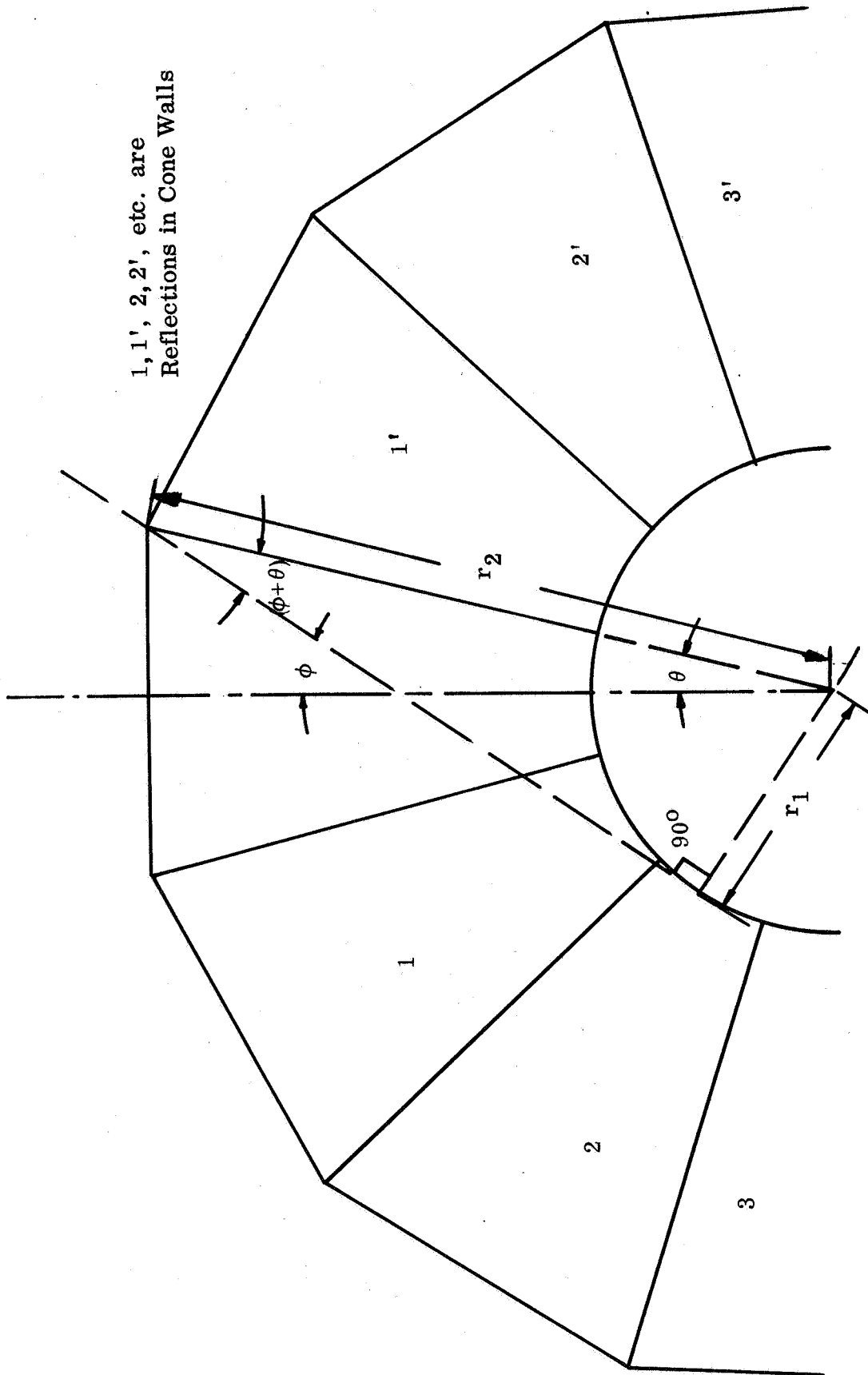
1, 1', 2, 2', etc. are
Reflections in Cone Walls

Figure 3    Maximum Look Angle $\phi$ For a Spherical Patch

9

Plots of $\ell/c$ versus $\theta$ are given in Figure 4 for maximum patch look angles of 30 degrees, 31.5 degrees, 45 degrees, and 60 degrees. Note that $\ell/c \longrightarrow \infty$ as $\theta \longrightarrow \phi$ (equation 5) and that the curve is broader for larger values of $\phi$. The values of optimum $\theta$ and minimum $\ell/c$ are given in Table 1 and the optimum patch aspect ratios for various combinations of vertical and horizontal look angles in Table 2.

Table 1

Optimum Cone Geometry for Given Maximum Look Angle

| $\phi$ | $\theta_{opt}$ | $(\ell/c)$ min |
|---|---|---|
| $30^O$ | $13^O$ | 10.48 |
| $31.5^O$ | $13.5^O$ | 9.314 |
| $45^O$ | $17^O$ | 3.69 |
| $60^O$ | $18^O$ | 1.520 |

Table 2

Optimum Patch Aspect Ratios for Given Maximum Look Angles

| Vertical | Horizontal | Aspect Ratio |
|---|---|---|
| $30^O$ | $60^O$ | 6.89 |
| $31.5^O$ | $60^O$ | 6.13 |
| $45^O$ | $60^O$ | 2.43 |
| $45^O$ | $45^O$ | 1.00 |
| $60^O$ | $60^O$ | 1.00 |

There are other optimizations possible in addition to the one carried out above to minimize the cone length to patch half width ratio. One would like to find an optimization procedure directly related to the thermal performance, for example. This might be accomplished by minimizing the radiative coupling between the patch and its cone (Section 1.3). The geometrical parameters which
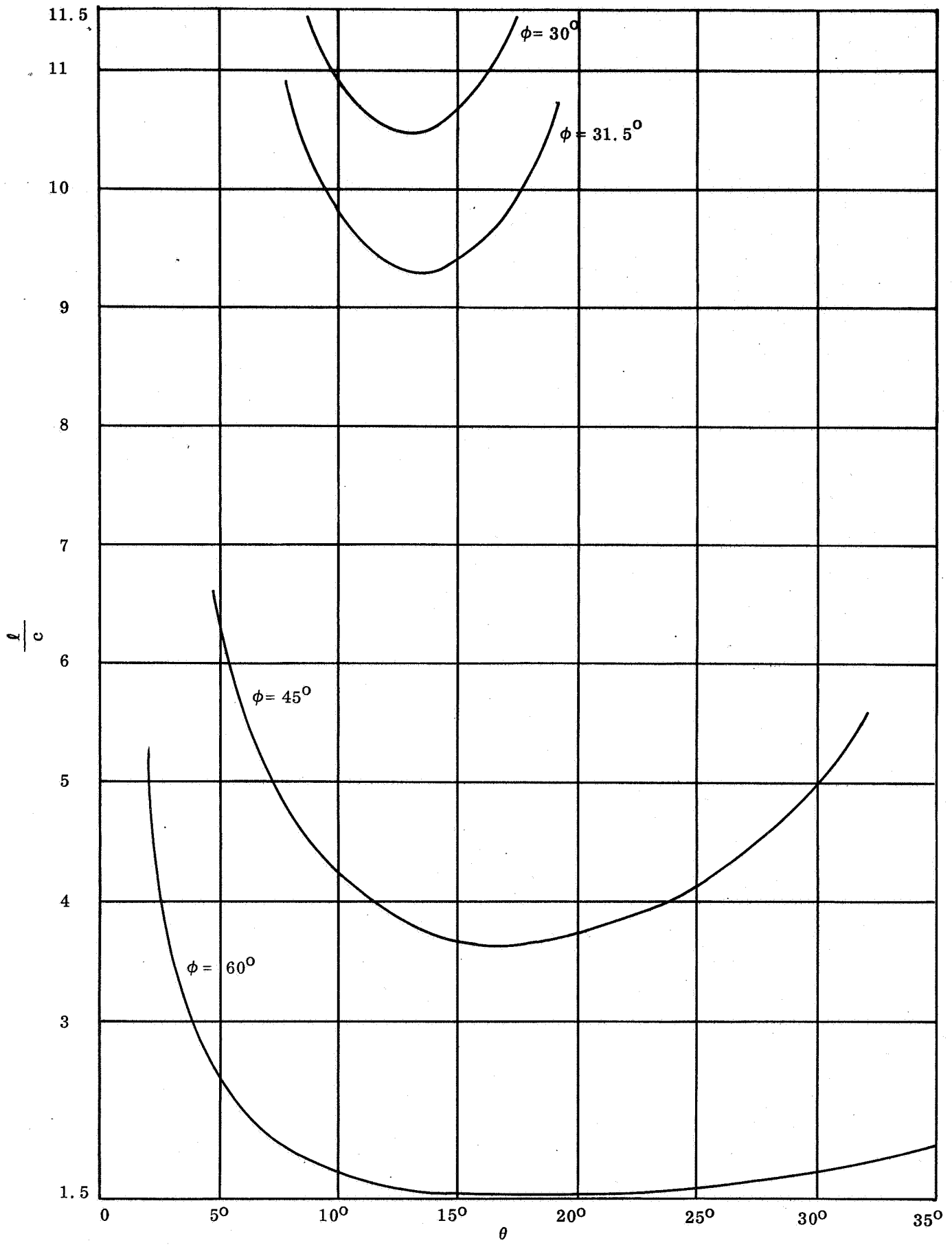
Figure 4   Relative Length Versus Cone Half Angle

11

influence radiative coupling are $\theta$ and $\phi$, and for a fixed $\phi$ the minimum occurs at $\theta = \phi$. This means $r_1/r_2 \longrightarrow 0$ and $\ell/c \longrightarrow \infty$, that is, either an infinitesimal patch or an infinitely long cone is required. Neither solution is practical, of course, and this approach to optimization was abandoned.

## 1.3  Radiative Coupling Between Patch and Cone

Equations are derived below for the effective emissivity and effective reflectivity of the cone structure as viewed from the patch in terms of the actual cone surface emissivity. The results are expressed as an effective patch-to-cone emissivity. The effective patch-to-cone emissivity is then related to the exchange factor used by Sparrow and others in the analysis of radiative coupling among surfaces having specular reflectivity.

### 1.3.1  Calculation of Effective Emissivity from Surface Emissivity

The black radiating patch in a radiant cooler views cold space via a low-emissivity, high-reflectivity cone structure. If $f_n$ is the fraction of radiant flux from the patch which reaches space after n reflections from the cone walls, the effective reflectivity of the cone, as seen from the patch, is

$$\rho_{pc} = \sum_{n=0} f_n \, \rho_g^n = \sum_{n=0} f_n \, (1 - \epsilon_g)^n \tag{8}$$

where $\rho_g$ is the reflectivity of the cone surface and $\epsilon_g$ its emissivity. The effective reflectivity of the cone is the fraction of radiant power emitted by the patch that reaches cold space. This concept is used in the study of cavities to express the fraction of incident radiation reflected back out of the cavity (see, for example, E. W. Treuenfels, JOSA 93, 1162, 1963). In the case of the radiant cooler, the cavity is in the form of a truncated conical perforation.

According to Kirchhoff's radiation law, the effective emissivity, $\epsilon_{pc}$, of the cone structure, as seen from the patch, is then $(1 - \rho_{pc})$. That is,

$$\epsilon_{pc} = 1 - \sum_{n=0} f_n \, (1 - \epsilon_g)^n \tag{9}$$

This is one of the three general methods employed for deriving equations for cavity emissivity (G. A. Rutgers, Handbuch der Physik, Bd. 26 (Springer-Verlag, Berlin, 1958), p. 129).

An expression for the effective patch-to-cone emissivity may also be obtained directly with the help of Figure 5. ABCD is a cross-section of a radiant cooler in which BC is the black patch. BC' and CB' are images of the patch
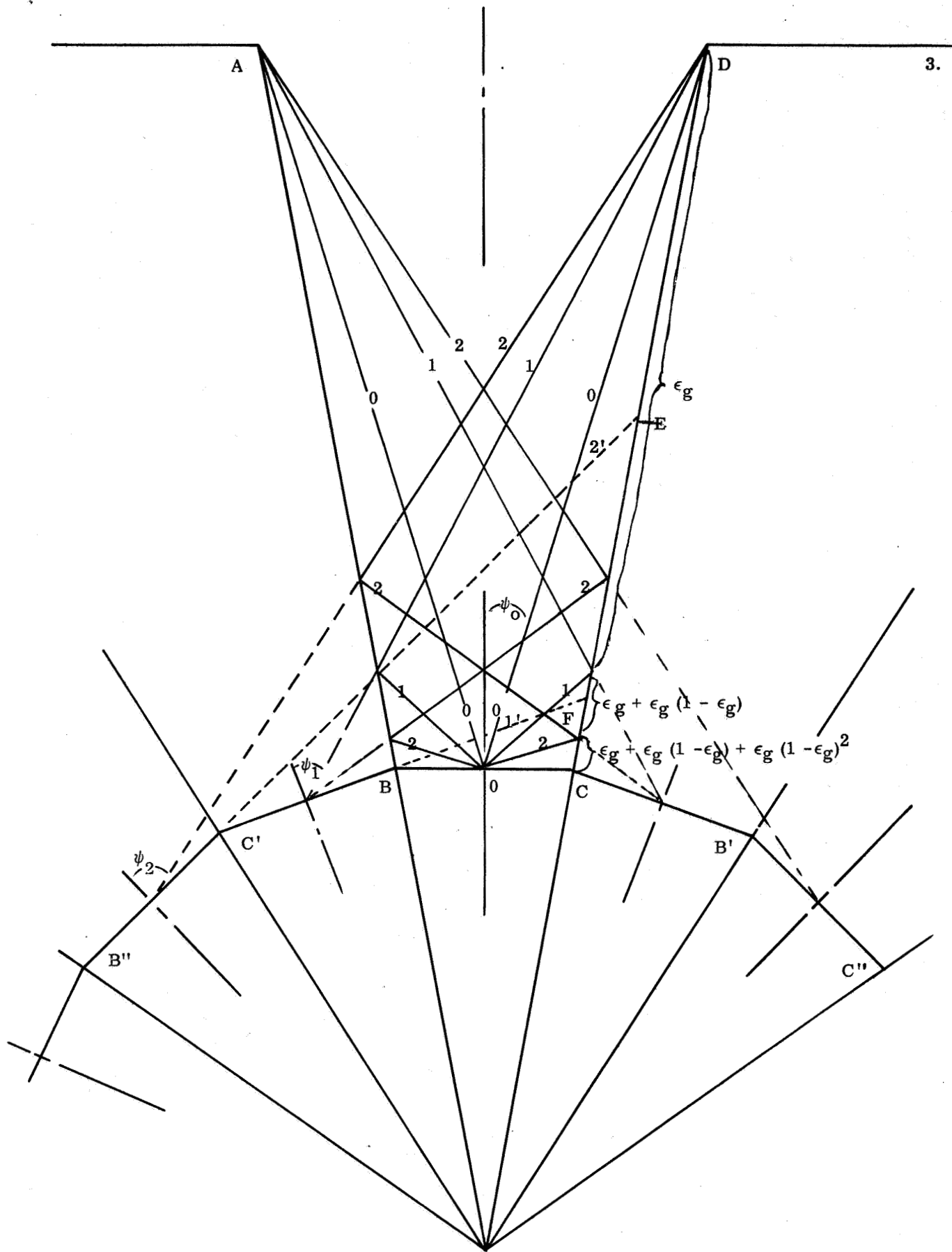
Figure 5   Calculation of Effective Patch-To-Cone Emissivity

13

formed by one reflection in the cone walls, C'B" and B'C" are images of the patch by two reflections. The cone walls are assumed to be specularly reflecting and the patch to have an absorptivity of unity. The technique of multiple-reflections shown in the sketch has been used by Sparrow and Lin to determine the emissivity of a specularly reflecting V-groove cavity ("Absorption of Thermal Radiation in V-Groove Cavities", U. of Minn. for NASA-Lewis, N62 10682, July 1962). It has also been employed by Williamson (JOSA 42, 712, 1952) and Hanel (ARS Journ. 31, 246, 1961) in the study of specularly reflecting cone channels.

The view of cold space and the cone walls from the patch will be approximated by the view from the center of the patch. The fraction, $f_0$, of radiation emitted by the patch between the normal to the patch and the rays 0 goes directly to space without reflection from the cone and is equal to $F_{ps}$, the view factor from the patch to space (i. e. , the fraction of emitted radiation going directly to space). Rays between 0 and ray 1 are reflected once from the cone wall before going to space; rays between 1 and 2 are reflected twice and between 2 and 90 degrees to the patch normal, three times. The fraction of patch radiant flux which reaches cold space is then

$$\rho_{pc} = f_0 + f_1 \rho_g + f_2 \rho_g^2 + f_3 \rho_g^3 + \cdots = \sum_{n=0} f_n \rho_g^n \qquad (10)$$

The radiant flux from the patch which is absorbed by the cone wall is then given by

$$\Phi_{p-c} = \sigma T_p^4 A_p (1 - \rho_{pc}) \qquad (11)$$

where $T_p$ is the patch temperature and $A_p$ the patch radiating area. The radiant flux from the patch therefore either goes to cold space or is absorbed in the cone walls. None is returned to the patch because of the outward sloping, specularly reflecting walls.

When reversed in direction, the path by which rays go to space via reflections from the cone walls become the paths by which radiation from the cone walls reaches the patch. F. E. Nieodemus (Appl. Opt. 4, 767, 1965) shows that, when the usual reciprocity relationship holds, the reflectance $\rho$ for a ray incident on an opaque surface element is related by Kirchhoff's law, $1 - \rho = \epsilon$, to the emissivity $\epsilon$ of that element for a ray emitted along the same line in the opposite sense (See also E. R. G. Eckert and E. M. Sparrow, Int. J. Heat Mass. Transfer 3, 50, 1961). We may therefore conclude that since $(1 - \rho_{pc})$ is the effective absorptivity for radiation going from the patch to space, that it is also the effective emissivity for radiant transfer from the cone walls to the patch. This is shown by means of Figure 5.

14

Radiation from the cone wall may reach the patch by a direct path or by reflection off the cone wall. All the cone wall can see the patch directly. The cone wall between D and F can see the patch by one reflection off the walls: this area is determined by the rays 1 and 1' from the image of the patch formed by one reflection. This once-reflected cone radiation may be accounted for by assigning an emissivity $\epsilon_g (1 - \epsilon_g)$, in addition to the emissivity $\epsilon_g$ due to direct coupling, to the cone wall area between 90 degrees to the patch normal and the boundary where ray 1 from the patch center first strikes the wall. The once-reflected wall radiation effectively comes from this area, since it is reflected from the area before being absorbed by the patch. Similarly, the cone wall between D and E can see the patch by two reflections in the cone wall; this area is determined by rays 2 and 2' from the image of the patch formed by two reflections. The twice reflected radiation may be accounted for by assigning a third emissivity component of $\epsilon_g (1 - \epsilon_g)^2$ to the cone wall area between 90 degrees to the patch normal and the boundary where ray 2 from the patch center first strikes the cone wall.

The above procedure may be extended until a reflection m is reached such that the mth reflection of the patch in the cone walls cannot see the cone walls. In the attached sketch, the maximum number of wall reflections for wall emission is two, so that m is three. The radiant power transfer from the cone wall to the patch can therefore be determined by assigning an emissivity.

$$\epsilon_n = \epsilon_g \ [1 + (1 - \epsilon_g) + \cdots + (1 - \epsilon_g)^{n-1}] \tag{12}$$

to the wall area $A_n$, where $A_n$ is the wall area initially intercepted by rays from the patch center that require n reflections to go to cold space. The above is a geometrical progression and may be summed to give

$$\epsilon_n = [1 - (1 - \epsilon_g)^n] \tag{13}$$

The radiant power transfer from the cone walls to the black patch is then

$$\Phi_{c-p} = \sigma T_c^4 \ \sum_{n=0} \ A_n g_n \ [1 - (1 - \epsilon_g)^n] \tag{14}$$

where $g_n$ is the view factor from $A_n$ to the patch area $A_p$ (i.e., the fraction of diffuse radiation from $A_n$ which goes directly to $A_p$). But

$$A_n g_n = A_p f_n \tag{15}$$

where $f_n$ is the view factor from the patch to area $A_n$ (M. Jakob, Heat Transfer, Vol. II, Wiley and Chapman & Hall, 1957, p. 9). The view factor $f_n$ is equal to the fraction of patch radiation that requires n reflections in a perfectly reflecting

cone ($\rho_g = 1$) to reach cold space; it is also the view factor from the patch to space as seen by n reflections in the cone walls. Hence,

$$\Phi_{c-p} = \sigma T_c^4 A_p \sum_{n=0} f_n \ [1 - (1 - \epsilon_g)^n]$$  (16)

The sum over n may be rewritten $\sum_{n=0} f_n - \sum_{n=0} f_n (1 - \epsilon_g)^n$. But

$$\sum_{n=0} f_n = 1$$  (17)

(Jakob, op. cit., p. 10), that is, the sum of all view factors from the patch (over a hemisphere) is unity. Equation (16) then becomes

$$\Phi_{c-p} = \sigma T_c^4 A_p \ [1 - \sum_{n=0} f_n (1 - \epsilon_g)^n]$$  (18)

Finally, since the patch is black (absorptivity of unity), no wall radiation is reflected back to the walls, and the net radiative exchange between the cone walls and the patch is (equations 11 and 18)

$$\Delta \Phi_{c-p} = \Phi_{c-p} - \Phi_{p-c} = \sigma A_p (T_c^4 - T_p^4) \ [1 - \sum_{n=0} f_n (1 - \epsilon_g)^n]$$  (19)

The effective emissivity for cone wall-patch radiant exchange is therefore

$$\epsilon_{pc} = (1 - \rho_{pc}) = 1 - \sum_{n=0} f_n (1 - \epsilon_g)^n$$  (20)

as already obtained by application of Kirchhoff's law.

The angles $\psi_n$ (Figure 5) can be determined by means of the law of sines and law of cosines, which yield the equation

$$\sin \psi_n = \frac{r_2 \sin [(2n+1) \ \theta]}{[r_2^2 + r_1^2 \cos^2 \theta - 2 r_1 \cos \theta \, r_2 \cos ( <2n+1> \theta )]^{1/2}}$$  (21)

where

$\theta$ = cone half angle

$r_1$ = distance along cone surface from apex to patch

$r_2$ = distance along cone surface from apex to mouth

16

The geometry of the cooler is shown in Figure 2 in Section 1.2. For a given maximum patch look angle $\phi$ (equation 4) equation (21) may be written

$$\sin \psi_n = \frac{\sin [(2n+1)\ \theta]}{[1 + \sin^2 (\phi - \theta) \cos^2 \theta + \sin (\phi - \theta) \cos \theta \cos (<2n+1> \theta)]^{1/2}} \quad (22)$$

We will assume that the patch area is concentrated at its center, i.e., that the view factors from the center of the patch equal the values averaged over the patch area. For a truncated right circular cone in which rays at angles between $\psi_{n-1}$ and $\psi_n$ to the patch normal require n reflections to reach cold space, the view factor is given by

$$f_n = 1/\pi \int_{\varphi = 0}^{2\pi} \int_{\vartheta = \psi_{n-1}}^{\psi_n} \sin \vartheta \cos \vartheta\, d\,\vartheta\, d\,\varphi = \sin^2 \psi_n - \sin^2 \psi_{n-1} \quad (23)$$

The integral is written in terms of spherical coordinates at the patch center with the pole along the patch normal; $\vartheta$ is the pole angle and $\varphi$ the azimuthal angle. From equations (20), (22), and (25) we see that the effective patch-to-cone emissivity for a given maximum look angle depends only on the emissivity of the cone surface and the half angle of the cone.

## 1.3.2   Radiative Coupling Among Surfaces Having Specular Reflectivity

Radiative coupling among surfaces having specular reflectivity is treated in Chapters 5 and 6 of "Radiation Heat Transfer" by E. M. Sparrow and R. D. Cess (Brooks/Cole Pub. Co., Belmont, Calif., a Div. of Wadsworth Pub. Co., Inc., 1966). In his analysis, Sparrow makes use of a parameter called the exchange factor, which replaces the view (angle) factor used for diffusely reflecting surfaces. The exchange factor $E_{ij}$ from an area $A_i$ to an area $A_j$ is the fraction[1] of diffusely distributed flux from $A_i$ that arrives at $A_j$ both directly and by all possible intervening specular reflections.

The exchange factor is also used by O'Brien and Sowell in their analysis of radiant transfer through specular tubes (JOSA 57, 28, 1967), where it is represented by the symbol $\phi$. O'Brien and Sowell attribute the establishment of the exchange factor to Bobco (J. Heat Transfer, ASME Ser. C86, 123, 1964).

The exchange factor is related to the effective emissivity used in the analysis of the two-stage radiant cooler. This can be shown by considering the radiative exchange between areas $A_i$ and $A_j$ in an enclosure of specularly reflecting surfaces. In this case, the only diffusely distributed flux from a surface is that

---

1   This "fraction" may be greater than one.

17

emitted by the surface (i. e., diffuse reflectivity is zero). Black surfaces may be included as areas of zero specular reflectivity. The power from $A_i$ that is absorbed in $A_j$ is then.

$$\Phi_{ij} = A_i \, \epsilon_i \, \sigma T_i^4 \, E_{ij} \, \epsilon_j \qquad (24)$$

where

$$\epsilon_i = \text{emissivity of } A_i$$

$$T_i = \text{temperature of } A_i$$

$$\epsilon_j = \text{absorptivity of } A_j$$

This equation assumes the areas are gray, so that the absorptivity, $\alpha_K$, of a surface equals its emissivity, $\epsilon_K$. $A_i \, \epsilon_i \, \sigma T_i^4$ is the total power emitted by $A_i$, $E_{ij}$ is the fraction of total power reaching $A_j$ directly and by specular reflection, and $\epsilon_j$ is the fraction of power reaching $A_j$ that is absorbed in $A_j$. Similarly, the power from $A_j$ absorbed in $A_i$ is

$$\Phi_{ji} = A_j \, \epsilon_j \, \sigma T_j^4 \, E_{ji} \, \epsilon_i \qquad (25)$$

Using the reciprocity relation (Sparrow and Cess, equation 5-4a; O'Brien and Sowell, equation 4 and appendix)

$$A_i \, E_{ij} = A_j \, E_{ji} \qquad (26)$$

the net radiative exchange between surfaces i and j is (for $T_j > T_i$)

$$\Delta \Phi_{ij} = A_i \, \epsilon_i \, \epsilon_j \, E_{ij} \, \sigma(T_j^4 - T_i^4) \qquad (27)$$

In terms of the effective emissivity $\epsilon_{ij}$ from surface i to surface j, the net radiative exchange is (see equation 19)

$$\Delta \Phi_{ij} = A_i \, \epsilon_{ij} \, \sigma(T_j^4 - T_i^4) \qquad (28)$$

Comparison of equations (27) and (28) yields

$$\epsilon_{ij} = \epsilon_i \, \epsilon_j \, E_{ij} \qquad (29)$$

The effective emissivity, $\epsilon_{ij}$, in an enclosure of specularly reflecting surfaces (including black surfaces) is therefore the emissivity of the diffusely emitting surface i times the fraction of its emission absorbed in the receiving surface j.

Combining (29) and (26), we obtain the reciprocity relationship for effective emissivity,

$$A_i \, \epsilon_{ij} = A_j \, \epsilon_{ji} \tag{30}$$

Since $\epsilon_j \, E_{ij}$ is the fraction of diffuse radiation from surface i absorbed in surface j for an enclosure of black and specularly reflecting surfaces, its sum over all the surfaces must be unity

$$\sum_j \epsilon_j \, E_{ij} = 1 \tag{31}$$

That is, all the emission from $A_i$ is absorbed within the enclosure. In general, $A_i$ may be concave or see itself by reflection, so that the sum includes a term $\epsilon_i \, E_{ii}$. This relation is derived by O'Brien and Sowell (op. cit. , eq. 5 and appendix).

As an example of the determination of the exchange factor and effective emissivity, consider two plane-parallel specularly reflecting surfaces of infinite extent. The "fraction" of radiation from surface 1 that reaches surface 2 directly and by all possible intervening specular reflections is

$$E_{12} = 1 + (1 - \epsilon_2)(1 - \epsilon_1) + (1 - \epsilon_2)^2 (1 - \epsilon_1)^2 + \cdots \tag{32}$$

where

$$1 - \epsilon_1 = \text{reflectivity of surface 1}$$

$$1 - \epsilon_2 = \text{reflectivity of surface 2}$$

Equation (32) is a geometrical progression and can be summed to yield

$$E_{12} = \frac{1}{1 - (1 - \epsilon_2)(1 - \epsilon_1)} = \frac{1}{\epsilon_2 + (1 - \epsilon_2)\,\epsilon_1} \tag{33}$$

The effective emissivity from surface 1 to surface 2 is then

$$\epsilon_{12} = \epsilon_1 \, \epsilon_2 \, E_{12} = \frac{\epsilon_1 \, \epsilon_2}{\epsilon_2 + (1 - \epsilon_2)\,\epsilon_1} \tag{34}$$

This result is given in Table 6.3, p. 148, of R B. Scott, "Cryogenic Engineering", D Van Nostrand, 1959.

Sparrow considers the determination of the exchange factor for plane specularly reflecting surfaces (pp. 140-144) and for curved specularly reflecting surfaces (pp. 144-149). For radiation going from the diffusely emitting black patch to space via the specularly reflecting cone the exchange factor is (Sparrow and Cess, equation 5-2)

$$E_{ps} = \sum_n \rho_g^n f_n \tag{35}$$

where $\rho_g$ is the reflectivity of the cone surface. The factor $f_n$ is identical to the $f_n$ used in Section 1.3.1; it is given by any of the three following equivalent definitions.

$f_n$ = view factor from patch to cone wall area initially intercepted by rays from patch that require n cone reflections to go to cold space (Sparrow and Cess, equation 5-11).

$f_n$ = view factor from patch to space (cone mouth) as seen by n reflections in the cone wall.

$f_n$ = fraction of emitted patch radiation that requires n reflections in a perfectly reflecting ($\rho_g = 1$) cone to reach cold space (Sparrow and Cess, p. 139).

Equation (35) is of the same form as equation (5-22) in Sparrow and Cess, which applies to elements in a specularly reflecting cylindrical tube. It is also the form used by O'Brien and Sowell (op. cit., eq. 3) in their study of radiant transfer through specular tubes.

Comparison of equation (35) with equation (8) shows that $E_{ps}$ is equal to the effective reflectivity, $\rho_{pc}$, of the cone for radiation going from the patch to the cone mouth (cold space). That is, the reflectivity through the truncated cone from the patch end is equal to the fraction of diffuse emission from the patch that reaches the cone mouth directly and by all intervening specular reflections from the cone. The effective patch-to-cone emissivity is then

$$\epsilon_{pc} = 1 - \rho_{pc} = 1 - E_{ps} = \epsilon_g E_{pc} \tag{36}$$

That is, the fraction of radiation from the black patch that does not reach the cone mouth is absorbed in the cone walls.

## 1.4   First-Stage Cone

The first-stage cone consists of the outward sloping, specular surface (the cone) used to direct patch radiation to cold space and an attached cone end not visible from the patch. Sources of thermal loading on the first-stage cone are the outside cooler surface and external sources of radiation. Sufficient multilayer insulation (R. H. Kropschot, Chapter 6 in "Applied Cryogenic Engineering", Wiley, 1962) can be placed between the outer cooler surface and the cone to make the thermal load from the first source negligible compared to that from external sources. The most important external sources are the earth and the sun. The earth is a source of infrared radiation and reflected sunlight (earthshine).

First, consider the cone without an attached cone. Absorption of earth radiation in the cone is strongest in the vertical plane of the cooler. We will use the vertical plane values for absorption of earth infrared and earthshine. To offset this, cone absorption of spacecraft infrared will be neglected. Even then, the resultant heat load probably overstates the actual case. The cooler may be positioned so the spacecraft cannot be seen from the cone, or, if this is not possible, the spacecraft areas that are visible may be covered with a low emissivity material.

The thermal loads on the cone are balanced by its emission to the first-stage of the cooler and to the outside (by way of its opening or mouth). The average of vertical plane and horizontal plane values will be used for cone emissivities, since there is no concentration of emission around any particular direction.

Because its solar absorptivity is greater than its infrared absorptivity (emissivity), the largest thermal load on a low emissivity cone is produced by direct and earth reflected sunlight. However, coatings with a lower solar absorptivity seem to have a higher emissivity, which reduces the cone temperature but increases the radiant coupling from the cone to the first-stage patch. The function of the cone end is to balance the high $\alpha/\epsilon$ surface of the cone with a low $\alpha/\epsilon$ surface. The low $\alpha/\epsilon$ surface cannot be seen from the patch and so does not influence the radiant coupling to the patch. If the spacecraft areas seen by the cone end have a low emissivity (0.1), the ends will cool the cone in the absence of direct sunlight and keep the temperature rise within bounds in the presence of direct sunlight. The cone ends may be painted white on their outer surfaces or constructed of Alzak treated aluminum to achieve the desired low solar absorptivity and high infrared emissivity.

Besides the attachment of a cone end, the temperature of the first-stage cone may be reduced by the addition of sun or earth shields which lie outside the field of view of the patch (See Section 1.7). The shields reduce the thermal load

21

on the first-stage cone by replacing some or all of the earth and solar irradiation with infrared irradiation from a low emissivity surface at the temperature of the outer cooler box. The following analysis is for the case of no shields.

## 1.4.1 Thermal Balance Equation of the Cone

For sufficient multi-layer insulation between the outer cooler surface and the first-stage cone, the radiant flux absorbed by the (inner surface of the) cone is

$$A_c \, (\epsilon_{ce} \, W_e + \alpha_{ce} \, W_s) + A_m \, \alpha_g \, H_s$$

where

$A_c$ = surface area of the cone

$A_m$ = area of cone mouth

$\epsilon_{ce}$ = infrared absorptivity of the cone for earth radiation

$\alpha_{ce}$ = absorptivity of the cone for earthshine

$\alpha_g$ = solar absorptivity of cone surface

$W_e$ = average infrared emittance of the earth (Appendix I)

$W_s$ = average equivalent earthshine emittance (Appendix I)

$H_s$ = average cone mouth solar irradiance over an orbit

The term for absorbed direct solar flux assumes there are no multiple reflections of direct sunlight in the cone (i.e., a direct ray from the sun goes back out the cone mouth after one cone wall reflection).

The cone at a temperature $T_c$ emits a radiant power of $A_c \, \sigma T_c^4 \, \epsilon_{cx}$ out the cone mouth, where $\epsilon_{cx}$ is the effective external cone emissivity and $\sigma$ the Stefan-Boltzmann constant. The cone also emits a net radiant power to the first-stage patch and second-stage cone of

$$\Phi = A_c \, \sigma \, (T_c^4 - T_p^4) \, (\epsilon_{cp} + \epsilon_{cc2}) \qquad (37)$$

where

$T_p$ = temperature of the first-stage patch and second-stage cone

22

$$\epsilon_{cp} = \text{effective emissivity from the first-stage cone to the first-stage patch}$$

$$\epsilon_{cc2} = \text{effective emissivity from the first-stage cone to the second-stage cone}$$

Since $T_p^4$ is much less than $T_c^4$, we may approximate this by

$$A_c \quad \sigma T_c^4 (\epsilon_{cp} + \epsilon_{cc2})$$

Equating the absorbed radiant power to the emitted power, we obtain the thermal balance equation for the first-stage cone

$$A_c \ \sigma T_c^4 (\epsilon_{cx} + \epsilon_{cp} + \epsilon_{cc2}) = A_c (\epsilon_{ce} W_e + \alpha_{ce} W_s) + A_m \ \alpha_g \ H_s$$

Or

$$\sigma T_c^4 = \frac{\epsilon_{ce} W_e + \alpha_{ce} W_s + \alpha_g H_s \frac{A_m}{A_c}}{\epsilon_{cx} + \epsilon_{cp} + \epsilon_{cc2}} \tag{38}$$

In order to calculate the in-orbit cone temperature from equation (38) we must first determine the values of the effective absorptivities in the numerator and effective emissivities in the denominator.

To obtain the effective cone-to-patch emissivity, $\epsilon_{cp}$, consider the net radiative exchange between the cone and patch, which is given by equation (19) in Section 1.3.1

$$\Delta \Phi_{c-p} = \sigma A_p \quad [1 - \sum_{n=0} f_n (1 - \epsilon_g)^n] \quad (T_c^4 - T_p^4)$$

where

$$A_p = \text{radiating area of the first-stage patch}$$

$$\epsilon_{pc} = 1 - \sum_{n=0} f_n (1 - \epsilon_g)^n = \text{effective emissivity from the first-stage patch to the first-stage cone.}$$

$$f_n = \text{view factor from the patch to space (cone mouth) as seen by n reflections in the cone.}$$

$$\epsilon_g = \text{surface emissivity of the cone}$$

If the radiant exchange is written in terms of the cone area, $A_c$, we may define an effective emissivity from cone to patch, $\epsilon_{cp}$, by the equation

$$\sigma A_c \, \epsilon_{cp} \, (T_c^4 - T_p^4) = \sigma A_p \, \epsilon_{pc} \, (T_c^4 - T_p^4) \tag{39}$$

Or

$$\epsilon_{cp} = \frac{A_p}{A_c} \, \epsilon_{pc} \tag{40}$$

This may be considered a form of the reciprocity relationship between view factor and area (M. Jakob, "Heat Transfer" Vol. II, Wiley, 1957, p. 9) in which the view factor has been replaced by a parameter dependent on surface emissivity and view factors under multiple reflections (the radiative interchange factor used by Jakob on p. 5). The reciprocity relationship for effective emissivity was obtained in Section 1.3.2 from the relationship for the exchange factor of specular surfaces.

The effective emissivity from the first-stage cone to the second-stage cone is given by

$$\epsilon_{cc2} = \frac{A_{c2}}{A_c} \, \epsilon_{c2c} \tag{41}$$

where $A_{c2}$ is the outer surface area of the second-stage cone and $\epsilon_{c2c}$ is the emissivity from the second- to the first-stage cone. Since the second-stage cone has roughly the same geometric position in the cooler as the first-stage patch but has the same low emissivity surface as the first-stage cone, we have the approximate relation

$$\epsilon_{c2c} = 1/2 \, \epsilon_{pc} \tag{42}$$

where the factor 1/2 accounts for the low emissivity of the second-stage cone. Then

$$\epsilon_{cc2} = \frac{A_{c2}}{A_c} \times 1/2 \, \epsilon_{pc} \tag{43}$$

Using equation (40) this becomes

$$\epsilon_{cc2} = 1/2 \, \epsilon_{cp} \, \frac{A_{c2}}{A_p} \tag{44}$$

And the thermal balance equation (38) becomes

$$\sigma T_c^4 = \frac{\epsilon_{ce} W_e + \alpha_{ce} W_s + \alpha_g H_s \, \dfrac{A_m}{A_c}}{\epsilon_{cx} + \epsilon_{cp} \left(1 + \dfrac{1}{2} \dfrac{A_{c2}}{A_p}\right)} \tag{45}$$

24

## 1.4.1.1   Effective Cone External Emissivity

The cone views the external environment by way of its mouth. Thus, from the point of view of the cone, the external environment may be replaced by an equivalent area stretched tightly over the cone mouth. In a manner similar to that used to derive the expression for radiant power transfer from the cone walls to the black patch (equation 14, Section 1.3.1), one may derive an equation for the radiant transfer from the cone walls to the cone mouth (external environment). The result is

$$\Phi_{c-m} = \sigma T_c^4 \sum_{n=0} A_n' g_n' [1 - (1 - \epsilon_g)^n] \tag{46}$$

where $g_n'$ is the view factor from $A_n'$ to the cone mouth area $A_m$. $A_n'$ is the cone wall area last intercepted by rays from the cone that require $n-1$ reflections at the cone wall to go out the cone mouth. Figure 6 shows the $A_n'$ areas for the vertical section of the first-stage cone and for rays which exit through the center of the cone mouth. Note that $A_1'$ and $A_2'$ are divided into sections separated on the cone surface.

But (M. Jakob, "Heat Transfer" Volume II, Wiley, 1957, p. 9)

$$A_n' g_n' = A_m f_n' \tag{47}$$

where $f_n'$ is the view factor from the cone mouth to the area $A_n'$.[2] The view factor $f_n'$ is also equal to the fraction of radiation entering the mouth of a perfectly reflecting cone that requires $n$ cone reflections to go back out the cone mouth or to the black patch at the other end of the truncated cone. Substituting (47) into (46)

$$\Phi_{c-m} = \sigma T_c^4 A_m \sum_{n=0} f_n' [1 - (1 - \epsilon_g)^n]$$

$$\Phi_{c-m} = \sigma T_c^4 A_m \left\{ \sum_{n=0} f_n' - \sum_{n=0} f_n' (1 - \epsilon_g)^n \right\} \tag{48}$$

But (M. Jakob, op. cit., p. 10)

$$\sum_{n=0} f_n' = 1 \tag{49}$$

That is, all radiation which enters the cone mouth is reflected either to the patch (including the case of zero reflections) or back out the mouth in a perfectly reflecting cone. Or, in terms of the view factor, all radiation entering the mouth initially strikes either the cone wall or the black patch (for which $n = 0$ and $1 - (1 - \epsilon_g)^n = 0$).

---

2     Or the view factor from the cone mouth to the cone mouth and patch as seen as $n$ reflections in the cone wall.

$A_n'$ = cone wall area last struck by rays from cone that require $n - 1$ cone wall reflections to go out center of cone mouth

n = 1

n = 2

n = 3

n = 4

n = 5

$A_1'$

$A_2'$

$A_3'$

$A_4'$

$A_5'$

$A_2'$

$A_1'$

$\theta$

$r_1$

$r_2$
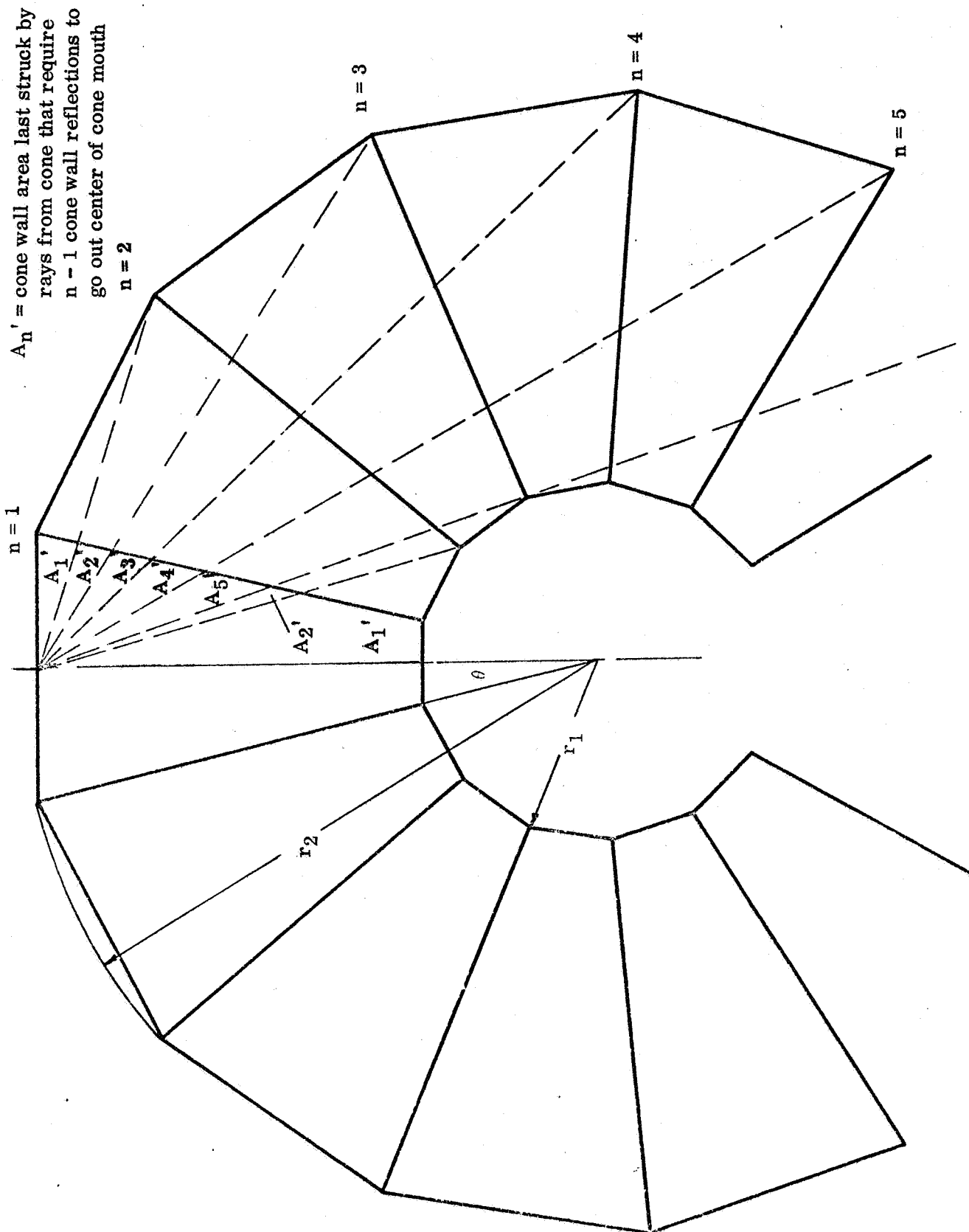
Figure 6  Vertical Plane of First Stage Reflected in Cone Walls

Combining (48) and (49), the equation for the radiant flux emitted to the outside by the cone becomes

$$\Phi_{c-m} = \sigma T_c^4 A_m (1 - \sum_{n=0} f_n' \rho_g^n) \tag{50}$$

where $\rho_g = 1 - \epsilon_g$ is the surface reflectivity of the cone. This may be written

$$\Phi_{c-m} = \sigma T_c^4 A_m (1 - \rho_{mx}) \tag{51}$$

where $\rho_{mx}$ is the effective or cavity reflectivity for radiation entering the cone mouth and equals the fraction of radiation incident on the mouth that is reflected back out the mouth and goes to the patch directly or by reflection. That is, it is the fraction entering that goes out both ends of the truncated cone cavity. The factor $1 - \rho_{mx}$ is the effective emissivity or absorptivity, $\epsilon_{mx}$, as generally applied to cavities.

One may then define an effective cone external emissivity by the equation

$$\Phi_{c-m} = \sigma T_c^4 A_m \epsilon_{mx} = \sigma T_c^4 A_c \epsilon_{cx} \tag{52}$$

where $A_c = \sum_{n=1} A_n'$ is the cone wall area.

Or

$$\epsilon_{cx} = \frac{A_m}{A_c} \epsilon_{mx} = \frac{A_m}{A_c} [1 - \sum_{n=0} f_n' (1 - \epsilon_g)^n] \tag{53}$$

The cone external emissivity, $\epsilon_{cx}$, is equal to the absorptivity of the cone walls for incident diffuse radiation (i.e., a source stretched tightly across the cone mouth), according to Kirchhoff's law.

## 1.4.1.2  Effective Cone Absorptivity For Earth Radiation

The view to earth from the mouth of the cone is the same as its view to a vertical semicircle whose radius subtends an angle equal to the angle from the spacecraft nadir to a tangent line to the earth and whose center lies on the nadir. If we set up spherical coordinates at the cone mouth, with the pole along a normal to the mouth, the number of reflections earth radiation undergoes at the cone walls before going back out the cone mouth is a step-wise function of the polar angle $\vartheta$ (See Figure 7) for a right circular cooler cone  That is, the range of polar angles can be divided into regions in which the absorptivity in the walls is a constant. Alternatively, the surface area of the earth seen from the cone mouth, or the equivalent area of the semicircle, can be divided into sub-areas, $A_{en}$, whose radiation is reflected n times at the cone walls upon entering the cone mouth. The effective absorptivity of the cone mouth for earth radiation is then

27

$$\sin \vartheta_n = \frac{\cos \varphi_O}{\cos \varphi_n}$$

Normal to Cone Mouth

$\varphi_O$

$\varphi_1$

$\varphi_2$

$\varphi_3$

$\vartheta_O$

$\vartheta_1$

$\vartheta_2$

$\vartheta_3$

$\vartheta_4$

$A_{e1}$

$A_{e2}$

$A_{e3}$

$A_{e4}$

Semi-circle generated by tangent lines to earth from cone mouth

$\vartheta = \vartheta_1$    $\vartheta = \vartheta_2$    $\vartheta = \vartheta_3$

$\vartheta_O = \pi/2$

$\vartheta_4 = \pi/2 - \varphi_O$
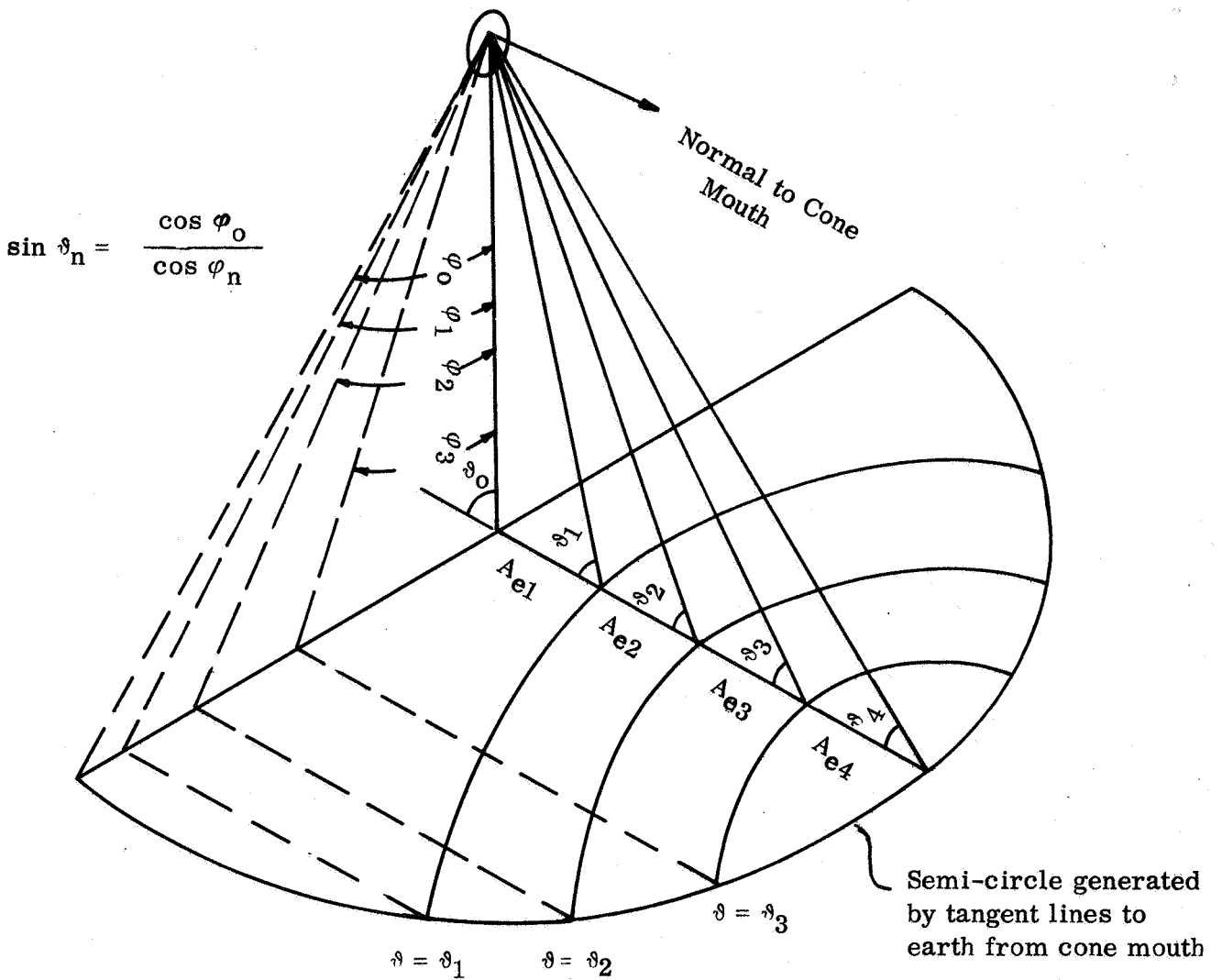
$\varphi_4 = 0$

Surfaces $\vartheta =$ constant are cones with axes along normal to cone mouth and intercept semi-circle in hyperbolae.

Figure 7    Coordinates and Angles for Calculation of Cone Mouth Absorptivity For Earth Radiation

28

$$a_{me} = \Sigma\, a_n\, F_m\text{-}A_{en} \tag{54}$$

where $a_n$ is the absorptivity produced by n cone-wall reflections and $F_m\text{-}A_{en}$ is the view factor from the cone mouth to the sub-area $A_{en}$.

For the spherical coordinate system shown in Figure 7, the view factor is given by

$$F_m\text{-}A_{en} = \frac{2}{\pi} \int_0^{\varphi_n} \int_{\vartheta_n}^{\vartheta_{n-1}} \sin\vartheta \cos\vartheta \, d_\vartheta \, d_\varphi \;+\; \frac{2}{\pi} \int_{\varphi_n}^{\varphi_{n-1}} \int_{\vartheta(\varphi)}^{\vartheta_{n-1}}$$

$$\sin\vartheta \cos\vartheta \, d_\vartheta \, d_\varphi \tag{55}$$

Integrating the first term fully and the second term with respect to the polar angle, the view factor becomes

$$F_m\text{-}A_{en} = \frac{1}{\pi}\, \varphi_n\, (\sin^2\vartheta_{n-1} - \sin^2\vartheta_n) + \frac{1}{\pi} \int_{\varphi_n}^{\varphi_{n-1}}$$

$$(\sin^2\vartheta_{n-1} - \sin^2\vartheta(\varphi))\, d_\varphi$$

But along the semicircle.

$$\sin^2\vartheta(\varphi) = \frac{\sec^2\varphi}{\sec^2\varphi_0} \tag{56}$$

and

$$\sin^2\vartheta_n = \frac{\sec^2\varphi_n}{\sec^2\varphi_0} \tag{57}$$

Thus

$$F_m\text{-}A_{en} = \frac{1}{\pi \sec^2\varphi_0}\; [\varphi_{n-1}\sec^2\varphi_{n-1} - \tan\varphi_{n-1}$$

$$-(\varphi_n\sec^2\varphi_n - \tan\varphi_n)] \tag{58}$$

Combining equations (54) and (58), we obtain

$$a_{me} = \frac{1}{\pi\sec^2\varphi_0} \sum_{n=0}^{\rho} (a_{n+1} - a_n)(\varphi_n\sec^2\varphi_n - \tan\varphi_n) \tag{59}$$

where $\rho + 1$ is the maximum number of cone-wall reflections. For the special case $\rho = 0$ (i.e., a maximum of one reflection),

$$a_{me}\,(\rho = 0) = a_1\, \frac{(\varphi_0 - \sin\varphi_0 \cdot \cos\varphi_0)}{\pi} = a_1\, F_{me} \tag{60}$$

29

where $a_1$ is the absorptivity for a single cone reflection and $F_{me}$ is the view factor from the cone mouth (an outside vertical cooler surface) to the earth.

The effective cone absorptivity for earth radiation, $a_{ce}$, is related to the effective cone mouth absorptivity for earth radiation, $a_{me}$, by the reciprocity relationship

$$a_{ce} = \frac{A_m}{A_c} a_{me} \tag{61}$$

## 1.4.2 Thermal Balance Equation of Combined Cone and Cone End

The thermal balance equation for a cone end by itself is, in the absence of shields

$$\epsilon_d A_d \sigma T_d^4 = A_d [\epsilon_s F_{ds} W_b + F_{de} (\epsilon_d W_e + \alpha_d W_s) + \alpha_d H_s] \tag{62}$$

where

$\quad A_d \quad = \quad$ area of cone end

$\quad T_d \quad = \quad$ temperature of cone end

$\quad \epsilon_d \quad = \quad$ emissivity of cone end

$\quad \epsilon_s \quad = \quad$ emissivity of spacecraft seen by end

$\quad F_{ds} \quad = \quad$ view factor from end to spacecraft

$\quad W_b \quad = \quad$ blackbody emittance at spacecraft temperature

$\quad F_{de} \quad = \quad$ view factor from end to earth

$\quad W_e \quad = \quad$ earth infrared emittance

$\quad W_s \quad = \quad$ equivalent earthshine emittance

$\quad H_s \quad = \quad$ average direct solar irradiance

$\quad \alpha_d \quad = \quad$ solar absorptivity of cone end

Adding this to the thermal balance equation for the interior area of the first-stage cone (equation 45) and setting the end temperature equal to the cone temperature $(T_c)$, we obtain the thermal balance equation for the combined cone and cone end and the equation

$$\sigma T_c{}^4 = \frac{\alpha_{ce} W_s + \epsilon_{ce} W_e + \alpha_g H_s \dfrac{A_m}{A_c} + \dfrac{A_d}{A_c}[\epsilon_s F_{ds} W_b + F_{de}(\epsilon_d W_e + \alpha_d W_s) + \alpha_d H_s]}{\epsilon_d \dfrac{A_d}{A_c} + \epsilon_{cx} + \epsilon_{cp}\left(1 + \dfrac{1}{2}\dfrac{A_{c2}}{A_p}\right)} \tag{63}$$

## 1.5 First-Stage Patch

In orbit the thermal coupling between the first-stage patch and its surroundings is very nearly all radiative. Upon removal of the caging mechanism, the only conductive coupling is by means of the in-orbit support, whose thermal inputs are negligible (see Section 1.5.1). The radiative transfer through the optical opening can also be neglected[3] (see Section 2.1.7) and, finally, absorption and emission by the inner walls of the second-stage cone, including coupling to the second-stage patch, have only a very small influence on the temperature of the first-stage patch and will not be considered here.

If we assume the first-stage patch and the second-stage cone attached to it are effectively located at the center of the first stage (i.e., geometrical position for radiative exchange with the first-stage cone), the net radiative exchange between the first stage and its cone is then (equations 37, 40, and 44)

$$\Delta \Phi_{c-p1} = A_{p1}\, \epsilon_{pc}\, \sigma(T_c{}^4 - T_{p1}{}^4)\left(1 + 1/2\,\frac{A_{c2}}{A_{p1}}\right) \tag{64}$$

where

$A_{p1}$ = radiating area of first-stage patch

$\epsilon_{pc}$ = effective emissivity from first-stage patch to first-stage cone (Section 1.3.1)

$T_c$ = temperature of first-stage cone

$T_{p1}$ = temperature of first-stage patch and second-stage cone

$A_{c2}$ = outside surface area of second-stage cone

And the first-stage radiant power to cold space is

$$\Phi_{p1-s} = A_{p1}(1 - \epsilon_{pc})\,\sigma T_{p1}{}^4\left(1 + \epsilon_g\,\frac{A_{c2}}{A_{p1}}\right) \tag{65}$$

---

3  In accordance with the basic design philosophy for the cooler.

where $\epsilon_g$ is the emissivity of the coating on the second-stage cone. The factor $(1 - \epsilon_{pc})$ is the effective reflectivity of the first-stage cone structure for all radiant power going from the first-stage to cold space. It is also called the cavity reflectivity (Section 1.3.1), in this case for radiation entering the small end of a truncated conical cavity. Radiation leaving the patch does not return because of the outward sloping, specularly reflecting cone walls; it is either absorbed in the cone walls (a fraction $\epsilon_{pc}$) or goes to cold space (a fraction $1 - \epsilon_{pc}$), directly or by reflection off the cone walls.

Equating equations (64) and (65), we obtain the thermal balance equation for the first-stage patch that determines its equilibrium temperature. The equilibrium radiant emittance of the first-stage patch is then given by

$$\sigma T_{p1}{}^4 = \frac{\epsilon_{pc}\,(1 + 1/2\,\dfrac{A_{c2}}{A_{p1}})\,\sigma T_c{}^4}{1 + \dfrac{A_{c2}}{A_{p1}}\,[\,\epsilon_g + \epsilon_{pc}\,(1/2 - \epsilon_g)\,]} \tag{66}$$

## 1.6  Second-Stage Patch

Unlike the first-stage patch, conductive inputs to the second-stage patch cannot be neglected. The second-stage patch is not caged, but held in place by a low-conductivity support tube designed to survive the vibration environment (see Appendix II). Even with the patch caged , however, it would be necessary to include the conductive input from the in-orbit support and the electrical leads. This is a consequence of the temperature range covered.

Thermal coupling at the temperatures of the first-stage cone and patch is predominately radiative, i.e., depends on the difference in the fourth power of the temperatures. However, as the temperatures are lowered, thermal coupling becomes progressively more conductive, i.e., includes a term which depends on the difference in temperatures. This change in the nature of the thermal coupling with decreasing temperature holds in general for two-stage cryogenic devices (see, for example, R. B. Scott, "Cryogenic Engineering", D. Van Nostrand, 1959, p. 211).

The second-stage patch has a radiating area $A_{p2}$ which emits a power

$$(1 - \epsilon_{pc}^{(2)})\,\sigma A_{p2}\,T_{p2}{}^4$$

to cold space at a temperature $T_{p2}$. The factor $1 - \epsilon_{pc}^{(2)} = \rho_{pc}^{(2)}$ is the effective reflectivity of the second-stage cone structure for radiation going to space from the second-stage patch. This radiant power is balanced by the conductive and radiative thermal inputs to the second-stage. The conductive input is given by

$$K_c \, (T_{p1} - T_{p2})$$

where $K_c$ = conductive coupling coefficient between stages

$T_{p1}$ = temperature of first-stage patch

The radiative input is

$$\epsilon_{pc}^{(2)} \, \sigma A_{p2} \, (T_{p1}^{\,4} - T_{p2}^{\,4})$$

where $\epsilon_{pc}^{(2)}$ is the effective emissivity from the second-stage patch to the second-stage cone.

Equating the radiant power to cold space to the thermal inputs, we obtain the thermal balance equation for the second-stage patch,

$$(1 - \epsilon_{pc}^{(2)}) \, \sigma A_{p2} \, T_{p2}^{\,4} = K_c \, (T_{p1} - T_{p2}) + \epsilon_{pc}^{(2)} \, \sigma A_{p2} \, (T_{p1}^{\,4} - T_{p2}^{\,4}) \qquad (67)$$

This may be rewritten as

$$\sigma A_{p2} \, T_{p2}^{\,4} + K_c \, T_{p2} = \epsilon_{pc}^{(2)} \, \sigma A_{p2} \, T_{p1}^{\,4} + K_c \, T_{p1} \qquad \bullet \; (68)$$

## 1.7   Shielded First-Stage Cone

A simple earth shield by itself or in combination with a sun shield (see Sections 2.1.3 and 2.2.2) can be used to reduce the thermal load on the first-stage cone. The shield should lie outside the field of view of the patch and be attached to the outer cooler surface. The outer surface can be designed to attain a temperature below that of the main spacecraft structure (Section 1.7.2)

## 1.7.1   Thermal Balance Equation

With the earth shield in place, the thermal balance equation of the combined cone and cone end yields (see equation 45)

$$\sigma T_c^{\,4} = \cfrac{\alpha_{ce}^s \, W_s + \epsilon_{ce}^s \, W_e + \epsilon_{ct} \, \epsilon_t \, W_t + \alpha_g \, H_s \, \dfrac{A_m}{A_c} + \dfrac{A_d}{A_c} \, [\epsilon_s \, F_{ds} \, W_b + F_{de}^s \, (\epsilon_d \, W_e + \alpha_d \, W_s)}{\epsilon_d \, \dfrac{A_d}{A_c} + \epsilon_{cx} + \epsilon_{cp} \, (1 + \dfrac{1}{2} \, \dfrac{A_{c2}}{A_{p1}})}$$

$$\underline{+ \, \epsilon_d \cdot \epsilon_t \, F_{dt} \, W_t + \alpha_d \, H_s \, ]} \qquad (69)$$

where $F_{dt}$ = view factor from cone end to earth shield

$\epsilon_t$ = emissivity of shield

33

$\epsilon_{ct}$ = effective absorptivity of cone for shield radiation

$W_t$ = blackbody emittance of shield

The superscript s denotes that a (partial) shield is between the cone and earth; the absorptivity values are then for that part of the earth visible from the center of the cone mouth with the shield in place.

Equation (69) is based on the fact that there are no multiple reflection effects between the cone and shield to enhance absorption. That is, no radiation emitted by the shield is first reflected off the cone end and then off the shield so as to return to the end. This is true as long as the shield is specularly reflecting.

The effective cone absorptivity for shield infrared is given by

$$\epsilon_{ct} = \frac{A_m}{A_c} \Sigma \epsilon_n F_{m-tn} \tag{70}$$

where $\epsilon_n$ = $1 - (1 - \epsilon_t)^n$ = absorptivity produced by n cone wall reflections

$F_{m-tn}$ = view factor from cone mouth to sub-area of shield whose radiation is reflected n times at cone wall upon entering cone mouth

This is the same form of equation as that for the effective cone absorptivities for earth radiation (Section 1.4.1.2). It can be used when no shield emission reaches the cone mouth after (specular) reflection at the shield wall.

Similarly, the absorptivity of the cone for earth radiation becomes

$$a_{ce}^s = \frac{A_m}{A_c} \Sigma a_n F_{m-Aen}^{vis.} \tag{71}$$

where $a_n = 1 - (1 - a)^n$ = absorptivity produced by n reflections off a cone of surface absorptivity a

$F_{m-Aen}^{vis.}$ = view factor from cone mouth to visible part of earth whose radiation is reflected n times in the cone

### 1.7.2 Outer Cooler Surface

The radiant heat loads on the outside surface of the two-stage radiant cooler together with the infrared emissivity and solar absorptivity of the surface determine the temperature of the surface. Because of the large thermal time constants of components between the outside surface and the first-stage patch, only average values of the thermal loads need to be considered.

34

The outside of the two-stage cooler is sketched in Figure 8. Side 1 faces the radiometer baseplate, side 2 views the earth and cold space, and sides 3 and 4 view the earth, radiometer baseplate, and cold space. In addition, sides 3 and 4 are exposed to direct sunlight during part of an orbit. The spacecraft is assumed to be earth-oriented with the cooler on the earth side and to be travelling a circular, sun-synchronous polar orbit. The fact that some direct sunlight falls on side 2 in the vicinity of the poles is offset by assuming the spacecraft provides no daytime shading of sides 3 and 4. In a double-ended cooler (Section 2.1), sides 5 and 6 are the openings to the first-stage cone; thermal flux entering these areas loads the cone and not the outer surface. In a single-ended cooler (Section 2.2), only side 6 is a cone opening. Side 5 is then assumed to view other instruments at close range; it is therefore included in the thermal balance equation, but has zero area for a double-ended cooler.

The contribution of the inward-facing surfaces of the outer cooler sides is negligible compared to the power absorbed and radiated by the outward-facing surfaces. The inward surfaces are thermally isolated from the areas they face (the first-stage cone) by multilayer insulation. Finally, it is assumed that all the outer surfaces, areas 1 through 5, are in good thermal contact (i.e., have high thermal conductivity bases which are efficiently joined), so that the outer cooler surface is isothermal.

The net radiant flux absorbed by the horizontal area $A_1$ facing the radiometer baseplate is

$$A_1 \ \frac{\epsilon_1}{2} \ (W_b - \sigma T_s^4)$$

assuming that the two surfaces are plane-parallel and both covered with a material of emissivity $\epsilon_1$. $W_b$ is the blackbody emittance of the radiometer baseplate (spacecraft) and $T_s$ the temperature of the outer cooler surface.

We will neglect the conductive thermal input to $A_1$ from the baseplate. By careful design, it can be made less than the above radiative input, which would increase $T_s$ by about 1 percent. This is less than the variation in calculated temperature produced by the uncertainty in the $\alpha/\epsilon$ ratio of sides 2, 3, and 4.

Similarly, the net radiant flux absorbed by the vertical area $A_5$ is

$$A_5 \ \epsilon_1 \ (W_b - \sigma T_s^4)$$

when the surface has the same emissivity as $A_1$. This assumes $A_5$ faces effectively black surfaces at the baseplate temperature.
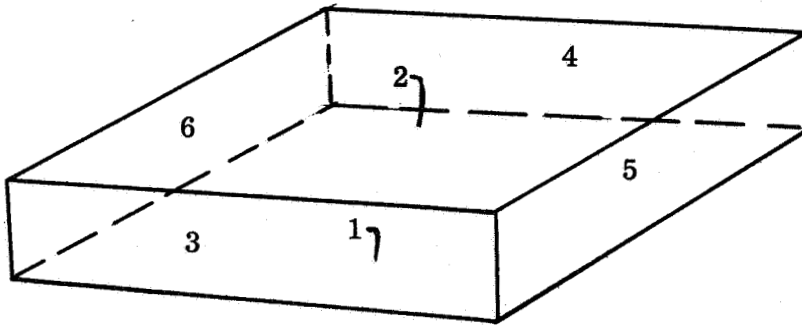
Figure 8   Outside of Two-Stage Cooler

The radiant flux absorbed by side 2 is given by

$$\epsilon_2 \, A_1 \, F_{2e} \, W_e + \alpha_2 \, A_1 \, F_{2e} \, W_s$$

where $\epsilon_2$ = emissivity of sides 2, 3, and 4

$A_1$ = $A_2$ = area of side 2

$\alpha_2$ = solar absorptivity of sides 2, 3, and 4

$F_{2e}$ = view factor from area 2 to earth

$W_e$ = average infrared emittance of the earth

$W_s$ = average equivalent earthshine (reflected sunlight) emittance of the earth.

The view factor $F_{ij}$ from surface i to surface j is the fraction of radiation emitted by i that strikes j. Thus the radiant infrared flux emitted by the earth which strikes the area $A_2$ is $A_e F_{e2} W_e$ where $A_e$ is the area of the earth's surface which can be seen from area 2. However, (M. Jakob, "Heat Transfer", Vol. II, Wiley, 1957, p. 9) $A_e F_{e2} = A_2 F_{2e}$ for diffuse emitters. Since we can ignore multiple reflections between the earth and side 2, the infrared earth flux absorbed by side 2 is $\epsilon_2 A_2 F_{2e} W_e$.

Finally, the radiant flux absorbed by sides 3 and 4 is

$$2 \, A_3 \left( \epsilon_2 \, F_{3e} \, W_e + \alpha_2 \, F_{3e} \, W_s + \epsilon_2 \, F_{3b} \, W_b + \frac{S_o \, \alpha_2}{2 \, \pi} \cdot \sin \phi_s \right)$$

where $F_{3e}$ = view factor to earth from side 3

$F_{3b}$ = view factor to radiometer baseplate from side 3

$S_o$ = solar constant = 0.14 watts/cm$^2$

$\phi_s$ = angle between orbit normal and vector to sun

The factor $S_o \, \alpha_2 / 2 \pi$ is the average direct solar irradiance absorbed by side 3 (or side 4) in a high-noon ($\phi_s$ = 90$^o$) sun-synchronous, near-polar orbit. It was calculated from

$$\alpha_2 \, S_o \cdot \frac{1}{4} \cdot \frac{2}{\pi} \int_0^{\pi/2} \cos \theta \cdot d\theta = \frac{\alpha_2 \, S_o}{2 \, \pi} \qquad (72)$$

It is assumed that the spacecraft shades $A_3$ during the nighttime portion of the orbit, but not the daytime. The area $A_3$ then intercepts sunlight directly one-quarter of the time. The remaining accounts for the fact that the irradiance is proportional to the fraction of $A_3$ projected in the direction of the sun, and gives an average value for this factor.

The angle $\theta$ is measured in the plane of the orbit from the normal to the side to the intersection line of the orbital plane and the ecliptic. The cosine of the angle between the normal to the side and the vector to the sun is then $\cos\theta \cdot \sin\phi_s$.

Equating the absorbed power to the power emitted by sides 2, 3, and 4, we obtain the thermal balance equation for the outer surface of the two stage cooler

$$\sigma A_1 \, \epsilon_2 \, T_s^{\,4} + 2 \, \sigma A_3 \, \epsilon_2 \, T_s^{\,4} = A_1 \, \frac{\epsilon_1}{2} \, (W_b - \sigma T_s^{\,4}) + A_5 \cdot \epsilon_1 \, (W_b - \sigma T_s^{\,4})$$

$$+ \; \epsilon_2 \, A_1 \, F_{2e} \, W_e + \alpha_2 \, A_1 \, F_{2e} \, W_s$$

$$+ \; 2 A_3 \, (\epsilon_2 \, F_{3e} \, W_e + \alpha_2 \, F_{3e} \, W_s + \epsilon_2 \, F_{3b} \, W_b + \frac{S_0 \, \alpha_2}{2 \, \pi} \; \sin\phi_s) \quad (73)$$

Dividing through by $A_3 \, \epsilon_2$ and arranging in terms of emittances, we obtain

$$\sigma T_s^{\,4} \, [2 + \frac{A_1}{A_3} + \frac{(A_1 + 2A_5) \, \epsilon_1}{2 \, A_3 \, \epsilon_2}] = W_b \, [2 \, F_{3b} + \frac{(A_1 + 2A_5) \, \epsilon_1}{2 \, A_3 \, \epsilon_2}]$$

$$+ \; W_e \, (2 \, F_{3e} + \frac{A_1}{A_3} \, F_{2e}) + \frac{\alpha_2}{\epsilon_2} \, W_s \, (2 \, F_{3e} + \frac{A_1}{A_3} \, F_{2e})$$

$$+ \; \frac{\alpha_2}{\epsilon_2} \cdot \frac{S_0}{\pi} \cdot \sin\phi_s \quad\quad\quad (74)$$

In general, sides 1 and 5 will have a low emissivity and sides 2, 3, and 4 a low $\alpha/\epsilon$ ratio.

## 2.0   SPECIFIC DESIGNS

The general procedures of Section 1.0 were applied to the design and analysis of two specific two-stage radiant coolers.  The coolers are for use on an earth-oriented spacecraft in a Nimbus-type orbit.  The cone surface is assumed to have a maximum emissivity of 0.086 and a minimum of 0.02; the corresponding solar absorptivities are 0.22 and 0.183.  The first design is for a double-ended cooler (i.e., the patches radiate to space from both sides) at a minimum altitude of 600 n mi and a maximum orbit plane to sun angle of 11 degrees.  The second design is for a single-ended cooler at 500 n mi and a maximum sun angle of 20 degrees.

## 2.1   Double-Ended Cooler

A double-ended two-stage radiant cooler is shown in Figure 9.  The cooler is designed for operation on an earth-oriented spacecraft in circular orbit at 750 nautical miles altitude.  The actual design was carried out for a 600 nautical mile altitude to allow for altitude errors and variations and for spacecraft wobble.  The cone structures limit the look angles of the black radiant patches so the only external object they see is cold space.  The cones are coated with a low emissivity surface for high reflectivity and low thermal coupling.  A pair of earth shields (only one is shown) may be added (Section 2.1.4) to reduce the thermal loading of the first-stage cone by earth radiation.

The cooler is separated from the spacecraft by supports (not shown in Figure 9) of low thermal conductivity material connected to the outer cooler surface (Section 2.1.2).  The first-stage cone and outer cooler surface (outer box) are also connected by low-conductivity tubes to allow thermal isolation of the two structures by multilayer insulation.

The outer surfaces of the cooler which receive direct sunlight are coated with a material of low solar absorptivity and high infrared emissivity to obtain as low an outer surface temperature as possible (Section 2.1.2).  The outer surface facing the spacecraft (radiometer base) is covered with a material of low infrared emissivity.

The first-stage patch is mechanically held during spacecraft launch and supported in orbit by means of a low thermal conductivity tube (Section 2.1.5).  The second-stage patch is supported from the outer patch by a similar tube, which is relatively stronger in order to survive the vibrational environment.  The supports are not shown in Figure 9.

Earth Shield

Connection To Primary (Scanner) Casting

Relay Optics Housing

First-Stage Patch

First-Stage Cone

Outer Surface

Second-Stage Cone

First-Stage Cone

Cone End

Multi-Layer Insulation
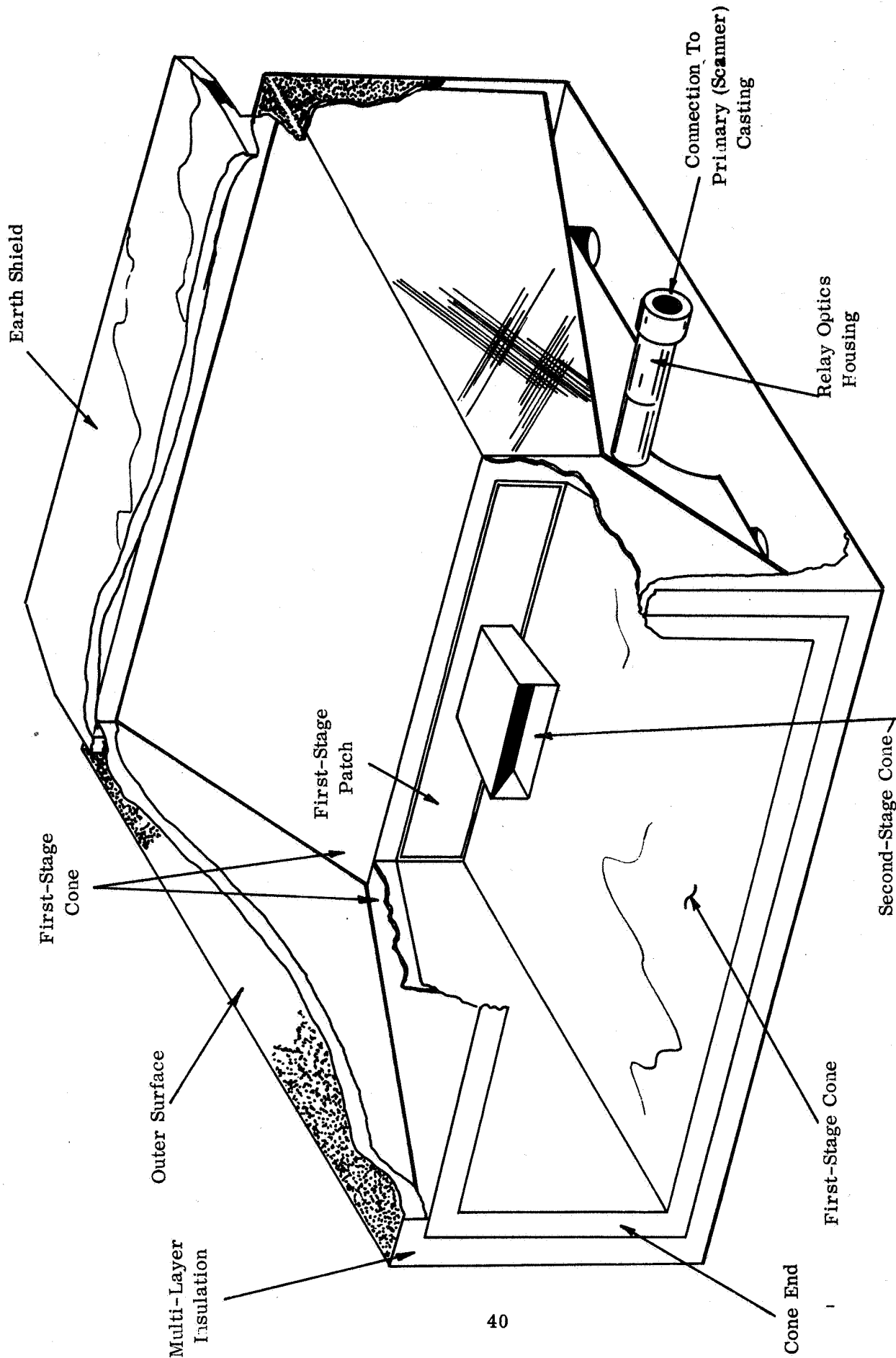
Figure 9  Double-Ended Radiant Cooler

40

The relay optics (Section 2.1.7) is designed for a low numerical aperture (small convergence angle or speed) through the first-stage cone to keep radiant coupling through the optical opening to a minimum. The use of a cooled interference filter mounted on the first-stage patch further reduces this source of thermal loading. Electrical leads are run through the centers of the support tubes, thus eliminating additional openings through the cone structures. The detector cell is mounted directly on the second-stage patch, so there is no cell housing separated from the patch. A separated housing tends to increase radiant coupling and to create vibrational problems.

The cooler was designed for a Nimbus-type orbit at an orbit normal to sun angle of 79 degrees. For a cone surface emissivity range of 0.02 to 0.086, the design equations predict a temperature range of about 86 to 112 degrees K for the first-stage patch and 64 to 80 degrees K for the second-stage. These results are for an attached earth shield (Section 2.1.4) at the higher emissivity.

## 2.1.1 Basic Design

The basic dimensions and cone angles of the double-ended two-stage radiant cooler are given in Figures 10 and 11. The dotted lines in each figure shows the vertical section of the stage and the solid lines the horizontal section. The cone angles in the second stage were decreased from their original values of 11 degrees (vertical) and 18 degrees (horizontal) in order to reduce thermal loading on the first-stage patch and second-stage cone by external sources just beyond the field-of-view of the patch. In addition, the total length of the second-stage cone was increased to 6.04 inches in the constructed model (Section 4.0) to allow for the non-zero (0.32 inch) patch thickness.

The geometry of the first stage was determined by minimizing the cone length to patch dimension ratios subject to a maximum vertical view angle of 31.5 degrees (angle between patch normal and tangent to earth from 600 nautical miles) and a maximum horizontal view angle of 60 degrees (procedure of Section 1.2). This set the vertical cone angle of the first stage at 13.5 degrees, the horizontal cone angle at 18 degrees, and the patch aspect ratio at 6.13.

The look angle of the second stage was initially set so that patch rays from the center of the cone opening in a cone 2.6 inches long did not strike the cone of the first stage in the vertical and horizontal planes. The patch aspect ratio was then determined by minimizing the cone length to patch dimension ratio in the vertical and horizontal planes subject to the above look angle constraint. This set the vertical cone angle of the second stage at 11 degrees, the horizontal cone angle at 18 degrees, and the patch aspect ratio at 6.98. The cone length of the second stage was then increased until the estimated increase in the second-stage temperature produced by radiant coupling between the patch and the first-stage
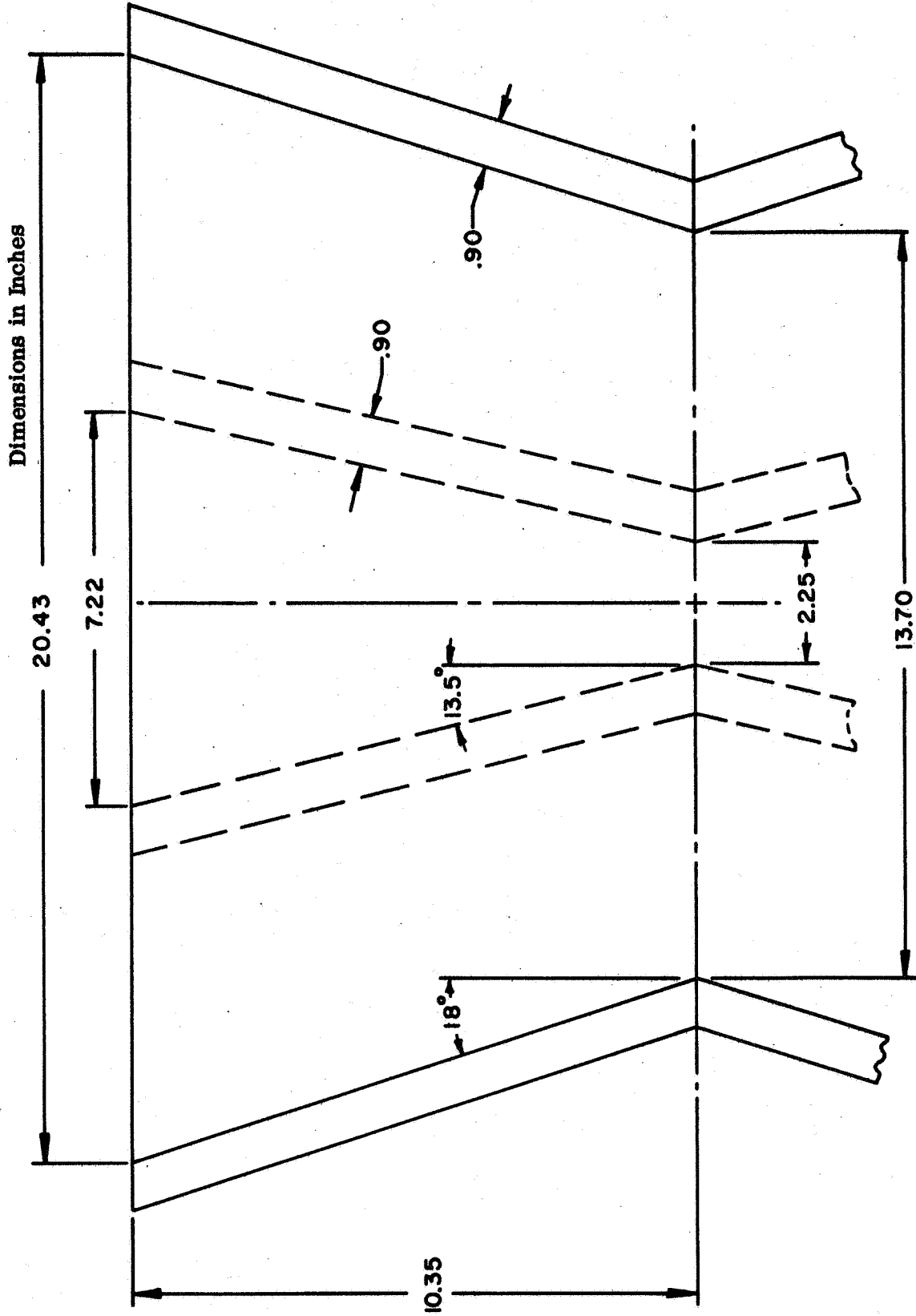
Figure 10  First-Stage Basic Design

Dimensions in Inches

20.43

7.22

2.25

13.70

13.5°

18°

.90

.90

10.35
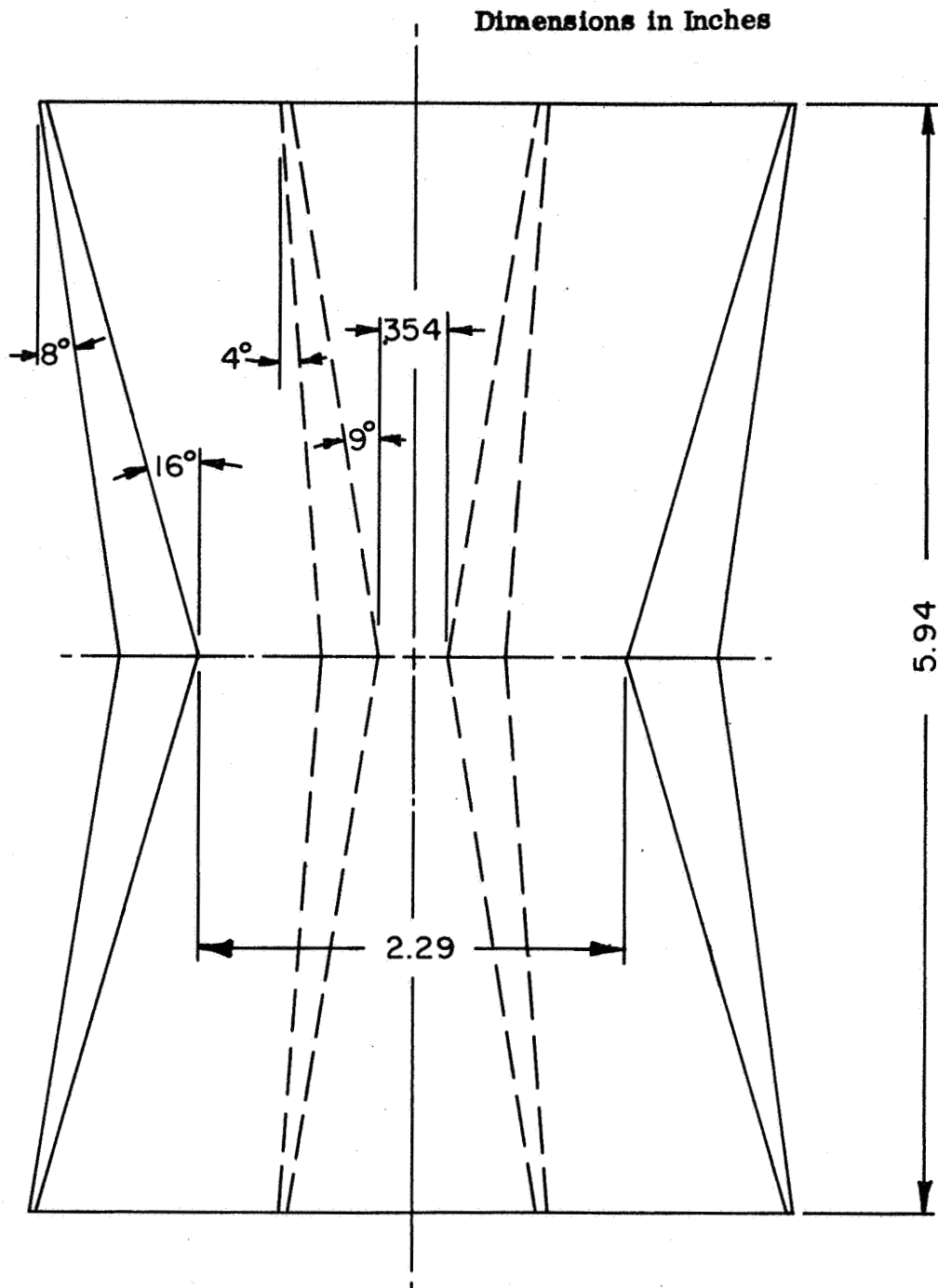
Figure 11   Second-Stage Basic Design

cone was reduced to the order of 1 degree K. This was done by considering all rays in the vertical and horizontal planes and not just those passing through the center of the end of the cone. The resultant cone length was 2.97 inches, which reduced the view factor (fraction of emitted patch radiation striking the first-stage cone) to zero in the horizontal plane and 0.025 in the vertical plane for a patch of zero thickness. After increasing the cone length, the length to patch dimension ratios are no longer minima, but they should be close to minima.

The second stage of the two-stage radiant cooler was then modified to reduce the loading on the first stage by radiant flux incident at angles beyond the maximum look angles of the first-stage patch. Such flux can be trapped between the cone for the first stage and the cone for the second stage over a small angular range starting with the maximum first-stage look angle. If the inside angle of the first-stage cone equals the outside angle of the second-stage cone in the vertical and horizontal planes, the two cones form radiant condensers to the first-stage patch in these planes, that is, any flux reflected between the two cones eventually strikes the first-stage patch. To reduce this thermal loading, the inside angles of the second-stage cone were reduced subject to the constraints that the second-stage patch area and cone length remain unchanged, and the small view factor ($\sim 0.025$) between the second-stage patch and first-stage cone be preserved. The outside angles of the second-stage cone were made smaller than the inside angles so that no radiant flux incident between cones at angles greater than the maximum look angle reaches the first-stage patch in either the vertical or horizontal planes. It was found that the cone angles in the vertical and horizontal planes could be varied by about ± 2 degrees with little or no change in the view factor. The inside cone angle in the vertical plane was therefore reduced from 11 degrees to 9 degrees and in the horizontal plane, from 18 degrees to 16 degrees. The outside cone angle was set at 4 degrees in the vertical plane and 8 degrees in the horizontal plane.

In the design shown, the determination of the second stage cone was carried out after fixing the size of the first stage. Specifically, the cone length of the first-stage was set at 10.35 inches (total cooler length of 20.7 inches).

2.1.2   Outer Cooler Surface

The temperature of the outer cooler surface can be determined from equation (74) in Section 1.7.2. The constructed models have an outer surface opening of 12.6 inches by 25.7 inches at the cone mouth ends of the cooler and a length of 20.7 inches. The area ratio is then

$$\frac{A_1}{A_3} = 2.04 \tag{75}$$

Since there is no outer surface perpendicular to the cone axis in a double-ended cooler, $A_5$ is zero.

44

The view factors to earth for a spacecraft nadir to earth tangent line angle of $\varphi_0$ are given by

$$F_{3e} = \frac{1}{\pi} (\varphi_0 - \sin \varphi_0 \cdot \cos \varphi_0) \qquad (76)$$

$$F_{2e} = \sin^2 \varphi_0 \qquad (77)$$

The first equation is taken from equation (60), Section 1.4.1.2, and the second is the view factor from the spacecraft to the circle formed by the earth tangent lines. At an altitude of 600 n mi, $\varphi_0$ is 58.5 degrees, and

$$F_{3e} = 0.1832$$

$$F_{2e} = 0.7270$$

We will assume that the view factor, $F_{3b}$, from a vertical outer surface to the spacecraft is 0.3.

From Appendix I, the equivalent earth emittances are

$$W_s = 1.65 \times 10^{-2} \text{ watts/cm}^2$$

$$W_e = 2.1 \times 10^{-2} \text{ watts/cm}^2$$

The values of $W_s$ is for a 600 n mi altitude ($\vartheta_0 = \frac{\pi}{2} - \varphi_0 = 31.5$ degrees) and an orbit normal to sun angle, $\phi_s$, of 90 degrees. For a black spacecraft at 35 degrees C, we also have

$$W_b = 5.1 \times 10^{-2} \text{ watts/cm}^2$$

The emissivity ratio, $\epsilon_1/\epsilon_2$, will be taken as 0.1 and the solar constant, $S_0$ as $14 \times 10^{-2}$ watts/cm$^2$. The temperature, $T_s$, of the outer surface of a double-ended radiant cooler is then the solution to the equation

$$4.142 \; \sigma T_s^4 = 7.464 \times 10^{-2} + 7.508 \times 10^{-2} \; \frac{\alpha_2}{\epsilon_2}$$

where $\alpha_2/\epsilon_2$ is the ratio for sides 2, 3, and 4. The outer surface temperature is listed in Table 3 for three values of $\alpha_2/\epsilon_2$.

45

Table 3

Temperature of Outer Cooler Surface

| $\alpha_2/\epsilon_2$ | $T_S$ ($^O$K) |
|---|---|
| 0.1 | 243 |
| 0.2 | 249 |
| 0.3 | 254 |

The outer cooler surface is mechanically connected to the spacecraft base and to the primary (scanner) casting. The connection to the base is by means of four fiberglas epoxy tubes. The housing containing the relay optics is connected to the outer cooler surface, which, in turn, is connected to the primary casting by a fiberglas epoxy spacer.

At a temperature $T_S$ the outer surface of the cooler radiates (and absorbs) a total power of

$$\Phi_S = 4.142 \; \epsilon_2 \; A_3 \; \sigma T_S^4 \tag{78}$$

where $\epsilon_2$ = emissivity of outer surfaces receiving sunlight

$A_3$ = area of a vertical outer surface

For $T_S$ = 249 degrees K

$\epsilon_2$ = 0.9

$A_3$ = 1683 cm$^2$

equation (78) yields

$$\Phi_S = 136 \text{ watts} \tag{79}$$

The outer surface reaches a temperature of 249 degrees K with the radiometer base at 308 degrees K. The temperature difference between the outer surface and the base is then 59 degrees K.

If we allow the supports to conduct 4 percent of the above power to the outer surface this will increase the temperature of the outer surface by about 1 percent or 2.5 degrees K. If there are four support tubes, each will then conduct 1.36 watts and have a cross-sectional area given by

$$A_1 = \frac{1.36\, \ell_1}{K\, \Delta T_1} \tag{80}$$

where $\ell_1$ = length of support tube

$K$ = thermal conductivity of tube material

$\Delta T_1$ = temperature drop from base to outer surface

If the tube is made of fiberglas epoxy (Synthane G-10), $K = 7 \times 10^{-4}$ cals/sec$^o$C cm = $7.46 \times 10^{-3}$ watt/in$^o$C (eem file system, sec. 3100, 3200, Synthane Technical Plastics, p. 7). The cross-sectional area for $\ell_1 = 1$ inch and $\Delta T_1 = 59$ degrees C is then

$$A_1 = 3.09 \text{ in}^2 \tag{81}$$

One can therefore use, for example, four rods of 4 inch outside diameter and 3.5 inch inside diameter directly connected to the base and outer cooler surface.

If the scanner head attains a maximum temperature of 25 degrees C with the base at 35 degrees C, the temperature drop across the fiberglas epoxy spacer between the scanner head and outer cooler surface will be 50 degrees C. If we allow 0.54 watt of conduction through a 1 inch thick spacer, its allowable cross-sectional area is 1.45 in$^2$. This is a connection of 2 inches outside diameter and quarter-inch wall. The spacer then increases the thermal load on the outer cooler surface by only 0.4 percent and its temperature by about 0.1 percent.

### 2.1.3  First-Stage Cone

The thermal balance equation for the first-stage cone without a cone end is given by (equation 45, Section 1.4.1)

$$A_c\, \sigma T_c^{\,4}\, [\epsilon_{cx} + \epsilon_{cp}(1 + \frac{1}{2}\, \frac{A_{c2}}{A_{p1}})] = A_c\, (\epsilon_{ce} W_e + \alpha_{ce} W_s + \frac{A_m}{A_c}\, \alpha_g H_s) \tag{82}$$

The values of $W_s$ and $W_e$ are given in Section 2.1.2. The value of average solar irradiance of the cone mouth over an orbit is given by

$$H_s = \frac{1}{4} \cdot S_o \cdot \cos \phi_s \tag{83}$$

for an orbit in the vicinity of a high noon. It is assumed that the spacecraft shades the cone mouth during the nighttime portion of the orbit, so the cone is in sunlight one-half the time. In addition, only one cone mouth is exposed at a given time, which accounts for another factor of one-half. For $\phi_s$ equal to 79 degrees

$$H_s = 6.678 \times 10^{-3} \text{ watts/cm}^2$$

47

The values of effective emissivities and effective absorptivities were determined for cone surface emissivities of 0.086 and 0.02 and for corresponding solar absorptivities of 0.22 and 0.183.

The effective patch-to-cone emissivity was calculated for the horizontal and vertical planes of the first stage of the basic cooler described in Section 2.1.1 using the procedure outlined in Section 1.3.1. This procedure assumes right circular cones having the geometry in the plane and that the patch area is concentrated at its center (i.e., is strictly true for rays from the center of the patch). The view factors, $f_n$, obtained during this calculation are listed in Table 4.

Table 4

View Factors for Calculation of Patch-to-Cone Emissivity $f_n$

| n | Vertical | Horizontal |
|---|----------|------------|
| 0 | 0.112 | 0.494 |
| 1 | 0.569 | 0.506 |
| 2 | 0.319 | 0 |

Neglecting the presence of the second-stage cone, radiation from the patch center requires no more than two reflections off the cone walls to go to cold space in the vertical plane and no more than one in the horizontal plane. The average coated surface (cone, back of patch, and cylinder) emissivity, $\epsilon_g$, of the single-stage cooler is 0.086. Using this value of surface emissivity, the patch-to-cone effective emissivity values are (equation 9, Section 1.3.1).

$\epsilon_{pc}$ (horizontal) = 0.044

$\epsilon_{pc}$ (vertical) = 0.103

And the average patch-to-cone emissivity is 0.0735. For

$$\frac{A_p}{A_c} = \frac{2.25 \times 13.70}{467} = 0.066$$

(dimensions of cooler described Section 2.1.1), the average effective cone-to-patch emissivity is, from equation (40), Section 1.4.1

$\epsilon_{cp}$ = 0.00485

48

Since the calculations of the view factors, $f_n$, were based on the geometry in the absence of a second-stage, the first-stage patch area $(A_p)$ used is the value without a second stage.

The equation for the effective external emissivity, $\epsilon_{cx}$, is derived in Section 1.4.1.1. The result is

$$\epsilon_{cx} = \frac{A_m}{A_c} \; [1 - \sum_{n=0} f_n' \; (1 - \epsilon_g)^n] \tag{84}$$

where $A_m$ = area of cone mouth

$f_n'$ = view factor from the cone mouth to the cone area last intercepted by rays from the cone requiring n-1 reflections at the cone wall to go out.

The view factors, $f_n'$, from the center of the cone mouth are given in Table 5 for right circular cones having the dimensions of the vertical and horizontal cooler planes described in Section 2.1.1.

Table 5

View Factors for Calculation of Cone External Emissivity

| n | $f_n'$ Vertical | Horizontal |
|---|---|---|
| 0 | 0.0116 | 0.306 |
| 1 | 0.1597 | 0.348 |
| 2 | 0.2189 | 0.308 |
| 3 | 0.238 | 0.038 |
| 4 | 0.229 | 0 |
| 5 | 0.1428 | 0 |

For a surface emissivity, $\epsilon_g$, of 0.086 and for $A_m/A_c$ equal to 0.316 (cooler dimensions in Section 2.1.1), the effective cone external emissivities are then

$\epsilon_{cx}$ (vertical) = 0.0718

$\epsilon_{cx}$ (horizontal) = 0.0285

and the average external emissivity is 0.05015.

49

The expression for the effective absorptivity of the cone mouth for earth radiation is derived in Section 1.4.1.2. The result is

$$a_{me} = \sum_{n=0} a_n F_m\text{-}A_{en} \qquad (85)$$

where $a_n$ = the absorptivity for n cone-wall reflections

$F_m\text{-}A_{en}$ = view factor from the cone mouth to the earth area whose radiation is reflected n times at the cone walls

The values of $F_m\text{-}A_{en}$ are given in Table 6 for a truncated right circular cone having the geometry of the vertical cooler plane (Section 2.1.1) together with

Table 6

Parameters for Calculation of Cone Mouth
Absorptivity for Earth Radiation

| n | $F_m\text{-}A_{en}$ | $a_n$ (ir) | $a_n$ (solar) |
|---|---|---|---|
| 1 | 0.03285 | 0.086 | 0.22 |
| 2 | 0.0555 | 0.1646 | 0.3916 |
| 3 | 0.06285 | 0.2364 | 0.5255 |
| 4 | 0.0320 | 0.3021 | 0.6299 |

the values of $a_n$ for earth infrared and earthshine. The cone surface is assumed to have an infrared absorptivity (emissivity) of 0.086 and a solar absorptivity of 0.22. Using the parameters listed in Table 6 in equation (85), we obtain

$$a_{me} \text{ (ir)} = \epsilon_{me} = 0.0365$$

$$a_{me} \text{ (solar)} = \alpha_{me} = 0.0822$$

And the effective cone absorptivities are, for an area ratio $A_m/A_c = 0.316$.

$$\epsilon_{ce} = 0.0115$$
vertical values
$$\alpha_{ce} = 0.0260$$

The gold emissivity value of 0.086 is an estimate of the average value for all gold-coated surfaces in the single-stage, 200 degrees K radiant cooler. This represents a worst case; removal of the cylindrical structure and the gold-coating of one side of the radiant patch should decrease this value. In order to represent a "best" case and give a range of possible temperatures, we have selected the values of $\epsilon_g = 0.02$ for infrared emissivity and $\alpha_g = 0.183$ for solar absorptivity of the cone surfaces. These values were measured for evaporated gold by W. B. Fussell, J. J. Triolo, and J. H. Henniger (article 11 in NASA SP-31, "Measurement of Thermal Radiation Properties of Solids", ed. by J. C. Richmond, 1963). The effective emissivity and absorptivity values necessary to calculate the temperatures of the first-stage cone and patch are listed in Table 7 for these values of emissivity and absorptivity.

Table 7

Effective Emissivities and Absorptivities
for $\epsilon_g = 0.02$ and $\alpha_g = 0.183$

|  | Vertical | Horizontal | Average |
|---|---|---|---|
| $\epsilon_{cp}$ | 0.00156 | 0.000651 | 0.0011 |
| $\epsilon_{cx}$ | 0.01812 | 0.00676 | 0.00940 |
| $\epsilon_{ce}$ | 0.00285 | – | – |
| $\alpha_{ce}$ | 0.0224 | – | – |
| $\epsilon_{pc}$ | 0.024 | 0.010 | 0.017 |

The value of $A_m/A_c$ is 0.316 and of $A_{c2}/A_1$, 0.810 (value for constructed models). The thermal balance equation (82) for the cone without an end is then

$$5.696 \times 10^{-2} A_c \, \sigma T_c^4 = 11.348 \times 10^{-4} A_c \tag{86}$$

for $\epsilon_g = 0.086$ and $\alpha_g = 0.22$. And for $\epsilon_g = 0.02$ and $\alpha_g = 0,183$, it is

$$1.095 \times 10^{-2} A_c \, \sigma T_c^4 = 8.156 \times 10^{-4} A_c \tag{87}$$

The thermal balance equation of the cone end by itself is given by equation (62) in Section 1.4.2,

$$\epsilon_d A_d \, \sigma T_d^4 = A_d \, [\epsilon_s F_{ds} W_b + F_{de} \, (\epsilon_d W_e + \alpha_d W_s) + \alpha_d H_s] \tag{88}$$

51

The view factor from the cone end to earth, $F_{de}$, is the same as from a vertical cooler surface (Section 2.12) or 0.1832 from a 600 n mi altitude. Then for

$$\epsilon_s = 0.1$$

$$\epsilon_d = 0.9$$

$$\alpha_d = 0.18$$

$$F_{ds} = 0.3$$

$$W_b = 5.1 \times 10^{-2} \text{ watts/cm}^2 \text{ (spacecraft at 35 degrees C)}$$

equation (88) becomes

$$0.9 A_d \sigma T_d^4 = 6.7386 \times 10^{-3} A_d \tag{89}$$

for an orbit normal to sun angle of 79 degrees.

Adding equation (89) to equations (86) and (87), setting $T_d$ equal to $T_c$, and dividing by $A_c$, we obtain for the combined cone and cone end

$$(5.696 \times 10^{-2} + 0.9 \frac{A_d}{A_c}) \sigma T_c^4 = 11.348 \times 10^{-4} + 67.386 \times 10^{-4} \frac{A_d}{A_c},$$

$$\epsilon_g = 0.086 \text{ and } \alpha_g = 0.22 \tag{90}$$

$$(1.095 \times 10^{-2} + 0.9 \frac{A_d}{A_c}) \sigma T_c^4 = 8.156 \times 10^{-4} + 67.386 \times 10^{-4} \frac{A_d}{A_c},$$

$$\epsilon_g = 0.02 \text{ and } \alpha_g = 0.183 \tag{91}$$

For the cone dimensions given in Section 2.1.2 and for a 1-1/16 inch wide cone end, $A_d/A_c$ equals 0.1356. Equations (90) and (91) then yield

$$\sigma T_c^4 = 1.144 \times 10^{-2} \text{ watts/cm}^2$$

$$T_c = 212^o K, \ \epsilon_g = 0.086 \text{ and } \alpha_g = 0.22 \tag{92}$$

and

$$\sigma T_c = 1.300 \times 10^{-2} \text{ watts/cm}^2$$

$$T_c = 219^o K, \ \epsilon_g = 0.02 \text{ and } \alpha_g = 0.183 \tag{93}$$

## 2.1.4   <u>Earth Shield</u>

      A simple earth shield is shown in Figure 12; it is attached to the outer surface. The radiant power from the shield that is absorbed in the walls of the first-stage cone is negligible compared to the power from the earth absorbed in the walls. The shield reduces the cone temperature by 9.5 degrees K for a cone surface emissivity of 0.086 and solar absorptivity of 0.22. The shield was designed for the center of the cone mouth; it is assumed that the shielding of the center is equal to the average over the entire cone mouth.

      In order to determine the cone temperature from equation (69) in Section 1.7.1, we need the partial view factors from the cone mouth to the earth with the shield in place. With these view factors, we can evaluate the effective cone absorptivity for shield infrared from equation (70) and the absorptivities for earth radiations from equation (71). The shield is designed so that the view factor from the cone end to the shield (assumed equal to that from the center of the cone mouth) is equal to the decrease in view factor to the earth.

      The earth shield shown in Figure 12 was designed to block all radiation to the cone mouth from the sub-area 1 and part of the radiation from 2. No radiation from 3 and 4 is blocked. This is shown in Figure 12 by the shadow cast unto the semicircle (equivalent earth) by the shield from the center of the cone mouth. With the shield in place the view factor for $n = 1$ is therefore zero, while it is unchanged for $n = 3$ and $n = 4$ (values given in Section 2.1.3). It therefore remains to calculate the view factor for $n = 2$. For $n = 2$ the earth shield changes the upper limit of the polar angle in equation (55), Section 1.4.1.2. This equation gives the partial view factor, $F_m - A_{en}$, in terms of spherical coordinates at the center of the cone mouth, with the pole along the normal to the mouth. The polar angle is $\vartheta$ and the azimuthal angle $\varphi$. With the shield in place the upper limit of the polar angle for $n = 2$ is not $\vartheta_1$ but the angle, $\vartheta_s$, determined by the straight line projected across the semicircle (See Figure 12).

      The view factor from the cone mouth to the visible part of earth whose radiation is reflected twice in the cone is then

$$F_{m-Ae2}^{vis.} = \frac{2}{\pi} \int_0^{\varphi_2} \int_{\vartheta_2}^{\vartheta_s} \sin\vartheta \cos\vartheta \, d\vartheta \, d\varphi + \frac{2}{\pi} \int_{\varphi_2}^{\varphi_1} \int_{\vartheta(\varphi)}^{\vartheta_s} \sin\vartheta \cos\vartheta \, d\vartheta \, d\varphi$$

Integrating with respect to the polar angle,

$$F_{m-Ae2}^{vis.} = \frac{1}{\pi} \int_0^{\varphi_2} (\sin^2\vartheta_s - \sin^2\vartheta_2) \, d\varphi + \frac{1}{\pi} \int_{\varphi_2}^{\varphi_1} (\sin^2\vartheta_s - \sin^2\vartheta(\varphi)) \, d\varphi \quad (94)$$

Shield may be located 2.18 inches below the cone mouth.
It then extends 3.55 inches horizontally.

Center of Cone Mouth

$\varphi_0'$

$\varphi$

Earth Shield or
Its Projection

$a \cdot \sec \varphi$

$a$

$90^o$

$90^o$

$a \tan \varphi_0'$

$\vartheta$

$s$

$a \tan \varphi_0'$

Center of Cone Mouth

c

Earth Shield

n = 1

n = 2

n = 3

n = 4
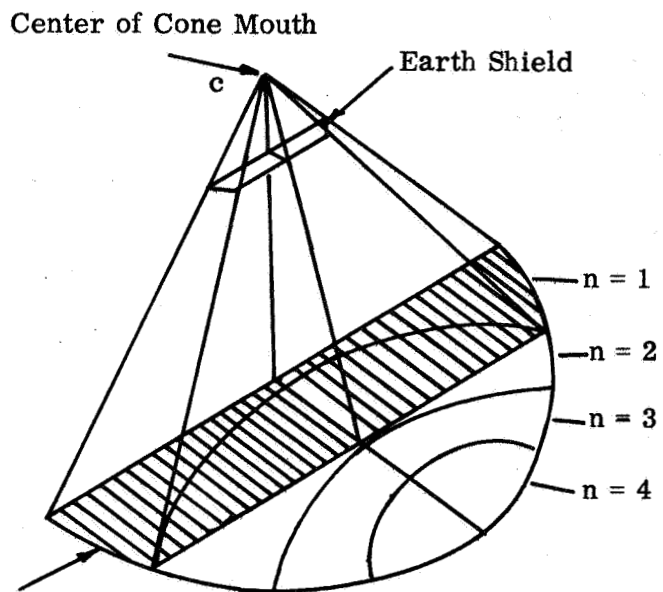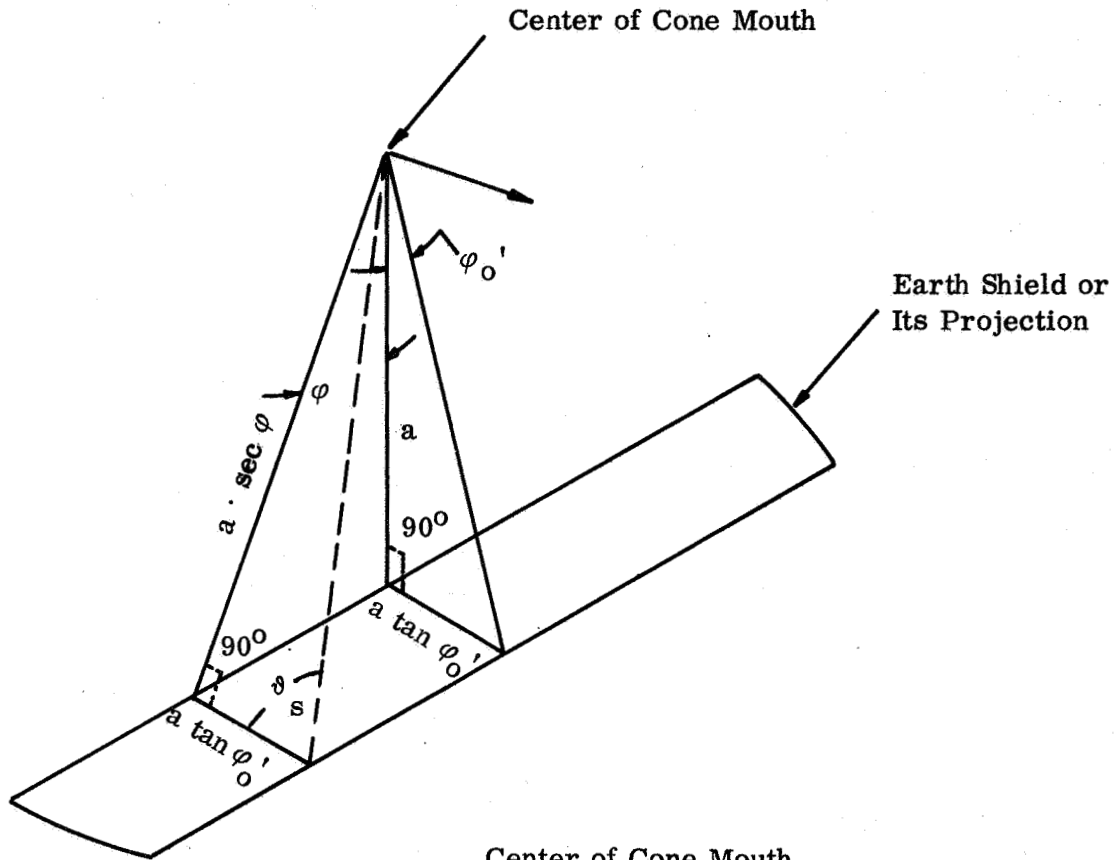
Semi-Circle Generated
by Tangent Lines to
Earth from C

Figure 12   Earth Shield For First-Stage Cone

54

The equation for $\sin^2 \vartheta (\varphi)$ is

$$\sin^2 \vartheta \ (\varphi) = \frac{\sec^2 \varphi}{\sec^2 \varphi_0} \qquad (95)$$

This is the relation between $\vartheta$ and $\varphi$ along the semicircle generated by tangent lines to the earth from the cone mouth.

Along the straight line projection on the semicircle (See Figure 12)

$$\sin^2 \vartheta_s = \frac{1}{1 + \cos^2 \varphi \cdot \tan^2 \varphi_0'} \qquad (96)$$

where $\varphi_0'$ is the vertical-plane angle subtended by the earth shield at the center of the cone mouth. The earth shield was designed for the straight line to intersect the semicircle at $\vartheta = \vartheta_1 = 71$ degrees 27 minutes (See Figure 7 in Section 1.4.1.2). Since $\varphi_0 = 58.5$ degrees is the angle between the nadir and the tangent line to the earth, equations (95) and (96) give

$$\tan \varphi_0' = \frac{\cos 71^0 \ 27'}{\cos 58.5^0} = 0.61$$

and $\varphi_0'$ is approximately 31.5 degrees.

Substituting equations (95) and (96) into (94), we obtain

$$F_{m-Ae_2}^{vis.} = \frac{1}{\pi} \int_0^{\varphi_1} \frac{d\varphi}{1 + \cos^2 \varphi \cdot \tan^2 \varphi_0'} - \frac{\varphi_2}{\pi} \sin^2 \vartheta_2$$

$$- \frac{1}{\pi} \int_{\varphi_2}^{\varphi_1} \frac{\sec^2 \varphi \, d\varphi}{\sec^2 \varphi_0}$$

Integrating (the first integral is given by G. Petit Bois, "Tables of Indefinite Integrals", Dover, 1961, p. 122) and rearranging terms

$$F_{m-Ae_2}^{vis.} = \frac{1}{\pi} \ [\cos \varphi_0' \cdot \arctan (\cos \varphi_0' \cdot \tan \varphi_1)$$

$$- \cos^2 \varphi_0 \ (\varphi_2 \sec^2 \varphi_2 + \tan \varphi_1 - \tan \varphi_2)] \qquad (97)$$

For  $\varphi_0'$  =  31.5 degrees

$\varphi_0$  =  58.5 degrees

$\varphi_1$  =  56 degrees 33 minutes

$\varphi_2$  =  51 degrees 45 minutes

$$F_{m-Ae_2}^{vis.} = 0.02085$$

The values given for $\varphi_1$ and $\varphi_2$ are for a truncated right circular cone having the geometry of the vertical cooler plane.

All the required view factors are listed in Table 8 together with the infrared and solar absorptivities for $\epsilon_g = 0.086$ and $\alpha_g = 0.22$.

Table 8

Parameters for Calculation of Cone Absorptivities with Earth Shield

| n | $F_{m-Aen}$ | $F_{m-tn}$ | $a_n$ (ir) | $a_n$ (solar) |
|---|---|---|---|---|
| 1 | 0 | 0.03285 | 0.086 | 0.22 |
| 2 | 0.02085 | 0.03465 | 0.1646 | 0.3916 |
| 3 | 0.06285 | 0 | 0.2364 | 0.5255 |
| 4 | 0.0320 | 0 | 0.3021 | 0.6299 |

$$F_{de}^s = 0.1157 \qquad 0.0675 = F_{dt}$$

Using equation (71) and the data in Table 8, the effective cone absorptivities are, for the shield shown in Figure 12 and a mouth to wall area ratio of 0.316,

$$\epsilon_{ce}^s = 0.00882$$

$$\alpha_{ce}^s = 0.0194$$

And from equation (71), the effective cone absorptivity for shield radiation is

$$\epsilon_{ct} = 0.00270$$

when the side of the shield facing the cone mouth has an emissivity, $\epsilon_t$, of 0.086.

The outside surface of the shield is part of the outer cooler surface. From Section 2.1.2, the emittance of the shield is

$$\epsilon_t W_t = \epsilon_g \sigma T_s^4 = 1.86 \times 10^{-3} \text{ watts/cm}^2$$

when $\alpha_2/\epsilon_2$ equals 0.2.

We are now in a position to determine the temperature of the shielded cone from equation (69). The parameters not changed by the addition of the shield are assumed to have the values given in Section 2.1.3. Then for an orbit normal to sun angle of 79 degrees and an altitude of 600 n mi, the shielded cone has a black-body emittance of

$$\sigma T_c{}^4 = 9.53 \times 10^{-3} \text{ watts/cm}^2$$

and a temperature of

$$T_c = 202.5^{\circ}K , \quad \epsilon_g = 0.086 \text{ and } \alpha_g = 0.22 \tag{98}$$

This is a reduction of 9.5 degrees K in the cone temperature.

The total power absorbed (and emitted) by the cone and cone end at the above temperature is (equation 90, Section 2.13)

$$\Phi_c = 1.10 \times 10^{-2} A_c \text{ watts, } A_c \text{ in square inches} \tag{99}$$

The inside surface area of the cone, $A_c$, is 933 square inches, so that

$$\Phi_c = 10.3 \text{ watts} \tag{100}$$

There are presently eight synthane G-10 supports of 1/2 inch outside diameter, 1/4 inch inside diameter, and 1-1/2 inches in length directly connected to the first-stage cone and outer box. In this case, the total conduction between the first-stage cone and outer box will be 0.275 watt for a temperature difference of 47 degrees C. This is about 2.7 percent of the power emitted by the cone and its ends and would raise the cone temperature by about 0.7 percent or 1.8 degree K.

## 2.1.5   First-Stage Patch

The temperature of the first-stage patch can be calculated from equation (66) in Section 1.5 and the data given in Sections 2.1.3 and 2.1.4. The required parameters are listed in Table 9 for the two sets of cone wall emissivities and solar absorptivities.

## Table 9

### Parameters for Determination of First-Stage Patch Temperature

| | | |
|---|---|---|
| $\epsilon_g$ | 0.086 | 0.02 |
| $\alpha_g$ | 0.22 | 0.183 |
| Earth Shield | Yes | No |
| $\epsilon_{pc}$ | 0.0735 | 0.017 |
| $A_{c2}/A_{p1}$ | 0.810 | 0.810 |
| $\sigma T_c^4$ (w/cm$^2$) | $9.53 \times 10^{-3}$ | $1.30 \times 10^{-2}$ |

The corresponding emittances and temperatures of the first-stage patch are

$$\left. \begin{array}{ll} \sigma T_{p1}^4 = 8.90 \times 10^{-4} \text{ watts/cm}^2 & \epsilon_g = 0.086 \text{ and} \\ T_{p1} = 112^{\circ}\text{K} & \alpha_g = 0.22 \end{array} \right\} \quad (101)$$

$$\left. \begin{array}{ll} \sigma T_{p1}^4 = 3.03 \times 10^{-4} \text{ watts/cm}^2 & \epsilon_g = 0.02 \text{ and} \\ T_{p1} = 85.5^{\circ}\text{K} & \alpha_g = 0.183 \end{array} \right\} \quad (102)$$

We therefore expect the temperature of the first stage will be in the range 86 to 112 degrees K for an in-orbit cooler. The upper limit is for a high gold emissivity and requires the use of an earth shield (Section 2.1.4) to prevent an even higher first-stage temperature ($\sim$ 117 degrees K). The actual emissivity value for an aluminized mylar cone surface was determined during the experimental study (Section 4.3).

An in-orbit support for the first-stage (first-stage patch and second-stage cone) is needed to maintain alignment after release of the caging mechanism used to hold the first stage during powered flight. The design of the support is shown in Figure 13. The support is a tube of low thermal conductivity material, such as fiberglas epoxy (Synthane G-10). This form of support has simplicity, high torsional rigidity, and high thermal resistance. Two tubes are used to support the patch and are mounted parallel to the long dimension of the patch.

NOTES:

△ MAT'L: POLYURETHANE ADHESIVE DUPONT ADIPRENE L-100 OR NARMCO POLYURETHANE RESIN 7343-100 PARTS BY WEIGHT. DUPONT MOCA OR NARMCO CURING AGENT 7139-11 PARTS BY WEIGHT.
CURING: 3 DAYS @ 75°F OR 4 HOURS @ 158°F OR 3 HOURS @ 212°F

BOND 2 HALVES OF TUBING TOGETHER BEFORE BONDING TO ITEM 1 & 11

BOND 2 HALVES OF TUBING TOGETHER BEFORE BONDING TO ITEMS 5 & 6

BOND THIS END OF TUBE TO ITEM 1 & 11 OPPOSITE END TO ITEM 6
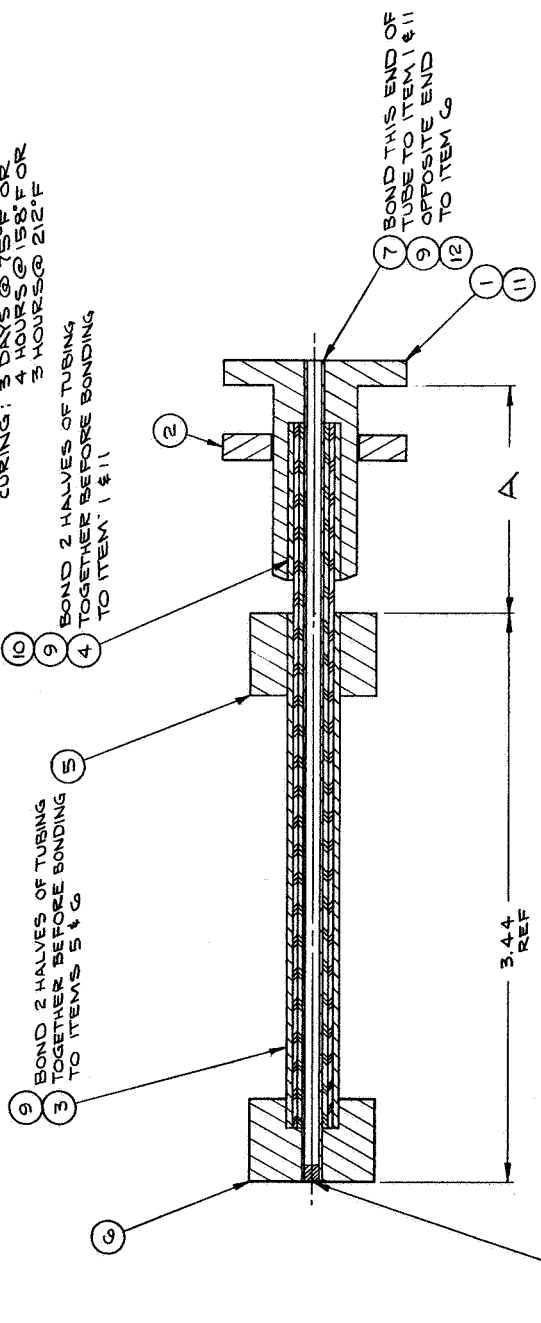
MAT'L: POLYURETHANE FOAM STAY FOAM 604 .10 LONG SLIGHT INTERFERENCE FIT IN ITEM 7 & 12

3.44 REF

| QTY G2 | QTY G1 | ITEM | PART NUMBER | DESCRIPTION |
|---|---|---|---|---|
| 1 | | 12 | B 4710058-G2 | TUBE SUPPORT |
| | 1 | 11 | B 4720140-1 | SUPPORT, OUTER, IN-ORBIT |
| 2 | | 10 | B 4710059-4 | TUBE, REFLECTOR |
| AR | AR | 9 | △ | ADHESIVE |
| | 1 | 8 | THIS DWG-8 | PLUG |
| 1 | | 7 | B 4710058-G1 | TUBE, SUPPORT |
| | 1 | 6 | B 4710062-1 | SUPPORT, INNER, IN-ORBIT |
| 1 | | 5 | B 4710061-1 | SPACER, SUPPORT, IN-ORBIT |
| | 2 | 4 | B 4710059-2 | TUBE, REFLECTOR |
| 2 | 2 | 3 | B 4710059-1 | TUBE, REFLECTOR |
| | 1 | 2 | B 4710065-1 | SPACER, WASHER |
| 1 | | 1 | B 4710060-1 | SUPPORT, OUTER, IN-ORBIT |

LIST OF MATERIAL

Figure 13  In-Orbit Support For First-Stage Patch

59

The tube is gold coated on the outside and wrapped with two layers of aluminized mylar to reduce radiative coupling from its surface area. Radiative coupling is further reduced by cylindrical inserts mounted to the cone and first-stage patch; these inserts are gold coated on their inner surface. The tube and its wrapping may be vented to space through the opening at the cone end of the support.

The thermal inputs to the first stage from the in-orbit support produce only a small percentage increase in the temperature of first-stage patch, as shown by the following calculations.

The conductive thermal input down the support tubes given by

$$\Phi_c = \frac{2 \Delta T}{\ell} [K_s A_s + K_g A_g] \tag{103}$$

where $\Delta T$ = temperature difference between first-stage cone and patch

$\ell$ = length of tube between contacts

$K$ = thermal conductivity

$A$ = cross-sectional area

$s$ = tube material

$g$ = gold coating on tube

The tube is 4 inches long and has a 1/4 inch outside diameter and a 1/32 inch wall. A gold thickness of 0.1 micron is needed for high reflectivity (low emissivity) on the outer surface of the tube. The conductive input is then

$$\Phi_c = 0.0916 \Delta T \text{ milliwatts}$$

for $K_s = 2.94 \times 10^{-3}$ watt/cm$^\circ$C and $K_g = 2.93$ watt/cm$^\circ$C.

The temperature difference is 90.5 degrees C at the high cone surface emissivity of 0.086 and 133.5 degrees C at the low emissivity of 0.02. The corresponding conductive inputs are 8.29 and 12.2 milliwatts.

To estimate the radiative coupling from the outside surface of the support, we will assume the tube has an effective temperature given by

$$T_r^4 = 1/2 (T_c^4 + T_{pl}^4)$$

60

The equation for the radiative coupling is then

$$\Phi_r = \frac{\epsilon}{(n+1)} \pi r_o \, \ell \, \sigma (T_c^4 - T_{p1}^4) \tag{104}$$

for the two tubes, where

$$\epsilon \quad = \quad \text{emissivity of coated surfaces}$$

$$n \quad = \quad \text{effective number of perfect radiative shields} \\ \text{between tube and patch}$$

This equation assumes the outer surface of the tube and inner surface of the patch (cylindrical inserts) as well as the radiative shields have an emissivity $\epsilon$. Two layers of aluminized mylar, such as a pair of Dimplar multilayer insulation sheets, are equivalent to about one perfect radiant shield coated on both sides. For the above tube, $\epsilon = 0.1$, and $n = 1$,

$$\Phi_r = 0.507 \, (\sigma T_c^4 - \sigma T_{p1}^4) \text{ mw}, \quad \sigma T^4 \text{ in mw/cm}^2$$

For a cone surface emissivity of 0.086 and an attached earth shield, $\Phi_r$ equals 4.38 milliwatts; for a cone surface emissivity of 0.02 and no earth shield, $\Phi_r$ is 6.43 milliwatts.

The total thermal input to the first-stage patch is about 12.7 milliwatts at $\epsilon_g = 0.086$ and 18.6 milliwatts at $\epsilon_g = 0.02$. The first-stage patch (as constructed) has a surface area of 453 cm$^2$; it radiates 403 milliwatts at 112 degrees K ($\epsilon g = 0.086$) and 137 milliwatts at 85.5 degrees K ($\epsilon_g = 0.02$). The thermal inputs are then 3.1 percent of first-stage power at $\epsilon_g = 0.086$ and 13.6 percent at $\epsilon_g = 0.02$. The respective increases in the temperature of the first-stage patch are 0.8 percent (0.9 degrees K) and 3.4 percent (2.9 degrees K).

## 2.1.6 Second-Stage Patch

The second-stage cone is designed so that the second-stage patch sees none or only a very small fraction of the first-stage cone. The radiative input to the patch is then from the second-stage cone. The conductive input is from the support tube and electrical leads.

The temperature range of the second-stage patch is determined below for the range of cone surface emissivities used in the first-stage and for a support that has passed sinusoidal vibration tests.

## 2.1.6.1 Patch Support

The support for the second stage is shown in Figure 14. It is similar to the in-orbit support for the first stage (Section 2.1.5), except that it is considerably more rugged (in relation to the mass it supports) in order to survive powered launch. The hollow support rod is made of fiberglas epoxy (Synthane G-10) and is 1-5/8 inches long. An assembly using this support has passed sinusoidal vibration tests as the Nimbus prototype levels (Appendix II ).

Because of the lower temperature range, the conductive input through a gold coating on the tube is larger than the increase in radiative input upon removal of the coating and the multilayer insulation around the tube. The gold coating and multi-layer insulation will therefore be used only on the first-stage (in-orbit) support. However, by enclosing the tube in concentric, gold-coated shields attached to the two patches, the radiative coupling from the tube is reduced to a very small fraction of the power radiated by the second-stage patch.

The tube patch support has several advantages over the wire supports employed in the single-stage radiant cooler of the Nimbus High Resolution Infrared Radiometer.[4] It has high torsional rigidity, so that cell alignment is more accurate. Its hollow center can be used to carry electrical leads, thus eliminating additional holes in the cone structure. It supports the patch from a single contact area, thus reducing thermal contraction problems. Finally, a damping mechanism can be attached in the area of connection to the first stage to aid in surviving the vibration environment.

The conductive coupling coefficient of the support tube is given by

$$K_c = K \frac{A}{\ell} \tag{105}$$

where  K   =   thermal conductivity of rod material

   A   =   cross-sectional area of tube

   $\ell$   =   $\cdot$ length of tube

The thermal conductivity of Synthane G-10 is 0.7 cals/sec cm degrees C = 0.746 x $10^{-2}$ watt/inch degree C (eem file System, Sec. 3100, 3200, Synthane Technical Plastic, p. 7). Also the minimum inside diameter of Synthane rods is 3/32 inch. The outside diameter is 1/8 inch. The conductive coefficient for a tube 1-5/8 inches long is then 0.0247 mw/degree K.

---

4        Contract NAS5-668

Figure 14   Second-Stage Patch Assembly

If there are five 1-5/8 inch long electrical leads of B&S No. 40 (3.145 x $10^{-3}$ inch diameter) drawn Monel, their conductive coefficient is 0.0092 mw/degree K. The thermal conductivity of drawn Monel at 100 degrees K is 0.152 watt/cm degree C = 0.386 watt/inch degree C. The thermal conductive coupling coefficient between stages is then

$$K_c = 0.0339 \text{ mw/degree K}$$

Radiative coupling from the outer surface of the support rod to the second-stage tube shield is given by

$$\Phi_r = \epsilon \, 2 \, \pi \, r_0 \, \ell \, \sigma \, (T_r^4 - T_{p2}^4) \tag{106}$$

assuming the entire rod radiated at an effective temperature, $T_r$. The other factors are

$\epsilon$  =  emissivity of tube shield

$r_0$  =  outside radius of tube

$\ell$  =  length of tube between supports

For

$\epsilon$  =  0.1

$2 \, r_0$  =  1/8 inch

$\ell$  =  1-5/8 inch

$T_{p2}$  =  79 degrees K

$T_r^4$  =  1/2 $[(111)^4 + (79)^4]$

The radiative coupling from the support tube is then

$$\Phi_r = 0.131 \text{ milliwatts}$$

Including the side areas, the second-stage patch as finally constructed has a surface area of 2.62 $\text{in}^2$ and a radiant power of 3.73 milliwatts at 79 degrees K. The above radiative power is about 3.5 percent, which would increase the patch temperature by about 0.9 percent or 0.7 degrees K.

## 2.1.6.2　Temperature Range

The effective patch-to-cone emissivity for the second stage, $\epsilon_{pc}^{(2)}$, was calculated for $\epsilon_g$ equal to 0.02 and 0.086 (Section 1.3.1). Values were determined for truncated right-circular cones having the geometry of the vertical and horizontal cooler planes. The results are listed in Table 10 together with the average values.

### Table 10

### Patch-to-Cone Effective Emissivity of Second Stage

| $\epsilon_g$ | Vertical | Horizontal | Average |
|---|---|---|---|
| 0.02 | 0.038 | 0.014 | 0.026 |
| 0.086 | 0.156 | 0.062 | 0.109 |

For a conductive coupling coefficient of 0.0339 mw/degrees K the temperature, $T_{p2}$, of the second-stage patch satisfies (equation 91, Section 1.6)

$$4.79 \times 10^{-8} \, T_{p2}^{4} + 0.0339 \, T_{p2} = 4.62 \text{ milliwatts}$$

when $\epsilon_g$ equals 0.086 and the first stage patch is at 112 degrees K (Section 2.1.5). The patch radiating area is 1.31 square inches with an 0.030 inch patch-to-cone gap (Section 2.1.1). The solution is

$$T_{p2} = 79.5 \text{ degrees K} \tag{107}$$

For $\epsilon_g$ equal to 0.02, the first-stage patch is at 85.5 degrees K and the second-stage patch temperature satisfies

$$4.79 \times 10^{-8} \, T_{p2}^{4} + 0.0339 \, T_{p2} = 2.96 \text{ milliwatts}$$

The solution is

$$T_{p2} = 63.9 \text{ degrees K} \tag{108}$$

The above results are for a thin patch (See Section 1.3.1), i.e. for a patch whose area is perpendicular to the cone axis. In the cooler models actually constructed (Section 4.3.2), the patch thickness was made comparable to its width to provide for attachment of the support tube and mounting of the infrared detector. The radiative coupling between the patch and cone is about twice as large for the side areas because of the increased number of cone-wall reflections needed for patch radiation to reach space. This increased coupling, however, is more than

offset by the greater patch radiating area (which reduces the relative importance of the conductive coupling). The above model is therefore useful in the design of the second stage and in the prediction of patch temperature.

2.1.6.3   Detector Joule Heating

Detector joule heating produces an increase in the radiant power from the second-stage patch and a decrease in the conductive coupling at a fixed first-stage temperature. No change in the net radiative coupling to the first stage is produced by a change in the second-stage temperature (See equation 68, Section 1.6). This may be expressed as

$$J = A_{p2} \, \sigma (T_m^4 - T_{p2}^4) + K_c (T_m - T_{p2}) \tag{109}$$

where $T_m - T_{p2}$ is the increase in patch temperature produced by the joule heat.

A photoconductive detector on loan from the Honeywell Research Center, Boston, has a resistance of 193 ohms and an optimum (maximum detectivity) bias current of 0.9 ma; a detector purchased for use in the second-stage patch has a resistance of 171 ohms and the same optimum bias. The joule heats from the two detectors are then 0.156 and 0.139 milliwatts, respectively. For

$$A_{p2} = 2.62 \text{ in}^2 \text{ (value for constructed patch)}$$

$$T_{p2} = 77^O K$$

$$K_c = 0.0339 \text{ mw}/^O K$$

equation (109) then yields

$$T_m = 77.7^O K \tag{110}$$

to the nearest 0.1 degree K for either detector. The joule heating therefore produces a temperature rise of 0.7 degree K or 0.9 percent.

Detector joule heating can be eliminated by the use of a photovoltaic cell (See Part II, Section 4.0).

66

## 2.1.7   Relay Optic Design

The relay optic must be designed to minimize the radiative transfer from the optical structure to the patches through the optical opening. This radiative transfer can be made small by mounting the detector cell on a long edge of the second-stage patch, to minimize the cell-to-cone structure distance, and by reducing the speed of the optical beam as it enters the cooler, to minimize the size of the optical opening needed in the first-stage patch.

A design is shown in Figure 15 for use with an f/1 primary telescope and mechanical chopper. Radiation from the primary (chopper) focal plane is reflected by a flat mirror to an f/1.0 parabolic mirror, which collimates the radiation and directs it to an f/8 germanium focusing lens. The use of a collimated beam allows the separation between the parabolic mirror and focusing lens to be adjusted, so that the chopper-to-detector distance is not critical. The radiation from the f/8 lens is reflected off a 45 degree plane mirror through a 10.5 to 12.5 micron interference filter mounted on the first-stage patch. The beam is then increased in speed to f/2 by an aplanatic germanium lens, which focuses the radiation on the detector cell. The relay optic has a magnification of 2X.

If the primary telescope is a parabolic mirror (with folding flat secondary), it forms a pair of confocal parabolas with the first element of the relay optic. Such a pair is anastigmatic (E. H. Linfoot, "Recent Advances in Optics" Oxford, 1955, p. 277) that is, spherical aberration, coma, and astigmatism of the combination of the two parabolic mirrors are all zero. The f/8 germanium lens is designed for minimum spherical aberration. Its coma is then nearly zero because of the high refractive index of germanium (R. M. Scott, Proc. IRE 47, 1530, Sept. 1959). The germanium aplanatic lens has no spherical aberration or coma. Chromatic aberrations of both germanium lenses are negligible because of the low dispersion of germanium in the 10.5 to 12.5 micron band.

The f/1 parabolic mirror in the relay optic may be replaced with an f/1 germanium doublet. The first element in the doublet may be an aplanatic lens that reduces the speed to f/4 (i.e., by a factor equal to the refractive index of germanium). The beam can then be collimated by the second element, which may be bent for minimum spherical aberration.

If the mechanical chopper is replaced by an electronic chopper, the primary focus and the first member of the relay optic (f/1 parabola or germanium doublet) can be eliminated. This is accomplished by replacing the folding flat in the primary telescope with a negative parabolic surface confocal with the primary parabolic. The rays from the primary telescope are then collimated and go directly to the f/8 relay lens.

67

Second-Stage Patch,Detector

Ge Aplanatic Lens

First-Stage Patch

10.5–12.5 $\mu$ Filter

First-Stage Cone

Plane 45° Mirror

Ge Lens (f/8)

Parabolic Mirror (f/1)

Primary Focus (Plane of Chopper)

68
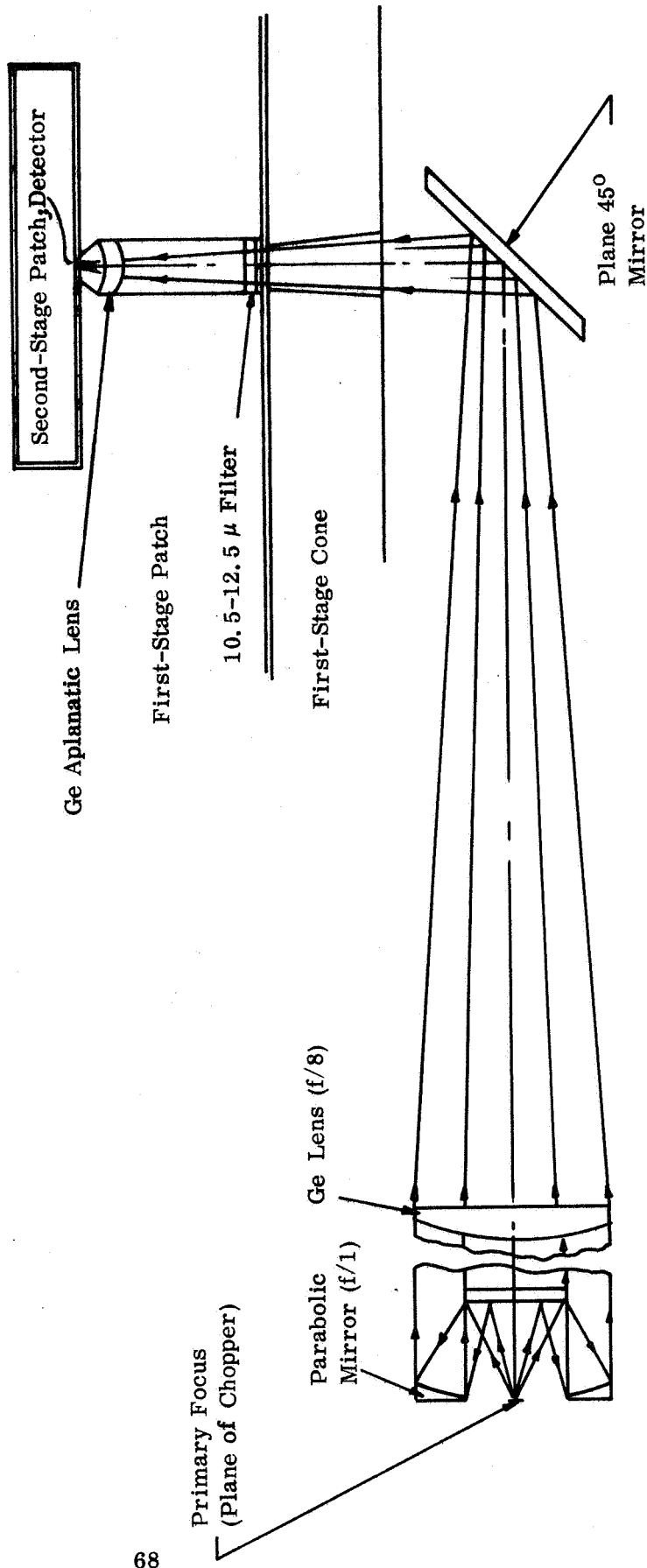
Figure 15   Relay Optics

In the relay design the cooler opening facing the optics is about one-half inch in diameter at the edge of the first-stage patch. The opening is large enough to allow for thermal contractions and initial (room temperature) alignment tolerances. As a result, the interference filter and aplanatic lens can be housed within the half-inch thick structure of the first-stage patch. In addition, none of the radiating (outside) patch area can "see" through the optical opening in the cone structure with this construction. The only coupling to the optics and its surroundings is then by means of the half-inch diameter opening. The coupling is radiative and given by

$$\Phi_O = A_O E \sigma (T_c^4 - T_{p1}^4) \tag{111}$$

where $A_O$ = area of optical opening

$E$ = effective emissivity

$T_c$ = temperature of first-stage cone

$T_{p1}$ = temperature of first-stage patch

For close-spaced geometry (R. B. Scott, "Cryogenic Engineering", Van Nostrand, 1959, p. 148)

$$E = \frac{\epsilon_1 \epsilon_2}{\epsilon_2 + (1 - \epsilon_2) \epsilon_1} \tag{112}$$

where $\epsilon_1$ = emissivity of interference filter

$\epsilon_2$ = emissivity of surroundings as seen back through optical opening

Measurement made on the 200 degrees K radiant cooler for HRIR Model F-5 (Contract No. NAS5-668) showed that $\epsilon_2$ is close to 0.5. The interference filter has a comparable emissivity value, so that E is about 0.33. For a half-inch diameter opening, the minimum value of $T_{p1}$ (85.5 degrees K, Section 2.1.5), and the maximum value of $T_c$ (219 degrees K, Section 2.1.3), the radiative coupling through the optical opening is

$$\Phi_O = 5.31 \text{ milliwatts}$$

This is less than 4 percent of the power radiated by the first-stage patch at 85.5 degrees K and would increase its temperature by less than 1 percent (0.8 degree K). At the higher patch temperature of 112 degrees K, the increase is about 1/4 degree K.

Next, consider the radiative transfer to the cell opening on the second-stage patch by way of the optical opening. The cell opening views the first-stage patch at angles beyond the optical beam from the aplanatic lens. An f/2 aplanatic lens subtends a half angle $\vartheta$ which satisfied the relation

$$\sin \vartheta = 1/4 \qquad (113)$$

The normalized projected solid angle or view factor ($\sin^2 \vartheta$) from the cell opening to the aplanatic lens is then 1/16 and to the first-stage patch 15/16. The interference filter is seen through the lens, which is transparent to a high percentage of the radiation from the first-stage cone and patch. The filter transmits about 0.10 of the total power radiated by a 219 degree K source (maximum temperature of the first-stage cone, Section 2.1.3) and a negligible fraction of the total power from a 85.5 degree K or 63.9 degree K source (minimum temperatures of the patches, Section 2.1.5 and 2.1.6). The radiative coupling through the optical opening to the second-stage patch at 63.9 degrees K from the first-stage patch at 85.5 degrees K and relay optics is therefore

$$\Phi_{02} = A_{02} \, \sigma \, \left\{ [(85.5)^4 - (63.9)^4] + \frac{0.10 \times 0.5}{16} (219)^4 \right\}$$

$$\Phi_{02} = 1.61 \, A_{02} \text{ milliwatts} \qquad (114)$$

where $A_{02}$ is the area of the detector cell opening in square inches. This equation assumes that the cell opening and first-stage patch are black and that the relay optics as seen from the detector has an emissivity of 0.5. For a 0.10 inch diameter opening over the cell

$$\Phi_{02} = 0.013 \text{ milliwatt}$$

This is less than 1 percent of the power radiated by the second-stage patch at 63.9 degrees K and would increase its temperature by about 1/4 percent (0.16 degree K).

The relay optics will be housed within a fiberglas epoxy tube. There will be about a 4 inch length between the outer surface and its connection to the first-stage cone. If the rod is connected to the outer surface without insulating washers (to ensure proper optical alignment) and has a 2 inch outside diameter and 1/16 inch wall, it will conduct

$$\Phi_0 = 3.33 \times 10^{-2} \text{ watt}$$

from the outer surface to the cone. This is less than 0.4 percent of the external power absorbed in the cone and would increase the cone temperature less than 0.1 percent (0.2 degree K).

70

## 2.2   Single-Ended Cooler

The single-ended two-stage radiant cooler has two main advantages over the double-ended design.  First, its placement on the spacecraft is less critical because it views cold space in only one direction and its horizontal view angle is ± 45 degrees from the cone axis rather than ± 60 degrees.  Secondly, the volume and weight are 3/4 or less that of the double-ended version.

The cooler was designed to operate in a Nimbus-type orbit, where it can expect to have its mouth illuminated by direct sunlight part of the time during a year in orbit.  For this reason, the cone mouth and cone end are completely shielded from direct sunlight to a minimum orbit normal to sun angle of 70 degrees. [5]  Over the 90 to 70 degree range of sun angles, the patch reaches a temperature range of 81 degrees K to 61 degrees K at a spacecraft altitude of 500 nautical miles.  The cone surface emissivity range is 0.086 to 0.02, and a minimum practical in-orbit patch support is used (Section 2.2.4.2).  If the patch is allowed to reach a maximum temperature range of 85 degrees K to 90 degrees K, the in-orbit support can be strengthened and the dependence on the patch caging mechanism reduced (Section 2.2.4.3).

### 2.2.1   Basic Design

The basic design of the single-ended two-stage cooler is shown in Figures 16 and 17, which are sections in the vertical and horizontal planes through the axis of the cooler.  The design shown has maximum over-all dimensions, in inches, of about 13 x 20 x 16, compared to the double-ended design dimensions of about 10.5 x 23.5 x 20.7.  The shield (t) shades the cone end and cone mouth (first stage of cooling) from direct sunlight and reduces the thermal loading from earthshine and earth infrared.  The shield is an integral part of the outer box (Sections 1.7.2 and 2.1.2).

The cone end is made of Alzak or painted white and in combination with the cone acts as the first stage of cooling.  The cone end may be considered a first-stage patch from which the second-stage cone is suspended.  The shield then serves as the first-stage cone.

The cone and patch are designed for maximum patch look angles of 29 degrees in the vertical plane and 45 degrees in the horizontal plane.  The angle from the cone axis to the earth in the vertical plane is 29.2 degrees at a spacecraft altitude of 500 nautical miles.  The cone is supported from the outer box by means of Synthane G-10 tubes and is radiatively isolated from the outer box by multilayer insulation.  The patch is supported in orbit by means of Synthane G-10 tubes or a

---

5      According to the Nimbus D Experimenters Handbook, this angle may
        be as small as 60 degrees at the end of a year in orbit.

**EXTENSION FOR EARTH SHIELD**

7.51"

5.62"

6.26"

29°

MAXIMUM SUN ANGLE

30°

6.40"

2.095"

0.56"

6.57"

t — SHIELD
m — CONE MOUTH
d — CONE END
c — CONE
p — PATCH
MLI — MULTILAYER INSULATION

MAX PATCH LOOK ANGLE = 29°
CONE HALF ANGLE = 13.5°

EMISSION FROM CONE END
AND CONE MOUTH REQUIRES
0 TO 1 REFLECTION AT
SHIELD TO GO OUT SHIELD
MOUTH
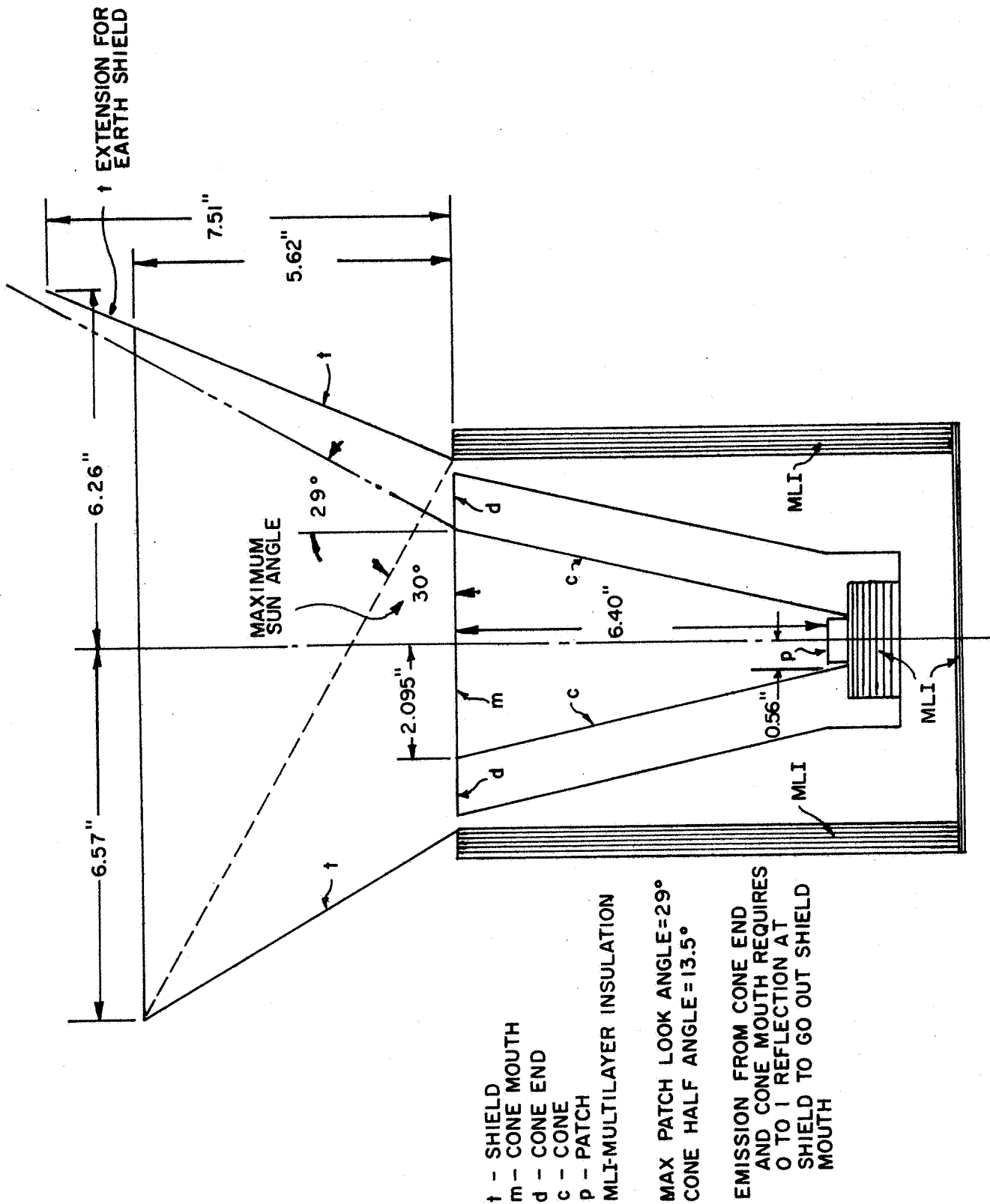
Figure 16 Single-Ended Two-Stage Radiant Cooler, Vertical Plane
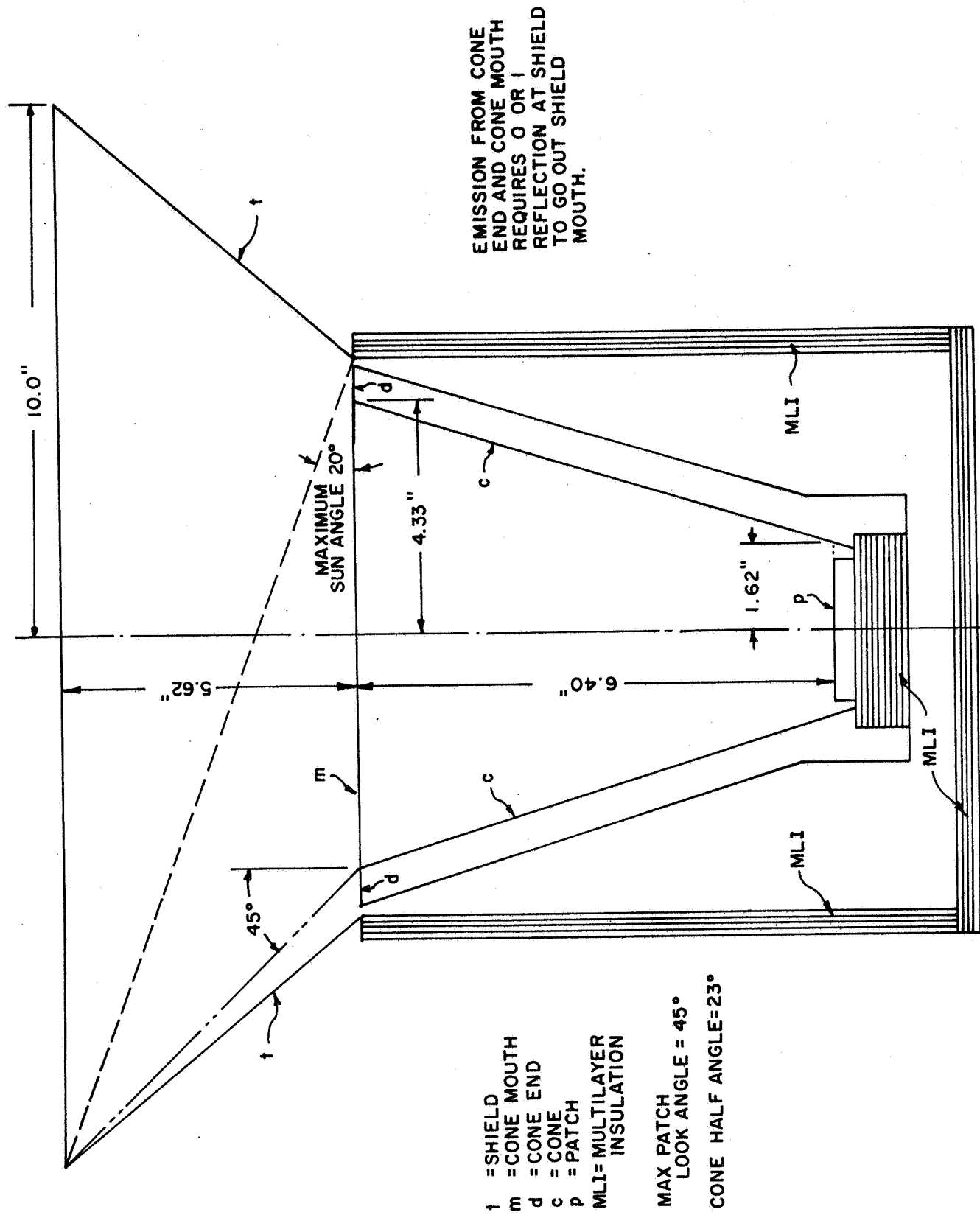
EMISSION FROM CONE
END AND CONE MOUTH
REQUIRES 0 OR 1
REFLECTION AT SHIELD
TO GO OUT SHIELD
MOUTH.

10.0"

MAXIMUM
SUN ANGLE 20°

4.33"

1.62"

5.62"

6.40"

45°

MLI

MLI

MLI

t

d

c

p

m

c

d

t

f  =SHIELD
m  =CONE MOUTH
d  =CONE END
c  =CONE
p  =PATCH
MLI= MULTILAYER
       INSULATION

MAX PATCH
   LOOK ANGLE = 45°

CONE HALF ANGLE=23°

73

Figure 17  Single-Ended Two-Stage Radiant Cooler, Horizontal Plane

wire suspension caged during launch by a retractable holding mechanism. The side of the patch not radiating to cold space is thermally isolated from the cone by multi-layer insulation.

2.2.2   Sun and Earth Shield

The cone mouth and cone end are shielded from direct sunlight in the horizontal plane to a maximum orbit plane to sun angle of 20 degrees. In the vertical plane, the shield in the direction opposite the earth is the same length (distance measured along the cone axis from the cone mouth to the shield mouth) as the shield in the horizontal plane. This provides shielding to a maximum orbit plane to sun angle of 30 degrees. The shield in the vertical plane in the direction of the earth subtends an angle of about 40 degrees from the cone axis at the center of the cone mouth, and extends beyond the other three shields. It acts as an earth shield to reduce thermal loading of the cone mouth and cone end.

All shields are designed so that they are not visible from the black patch, i.e., so that patch emission from the cone mouth does not strike the shields. In addition, the shield in the vertical plane in the direction opposite the earth is designed so that the cone mouth and cone end do not see the earth by reflection in this shield. This requires a minimum shield angle of 30.5 degrees, as shown in Figure 18 (31 degrees is used). Only directly incident earth infrared and earthshine are then absorbed in the cone mouth and cone end.

For the shield design shown in Figures 16 and 17, sunlight incident at 20 degrees or less to the orbit plane is reflected only once at the specular shield before going back out the shield mouth.

The shield is mechanically and thermally tied to the outer box (Section 1.7.2). Three of the outer surfaces are covered with a material, such as Alzak treated aluminum, of low $\alpha/\epsilon$ ratio. The sides facing the spacecraft and other instruments are covered with a low emissivity material to decrease radiant coupling to the spacecraft. The sixth side is the mouth of the shield. The change in altitude from 600 to 500 nautical miles and the covering of the additional side with low emissivity material (for a single-ended cooler) produce only small changes in the temperature calculations given in Section 2.1.2 for the double-ended cooler. In addition, when the shield is thermally tied to the outer box, the temperature of the combination is very close to that of the outer box by itself.

In the following calculations, we assume that the outer box is designed to attain an in-orbit temperature of 248 degrees K.

CONE AXIS

$t$

29°

$2\theta_s$

$d'$ AND $m'$

d AND m

$\theta_s$

$t$ = SHIELD
d AND m = CONE END AND
                 CONE MOUTH
$d'$ AND $m'$ = d AND m REFLECTED
                   IN $t$
$\theta_s$ = SHIELD ANGLE IN DIRECTION
          OPPOSITE EARTH

$$2\theta_s + 29° = 90°$$
$$\theta_s = 30.5°$$
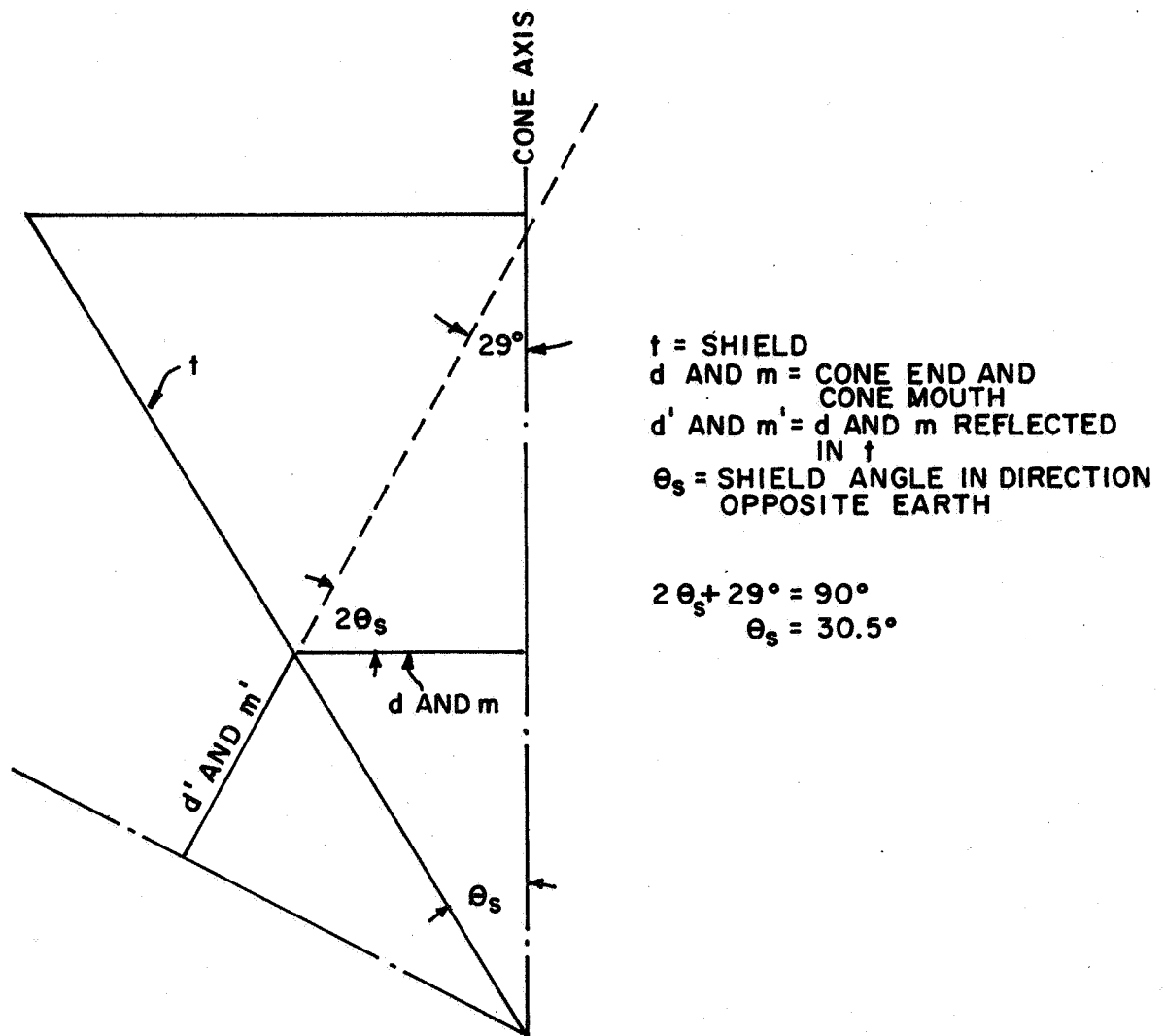
Figure 18    Minimum Vertical Shield Angle in Direction Opposite Earth

## 2.2.3 Cone

The cone half angle in the vertical plane is 13.5 degrees, which is close to the value (12.5 degrees) for the maximum patch half-width to cone length ratio at a minimum patch look angle of 29 degrees (see Section 1.2). The cone half angle in the horizontal plane is 23 degrees; the cone half angle of maximum patch half-width to cone length ratio at a maximum patch look angle of 45 degrees is 17 degrees. The angle was increased beyond 17 degrees, however, to reduce the radiative coupling between the cone and patch at only a small decrease in patch width in the horizontal plane (see Section 1.3).

Sources of thermal loading on the cone (cone mouth and cone end) are the shield and external sources. Sufficient multilayer insulation can be placed between the outer box and the cone to make the thermal load from the box negligible compared to that from external sources. The most important external source is still the earth, even with the extended earth shield attached.

Absorption of earth radiation in the cone mouth is strongest in the vertical plane of the cooler. We will use the vertical plane values for mouth absorption of earth infrared and earthshine. To offset this, cone absorption of spacecraft infrared will be neglected. Because the views from cone mouth and cone end to the spacecraft are limited by the shield, thermal loading from this source would be small in any case. The maximum look angles from the cone axis are 60 degrees in the vertical plane and 70 degrees in the horizontal plane at the outer edge of the cone end.

The thermal loads on the cone are balanced by its emission to the patch and to the outside. The average of vertical plane and horizontal plane values will be used for cone mouth emissivities, since there is no concentration of emission around any particular direction.

The blackbody emittance of the combined cone and cone end may be expressed in terms of parameters of the cone mouth rather than the cone wall (see equation 63, Section 1.4.2). For a cone shielded from direct sunlight, the result is

$$\sigma T_c^{\,4} = \frac{\epsilon_{me} W_e + \alpha_{me} W_s + \epsilon_{mt} W_t + \dfrac{A_d}{A_m}\left[ F_{de}\left(\epsilon_d W_e + \alpha_d W_s\right) + W_t\,\epsilon_d\,F_{dt} \right]}{\epsilon_d \dfrac{A_d}{A_m} + \epsilon_{mx} + \epsilon_{pc}\dfrac{A_p}{A_m}} \tag{115}$$

76

where $A_m$ = area of cone mouth

$A_d$ = area of cone end

$A_p$ = area of patch

$\epsilon_{me}$ = absorptivity of cone mouth for earth infrared

$\alpha_{me}$ = absorptivity of cone mouth for earthshine

$\epsilon_{mt}$ = absorptivity of cone mouth for shield infrared

$\epsilon_{mx}$ = effective cone mouth (cavity) emissivity

$\epsilon_{pc}$ = effective patch-to-cone emissivity

$\epsilon_d$ = emissivity of cone end

$\alpha_d$ = solar absorptivity of cone end

$W_e$ = average infrared emittance of the earth

$W_s$ = average equivalent earthshine emittance

$W_t$ = emittance of shield

$F_{de}$ = view factor from cone end to earth

$F_{dt}$ = view factor from cone end to shield

This equation holds when emissions from the cone end and cone mouth require 0 or 1 reflection at the shield to go out the shield mouth. Otherwise absorption of cone radiation in the shield (and emission of shield radiation to the cone) is enhanced by multiple reflections within the shield. The shield is designed to prevent such multiple reflections. The emittance of the shield is given by

$$W_t = \epsilon_g \, \sigma T_t^4 \tag{116}$$

where $\epsilon_g$ = emissivity of surface coating

$T_t$ = temperature of shield

## 2.2.3.1   Effective Emissivities and Absorptivities

In order to calculate the in-orbit cone temperature from equation (115), we must first determine the values of the effective absorptivities in the numerator and effective emissivities in the denominator. The approaches to these calculations are outlined below and the results listed.

The absorptivity of the cone mouth for shield infrared is given by

$$\epsilon_{mt} = \sum_n \epsilon_n F_{m-tn} \tag{117}$$

where $\epsilon_n$ = absorptivity produced by n cone wall reflections

$F_{m-tn}$ = view factor from cone mouth to sub-area of shield whose radiation is reflected n times upon entering the cone mouth

This equation holds when no shield emission reaches the cone mouth after reflection at the specular shield wall.

The view factors were determined from the center of the cone mouth for right circular coolers having the geometry of the vertical and horizontal planes. The value of $F_{m-tn}$ then depends only on the polar angle $\vartheta$ measured from the cone axis and is given by

$$F_{m-tn} = \sin^2 \vartheta_{n-1} - \sin^2 \vartheta_n \tag{118}$$

where the sub-area of the shield whose radiation is reflected n times in the cone occupies polar angles between $\vartheta_{n-1}$ and $\vartheta_n$. The values of $\vartheta_n$ were determined by the method of multiple reflections in the cone walls and can be calculated from the expressions

$$c_n^2 = r_2^2 + r_2^2 \cos^2 \theta - 2 r_2^2 \cos \theta \cos [(2n+1) \ \theta] \tag{119}$$

$$\sin \vartheta_n = \frac{r_2}{c_n} \sin [(2n+1) \ \theta] \tag{120}$$

where $r_1$ = distance along cone from apex to top of patch

$r_2$ = distance along cone from apex to cone mouth

$\theta$ = half angle of cone

The limiting value of $\vartheta_n$ is equal the angle from the cone axis to the shield. Below this angle, there is no shield to radiate to the cone. Thus $\vartheta_3$ equals 49 degrees 27 minutes in the vertical anti-earthward direction rather than 43 degrees 31 minutes.

Because the shield in the vertical plane is not symmetrical with respect to the cone axis, view factors were calculated for right circular shields having the geometries in the earthward and anti-earthward directions. The results are shown in Tables 11 and 12, and the view factors for the horizontal plane geometry are given in Table 13.

## Table 11

### Partial Shield View Factors for Vertical Plane
### Anti-Earthward Geometry

| n | $\vartheta_n$ | $\sin^2 \vartheta_n$ | $F_{m-tn}$ |
|---|---|---|---|
| 0 | $90^O$ | 1 | 0 |
| 1 | $71^O\ 57'$ | 0.9040 | 0.0960 |
| 2 | $57^O\ 29'$ | 0.7110 | 0.1930 |
| 3 | $49^O\ 27'$ | 0.5773 | 0.1337 |

## Table 12

### Partial Shield View Factors for Vertical Plane
### Earthward Geometry

| n | $\vartheta_n$ | $\sin^2 \vartheta_n$ | $F_{m-tn}$ |
|---|---|---|---|
| 0 | $90^O$ | 1 | 0 |
| 1 | $71^O\ 57'$ | 0.9040 | 0.0960 |
| 2 | $57^O\ 29'$ | 0.7110 | 0.1930 |
| 3 | $43^O\ 31'$ | 0.4741 | 0.2369 |
| 4 | $39^O\ 48'$ | 0.4097 | 0.0644 |

## Table 13

### Partial Shield View Factors for Horizontal Plane Geometry

| n | $\vartheta_n$ | $\sin^2 \vartheta_n$ | $F_{m-tn}$ |
|---|---|---|---|
| 0 | $90^O$ | 1 | 0 |
| 1 | $60^O\ 40'$ | 0.760 | 0.240 |

Note that the sum of partial view factors for a given geometry is equal to the view factor from the cone mouth to the shield, $F_{dt}$. The average vertical view factor is 0.5065, and the average of vertical and horizontal values is

$$F_{dt} = 0.373$$

For a cone wall emissivity $\epsilon_g$, the absorptivity produced by n cone wall reflections is

$$\epsilon_n = 1 - (1 - \epsilon_g)^n \tag{121}$$

Values of $\epsilon_n$ are listed in Table 14 for $\epsilon_g$ equal to 0.086 and 0.02.

### Table 14

### Absorptivity of n Cone Wall Reflections

$\epsilon_n$ for

| n | $\epsilon_g = 0.086$ | $\epsilon_g = 0.02$ |
|---|---|---|
| 1 | 0.086 | 0.02 |
| 2 | 0.1646 | 0.0396 |
| 3 | 0.2364 | 0.0588 |
| 4 | 0.3021 | 0.0776 |

The data in Tables 11 through 14 were used to calculate the absorptivity of the cone mouth for shield infrared by means of the summation (117). The results are given in Table 15 together with the average vertical value and the average of the horizontal and average vertical values.

### Table 15

### Absorptivity of Cone Mouth for Shield Radiation

| | Geometry | $\epsilon_{mt}$ for $\epsilon_g = 0.086$ | $\epsilon_{mt}$ for $\epsilon_g = 0.02$ |
|---|---|---|---|
| 1. | Vertical, earthward | 0.1150 | 0.0285 |
| 2. | Vertical, anti-earthward | 0.0716 | 0.0174 |
| 3. | Horizontal | 0.0206 | 0.0048 |
| 4. | Average of 1. and 2. | 0.0933 | 0.0230 |
| 5. | Average of 3. and 4. | 0.0570 | 0.0139 |

The absorptivities of the cone mouth for earth infrared and earthshine were calculated using the approach described in Section 1.4.1.2 and used in the analysis of the double-ended cooler in Sections 2.1.3 and 2.1.4. Values were calculated for a spacecraft altitude of 500 nautical miles and for the earth shield described in Section 2.2.2. The shield opposite the earth is such that only directly incident earth radiation is incident on the cone mouth.

If we set up spherical coordinates at the mouth of a right circular cone, with the pole along the cone axis, the number of reflections earth radiation undergoes at the cone walls before going back out the cone mouth is a step-wise function of the polar angle (see Figure 19). That is, the range of polar angles can be divided into regions in which the absorptivity of the cone mouth is constant. This allows the surface area of the earth visible from the cone mouth, or the area of the equivalent semicircle, to be divided into sub-areas, $A_{en}$, whose radiation is reflected n times at the cone walls upon entering the cone mouth. The effective absorptivity of the cone mouth for earth radiation is then

$$a_{me} = \sum_n a_n F_{m-en} \tag{122}$$

where  $a_n$  =  absorptivity produced by n cone wall reflections

$F_{m-en}$  =  view factor from cone mouth to the earth sub-area whose radiation is reflected n times at the cone walls

Values of $a_{me}$ for infrared and for earthshine were calculated for a right circular cone having the geometry of the vertical plane in the single-ended cooler. The values of $F_{m-en}$ were taken at the center of the cone mouth.

For the above spherical coordinate system, the partial view factor if given by (See Figure 20).

$$F_{m-en} = \frac{1}{\pi} \iint\limits_{\text{Visible } A_{en}} \sin \vartheta \cos \vartheta \, d\vartheta \, d\varphi \tag{123}$$

Integrating with respect to $\vartheta$, this becomes

$$F_{m-en} = \frac{1}{2\pi} \oint\limits_{\substack{\text{Visible boundary} \\ \text{of } A_{en}}} \sin^2 \vartheta \, (\varphi) \, d\varphi \tag{124}$$
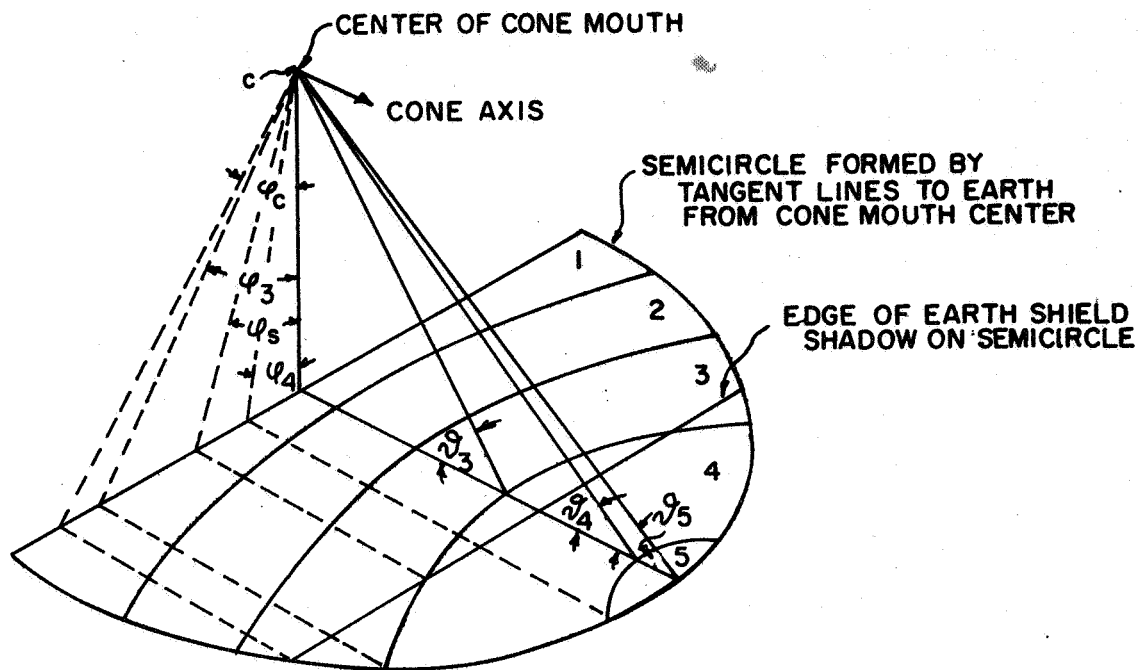
FIGURE 19    GEOMETRY FOR CALCULATION OF CONE MOUTH ABSORPTIVITY
FOR EARTH RADIATION
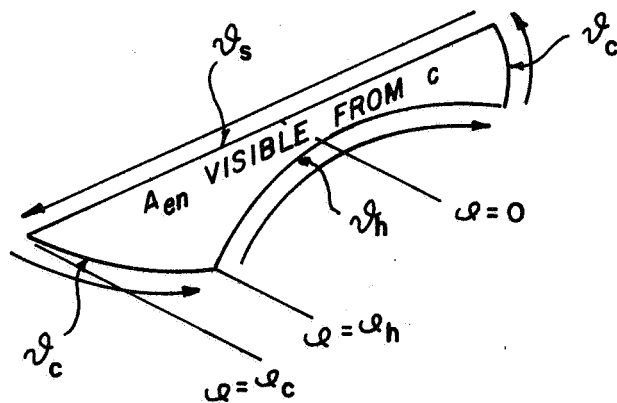


$$F_{m\text{-}en} = \frac{1}{2\pi}\int_{-\varphi_c}^{\varphi_c}\sin^2\vartheta_s\,d\varphi + \frac{1}{2\pi}\int_{\varphi_c}^{\varphi_n}\sin^2\vartheta_c\,d\varphi + \frac{1}{2\pi}\int_{\varphi_h}^{-\varphi_h}\sin^2\vartheta_h\,d\varphi + \frac{1}{2\pi}\int_{-\varphi_h}^{-\varphi_c}\sin^2\vartheta_c\,d\varphi$$

FIGURE 20    EVALUATION OF PARTIAL VIEW FACTOR

82

This integral is taken over the boundary of $A_{en}$ that is visible from the cone mouth center, as shown in Figure 20. As seen in Figure 19, only one sub-area, $A_{e5}$, can be seen in its entirety from the center of the cone mouth. Portions of two areas, $A_{e4}$ and $A_{e3}$, are visible. The rest of these two sub-areas plus the two remaining sub-areas, $A_{e2}$ and $A_{e1}$, are obscured by the earth shield and have zero view factors from the cone mouth center.

Applying equation (124) to sub-area 5, we obtain

$$F_{m-e5} = \frac{1}{2\pi} \int_{-\varphi_4}^{\varphi_4} \sin^2 \vartheta_4 \, d\varphi + \frac{1}{2\pi} \int_{\varphi_4}^{-\varphi_4} \sin^2 \vartheta_c(\varphi) \, d\varphi$$

where $\varphi_4$ is the value of $\varphi$ at which the cone $\vartheta = \vartheta_4$ intersects the semicircle and $\vartheta_c(\varphi)$ is $\vartheta$ as a function of $\varphi$ along the semicircle. In general a sub-area $A_{en}$ lies between the polar angles $\vartheta_n$ and $\vartheta_{n-1}$. Its boundary is further limited by the horizon $\vartheta_c(\varphi)$ and the edge of the earth shield or its projection. The above equation may be simplified to

$$F_{m-e5} = \frac{1}{\pi} \varphi_4 \cdot \sin^2 \vartheta_4 - \frac{1}{\pi} \int_0^{\varphi_4} \sin^2 \vartheta_c(\varphi) \, d\varphi$$

But, we also have

$$\sin^2 \vartheta_c(\varphi) = \frac{\sec^2 \varphi}{\sec^2 \varphi_0} \tag{125}$$

where $\varphi_0$ is the angle from the spacecraft nadir to the tangent line to the earth (60 degrees 49 minutes at 500 nautical miles). Substituting (125) into the preceding equation and integrating, we obtain

$$F_{m-e5} = \frac{1}{\pi} [\varphi_4 \cdot \sin^2 \vartheta_4 - \tan \varphi_4 \cdot \cos^2 \varphi_0]$$

To determine the other two view factors, it is necessary to know the value of $\vartheta$ as a function of $\varphi$ along the edge of the earth shield or its projection on the semicircle. This relationship is

$$\sin^2 \vartheta_s(\varphi) = \frac{1}{1 + \cos^2 \varphi \cdot \tan^2 \vartheta_0} \tag{126}$$

where $\vartheta_0$ is the vertical plane angle subtended by the earth shield at the cone mouth center (50 degrees 12 minutes for the design in Section 2.2.1).

Partial view factors 4 and 3 were obtained by applying equations (124) and (126). The results are

$$F_{m-e4} = \frac{1}{\pi} \left[ \cos \vartheta_0 \cdot \arctan (\cos \vartheta_0 \cdot \tan \varphi_S) - \cos^2 \varphi_0 (\tan \varphi_3 - \tan \varphi_4) \right.$$
$$\left. - \varphi_4 \cdot \sin^2 \vartheta_4 + (\varphi_3 - \varphi_S) \sin^2 \vartheta_3 \right]$$

$$F_{m-e3} = \frac{1}{\pi} \left[ \cos \vartheta_0 (\arctan <\cos \vartheta_0 \cdot \tan \varphi_c > - \arctan < \cos \vartheta_0 \cdot \tan \varphi_S >) \right.$$
$$\left. - (\varphi_3 - \varphi_S) \sin^2 \vartheta_3 - \cos^2 \varphi_0 (\tan \varphi_c - \tan \varphi_3) \right]$$

where $\varphi_n$ = value of $\varphi$ at intersection of cone $\vartheta = \vartheta_n$ with the semicircle

$\varphi_S$ = value of $\varphi$ at the intersection $\vartheta_S (\varphi) = \vartheta_3$

$\varphi_c$ = value of $\varphi$ at the intersection $\vartheta_c (\varphi) = \vartheta_S (\varphi)$

Note that the sum of $F_{m-e5}$, $F_{m-c4}$, and $F_{m-c3}$ is the view factor, $F_{me} = F_{de}$, from the cone mouth or cone end to the earth and has a value of 0. 0431.

The values of $\vartheta_n$ and $\varphi_n$ for n = 3, 4, 5 are listed in Table 16 for a right circular cone having the geometry of the vertical plane of the design shown in Section 2. 2. 1. These values were used to calculate

Table 16

Intersection of Cone $\vartheta = \vartheta_n$ with Earth Horizon

| n | $\vartheta_n$ | $\varphi_n$ |
|---|---|---|
| 3 | $43^O$ 31' | $44^O$ 55' |
| 4 | $29^O$ 42' | $10^O$ 13' |
| 5 | $29^O$ 11' | $0^O$ |

the three partial view factors for $\varphi_0$ = 60 degrees 49 minutes (spacecraft altitude of 500 nautical miles) and $\vartheta_0$ = 50 degrees 12 minutes (cooler design of Section 2. 2. 1). The angles $\varphi_S$ and $\varphi_c$ are then, from equations (125) and (126)

$\varphi_S$ = 28 degrees 40 minutes

$\varphi_c$ = 53 degrees 2 minutes

The view factors are given in Table 17 together with the values of $a_n$ for infrared and for earthshine. The $a_n$ were calculated for coatings on the cone walls of emissivity ($\epsilon_g$) 0. 086 and 0. 02 and solar absorptivity ($\alpha_g$) 0. 22 and 0. 183.

Table 17

Partial View Factors and Absorptivities

| n | $F_{m-en}$ | $\epsilon_g = 0.086$ | $\epsilon_g = 0.02$ | $\alpha_g = 0.22$ | $\alpha_g = 0.183$ |
|---|---|---|---|---|---|
| 5 | 0. 00053 | 0. 3621 | 0. 0950 | 0. 7113 | 0. 6360 |
| 4 | 0. 03545 | 0. 3021 | 0. 0776 | 0. 6299 | 0. 5545 |
| 3 | 0. 00713 | 0. 2364 | 0. 0588 | 0. 5255 | 0. 4547 |
| 2 | 0 | | | | |

The values in Table 17 were summed according to equation (122) to obtain the effective cone mouth absorptivities for earth infrared, $\epsilon_{me}$, and earthshine, $\alpha_{me}$. The results are listed in Table 18 for the above values of surface emissivity and surface solar absorptivity.

Table 18

Effective Cone Mouth Absorptivities for Earth Radiation

| $\epsilon_g$ | $\epsilon_{me}$ | $\alpha_g$ | $\alpha_{me}$ |
|---|---|---|---|
| 0. 086 | $1.26 \times 10^{-2}$ | 0. 22 | $2.65 \times 10^{-2}$ |
| 0. 02 | $3.22 \times 10^{-3}$ | 0. 183 | $2.32 \times 10^{-2}$ |

The effective cone mouth emissivity, $\epsilon_{mx}$, was calculated using the approach described in Section 1. 4. 1. 1 and used to determine the effective cone emissivity of the double-ended cooler in Section 2. 1. 3. The results are given in Table 19 for surface emissivities of 0. 086 and 0. 02.

Table 19

Effective Cone Mouth Emissivity

| $\epsilon_g$ | Vertical | Horizontal | Average |
|---|---|---|---|
| 0. 086 | 0. 2345 | 0. 1364 | 0. 185 |
| 0. 02 | 0. 0595 | 0. 0334 | 0. 0465 |

The effective patch-to-cone emissivity, $\epsilon_{pc}$, was calculated for the horizontal and vertical planes of the cooler using the technique outlined in Section 1.3.1. (See also Section 2.1.3.) This technique assumes a right circular cone having the geometry of the plane and that the patch is concentrated at its center (i.e., is strictly true for rays from the patch center). The results are listed in Table 20 for the two values of surface emissivity.

Table 20

Effective Patch-to-Cone Emissivity

| $\epsilon_g$ | Vertical | Horizontal | Average |
|---|---|---|---|
| 0.086 | 0.109 | 0.0581 | 0.0835 |
| 0.02 | 0.0262 | 0.01354 | 0.0199 |

## 2.2.3.2 Temperature Range

We now have all the emissivities and absorptivities needed to calculate the cone temperature from Equation (115). Conduction through the cone supports to the outer box is not included but will be covered in the next section. The value of average infrared earth emittance, $W_e$, is independent of spacecraft altitude and the average earthshine emittance, $W_s$, changes very little between 500 and 600 nautical miles. We will therefore use the values from Section 2.1.3, namely $W_e = 2.1 \times 10^{-2}$ watts/cm$^2$ and $W_s = 1.65 \times 10^{-2}$ watts/cm$^2$. The shield at a temperature, $T_t$, of 248 degrees K (Section 2.2.2) has an emittance of $1.84 \times 10^{-3}$ watts/cm$^2$ when coated with a surface of 0.086 emissivity. The cone end is assumed to be a surface whose emissivity, $\epsilon_d$, is 0.9 and solar absorptivity, $\alpha_d$, is 0.18. The view factors from the cone end, $F_{de}$ and $F_{dt}$, are given in the preceding section.

Using the vertical values of cone mouth absorptivities and the average values for the other absorptivities and emissivities, equation (115) yields for $\epsilon_g = 0.086$, $\alpha_g = 0.22$, and $A_p/A_m = 0.1$

$$\sigma T_c^4 = \frac{8.065 \times 10^{-4} + 16.30 \times 10^{-4} \frac{A_d}{A_m}}{0.9 \frac{A_d}{A_m} + 0.193} \qquad (127)$$

For a 0.9 inch wide cone end around the cone mouth, $A_d/A_m$ is 0.727, and equation (127) becomes

$$\sigma T_c^4 = 2.34 \times 10^{-3} \text{ watts/cm}^2$$

The cone temperature is then

$$T_c = 142.5 \text{ degrees K} \tag{128}$$

For a surface emissivity of 0.02, the shield emittance is reduced to 4.28 x $10^{-4}$ watts/cm$^2$, and equation (115) yields

$$\sigma T_c^4 = 1.77 \times 10^{-3} \text{ watts/cm}^2$$

for $\epsilon_g = 0.02$ and $\alpha_g = 0.183$. The cone temperature is then reduced to

$$T_c = 132.9 \text{ degrees K} \tag{129}$$

### 2.2.3.3  Cone Support

The temperature of the cone is increased by thermal conduction through the supports between the cone and outer box. Consider a support consisting of Synthane G-10 tubes, two 1-1/2 inches long, two 2-1/4 inches long, and all with 1/4 inch outside diameters and 3/16 inch inside diameters. This support conducts a power of

$$\Phi_s = 2KA \left( \frac{1}{\ell_1} + \frac{1}{\ell_2} \right) \cdot (T_t - T_c) \tag{130}$$

to the cone, where

$K$ = thermal conductivity = 7.46 x $10^{-3}$ watt/in degree C

$A$ = cross-sectional area of a tube = 2.15 x $10^{-2}$ square inches

$\ell_1$ = 1-1/2 inches

$\ell_2$ = 2-1/4 inches

$T_t$ = temperature of outer box and shield

$T_c$ = temperature of cone

For $T_t$ = 248 degrees K and $T_c$ = 142.5 degrees K, we have

$$\Phi_s = 0.0376 \text{ watt } (\epsilon_g = 0.086)$$

For $T_t$ = 248 degrees K and $T_c$ = 132.9 degrees K, we have

$$\Phi_s = 0.041 \text{ watt } (\epsilon_g = 0.02)$$

From equation (115) the total power radiated by the cone is given by

$$\Phi_c = A_m \left( \epsilon_d \frac{A_d}{A_m} + \epsilon_{mx} + \epsilon_{pc} \frac{A_p}{A_m} \right) \cdot \sigma T_c^4 \qquad (131)$$

For $\epsilon_g = 0.086$ and $\alpha_g = 0.22$, $T_c = 142.5$ degrees K in the absence of conduction through the support. The cone radiant power is then

$$\Phi_c = 0.464 \text{ watt } (\epsilon_g = 0.086)$$

For $A_d/A_m = 0.727$ and $A_m = 4.19 \times 8.66$ square inches. The cone support increases the power the cone must radiate to $0.464 + 0.0376 = 0.5016$ watt. This increases the emittance of a blackbody at the cone temperature to $2.53 \times 10^{-3}$ watts/cm$^2$ and the cone temperature to

$$T_c = 145.2 \text{ degrees K } (\epsilon_g = 0.086, \ \alpha_g = 0.22) \qquad (132)$$

This is an increase of 2.7 degrees K or about 2 percent.

For $\epsilon_g = 0.02$ and $\alpha_g = 0.183$, $T_c = 132.9$ degrees K in the absence of support conduction. The radiant power of the cone is then

$$\Phi_c = 0.291 \text{ watt } (\epsilon_g = 0.02)$$

Conduction through the support increases the power the cone must radiate to 0.332 watt. This increases the emittance of a blackbody at the cone temperature to $2.02 \times 10^{-3}$ watts/cm$^2$ and the cone temperature to

$$T_c = 137.4 \text{ degrees K } (\epsilon_g = 0.02, \ \alpha_g = 0.183) \qquad (133)$$

This is an increase of 4.5 degrees K or about 3 percent.

### 2.2.4 Patch

The patch is radiatively and conductively coupled to the cone. Conductive coupling is through the electrical leads and the in-orbit support. In addition, joule heating of the detector element introduces a thermal load to the patch. The side of the patch not emitting to cold space is radiatively isolated from the cone by a layer of multilayer insulation.

To begin with, the temperature range of the patch is calculated for radiative coupling only, i.e., for zero conduction and zero joule heating. The temperature range is then determined for a minimum in-orbit support, and the permissible in-orbit support established for maximum patch temperatures of 85 degrees K and 90 degrees K.

## 2.2.4.1 Temperature Range with Radiative Coupling Only

For only radiative coupling between the patch and cone, the patch temperature is given by

$$T_{pr} = (\epsilon_{pc})^{1/4} T_c \qquad (134)$$

when there is sufficient multilayer insulation between the cone and patch side facing away from cold space. For a cone surface emissivity of 0.086 and a solar absorptivity of 0.22, $\epsilon_{pc}$ equals 0.0835 (Section 2.2.3.1) and $T_c$ equals 145.2 degrees K (Section 2.2.3.3). The patch temperature is then

$$T_{pr} = 78.1 \text{ degrees K } (\epsilon_g = 0.086, \ \alpha_g = 0.22) \qquad (135)$$

For a cone surface emissivity of 0.02 and solar absorptivity of 0.183, $\epsilon_{pc}$ equals 0.0199 and $T_c$ equals 137.4 degrees K. The patch temperature is then

$$T_{pr} = 51.6 \text{ degrees K } (\epsilon_g = 0.02, \alpha_g = 0.183) \qquad (136)$$

## 2.2.4.2 Temperature Range with Joule Heating and Minimum In-Orbit Support

The addition of an in-orbit support and electrical circuitry introduces additional thermal inputs to the patch and increases its temperature. The in-orbit support and electrical leads add conductive coupling to the cone, and the bias current to the detector adds joule heat. To begin with, consider electrical circuitry designed for minimum thermal loading combined with a minimum practical in-orbit support.

The minimum electrical circuitry consists of three, 1 mil leads for the patch temperature measurement and control and two, 3.145 mil (No. 40) leads to the detector element. The detector requires larger diameter leads because of its low impedance (50 to 200 ohms). The minimum practical in-orbit support (i.e., one which is mechanically reasonable and introduces the least conductive coupling) will be taken as a six wire suspension of No. 40 titanium alloy.

The electrical leads introduce a conductive coupling coefficient between the cone and patch of

$$K_{c1} = \frac{K_1}{\ell_1} \Sigma A_j \qquad (137)$$

where $K_1$ = thermal conductivity of electrical wire

$\ell_1$ = length of a wire

$A_j$ = cross-sectional area of wire j

For the above five electrical leads made of drawn monel, $K_1 = 0.152$ watt/cm degrees C at 100 degrees K, and the conductive coefficient is

$$K_{c1} = 2.76 \times 10^{-3} \text{ mw/degrees K}$$

for $\ell_1 = 2.5$ inches. The in-orbit support introduces an additional conductive coefficient of

$$K_{c2} = 6 \frac{K_2 A_2}{\ell_2}$$

where $K_2$ = thermal conductivity of support wire

$A_2$ = cross-sectional area of a wire

$\ell_2$ = length of a wire

For titanium alloy, $K_2 = 5.0 \times 10^{-2}$ watt/cm degrees C at 100 degrees K, and the conductive coefficient is

$$K_{c2} = 6.58 \times 10^{-3} \text{ mw/degrees K}$$

for No. 40 (3.145 mil diameter) wires, each 0.9 inch long. The total conductive coupling coefficient is then

$$K_c = 9.34 \times 10^{-3} \text{ mw/degrees K}$$

For a conductive coupling coefficient $K_c$ between the cone and patch and a power J dissipated in the detector, the power radiated by the patch becomes

$$A_r \, \sigma T_p^4 = J + K_c (T_c - T_p) + A_r \, \sigma T_{pr}^4 \tag{138}$$

where $A_r$ = area of patch radiating toward cold space

$A_r \, \sigma T_{pr}^4$ = power radiated toward space for only radiative coupling

In addition to the radiation from the patch area directly facing cold space, about one-half the radiation from the patch area on the sides goes toward space. The other half of the side radiation strikes the multilayer insulation between the cone and the patch area facing away from space.

The patch is 0.4 inch thick (in order to accommodate the detector housing) and has a clearance to the cone of 0.05 inch on the side facing away from space. The patch dimensions, in inches, are 2.80 x 0.83 x 0.4, and the area radiating toward cold space is

90

$$A_r = 2.80 \times 0.83 + 0.4(2.80 + 0.83) = 3.78 \text{ in}^2$$

The power, $\Phi_p$, radiated toward space by a black patch is given in Table 21 for various patch temperatures.

Table 21

Patch Power Radiated Toward Space

| $T_p$, degrees K | $\Phi_p$, milliwatts |
|---|---|
| 51.6 | 0.98 |
| 78.1 | 5.14 |
| 80 | 5.65 |
| 85 | 7.21 |
| 90 | 9.05 |

For a cone wall emissivity of 0.086 and solar absorptivity of 0.22, $T_{pr}$ equals 78.1 degrees K and $T_c$ equals 145.2 degrees K. If J = 0.25 milliwatt (see Section 2.1.6.3) and $K_c$ = 9.34 x $10^{-3}$ mw/degrees K, the patch temperature must satisfy (equation 138)

$$1.38 \times 10^{-7} \ T_p^4 + 9.34 \times 10^{-3} \ T_p = 6.75 \text{ milliwatts}$$

for $A_r$ = 3.78 in$^2$. The solution is

$$T_p = 81.2 \text{ degrees K} \ (\epsilon_g = 0.086, \ \alpha_g = 0.22) \tag{139}$$

For an emissivity of 0.02 and a solar absorptivity of 0.183, $T_{pr}$ equals 51.6 degrees K and $T_c$ equals 137.4 degrees K. We then obtain from equation (138)

$$1.38 \times 10^{-7} \ T_p^4 + 9.34 \times 10^{-3} \ T_p = 1.23 \text{ milliwatts}$$

The solution is

$$T_p = 61.1 \text{ degrees K} \ (\epsilon_g = 0.02, \ \alpha_g = 1.83) \tag{140}$$

2.2.4.3    In-Orbit Support for Maximum Patch Temperature

We will now consider a second approach in which the patch is allowed to reach a prescribed maximum temperature (set, for example by detector sensitivity as a function of temperature). The maximum patch temperatures determines the conductive coupling coefficient and therefore the in-orbit support of maximum strength consistent with the thermal requirements. Such an in-orbit support tends to decrease the dependence on the patch caging mechanism during vibration.

91

The maximum patch temperature is the value attained for an emissivity of 0.086 and a solar absorptivity of 0.22. The allowable in-orbit support is determined for the electrical circuitry described in the previous section ($K_{c1}$ = 2.76 x $10^{-3}$ watt/cm degrees C and J = 0.25 milliwatt) and for maximum patch temperature of 85 degrees K and 90 degrees K.

At a maximum patch temperature, $T_p$, of 85 degrees K, equation (138) yields

$$60.2 \ K_c \ = \ 1.82 \text{ milliwatts}$$

$$K_c \ = \ 3.025 \text{ x } 10^{-2} \text{ mw/degrees K}$$

as the allowable total conductive coupling coefficient at an emissivity of 0.086 and a solar absorptivity of 0.22. Subtracting the conductive coupling, $K_{c1}$, produced by the electrical leads, we obtain the permissible conductive coefficient for the in-orbit support

$$K_{c2} \ = \ 2.745 \text{ x } 10^{-2} \text{ mw/degrees K}$$

This is the coefficient of a six wire suspension of 0.9 inch long, 6.4 mil diameter (approximately No. 34) titanium alloy wires. Another in-orbit support with about the same conductive coefficient consists of two Synthane G-10 tubes of 1/8 inch O.D. and 3/32 inch I.D., each 2.5 inches long.

At a maximum patch temperature of 90 degrees K, equation (138) yields

$$K_c \ = \ 6.63 \text{ x } 10^{-2} \text{ mw/degrees K}$$

at the maximum emissivity and solar absorptivity. Subtracting the coefficient for the electrical leads, the permissible coefficient for the in-orbit support becomes

$$K_{c2} \ = \ 6.35 \text{ x } 10^{-2} \text{ mw/degrees K}$$

This conductive coupling coefficient is produced by six titanium alloy wires of 9.7 mil diameter, each 0.9 inch long. Another in-orbit support with about the same conductive coupling consists of two Synthane G-10 tubes of 5/32 inch O.D. and 3/32 inch I.D., each 2.5 inches long.

The permissible in-orbit supports for maximum patch temperatures of 81.5, 85, and 90 degrees K are listed in Table 22 together with the corresponding minimum patch temperature (values attained for $\epsilon_g$ = 0.02 and $\alpha_g$ = 0.183). The results are for an electrical conductive coefficient of 2.76 x $10^{-3}$ mw/degrees K and a detector joule heating of 0.25 milliwatt.

Table 22

Permissible In-Orbit Supports
$$K_{c1} = 2.76 \times 10^{-3} \text{ mw/degrees K}$$
$$J = 0.25 \text{ mw}$$

| Patch Temperature Degrees K | | In-Orbit Supports Titanium Wires (6, 0.9 inch long) | Synthane G-10 Tubes (2, 2.5 inch long) | |
|---|---|---|---|---|
| Max. | Min. | Diam., mils | O. D. | I. D. |
| 81.2 | 61.2 | 3.145 | - | - |
| 85 | 69.8 | 6.4 | 1.8 inch | 3/32 inch |
| 90 | 78.1 | 9.7 | 5/32 inch | 3/32 inch |

## 3.0   TEST EQUIPMENT

The test equipment is used to determine the thermal performance of the two-stage radiant cooler under conditions simulating outer space operation (see Section 4.4). The equipment consists of a space chamber which contains a cold space reference (Section 3.1) cooled by a helium refrigerator. The temperature of the cold reference and radiant cooler are measured by means of resistance thermometers and thermocouples.

The main body of the T-shaped space chamber (Figure 21) is 36 inches in diameter and 45 inches long. The chamber is provided with a semiautomatic high vacuum pumping system and has been evacuated to a pressure of $5 \times 10^{-7}$ Torr measured at the top of its volume. The pressure should be no greater than about $2 \times 10^{-6}$ Torr for negligible heat transfer by the residual gas (Section 3.3).

The center access door of the chamber is used for insertion and removal of the cooler under test. The other two doors are used for mounting the copper cold reference and its aluminum shroud. The copper reference and aluminum shroud are shown inside the chamber in Figure 22. They are suspended from a stainless steel frame connected to the chamber by means of 304 stainless steel cables. The copper reference is painted with 3M Velvet Black on the two surfaces which face the cone mouths of the radiant cooler; it attains a maximum temperature of about 30 degrees K. The aluminum shroud reaches a maximum of about 100 degrees K. The cold reference is made of OFHC[6] copper and the shroud of 1100 aluminum.

The helium refrigerator used to cool the cold reference and shroud is a Norelco Model A-20, manufactured by North American Philips Company, Cryogenic Division, Ashton, Rhode Island. It can be seen connected to the rear of the space chamber in Figures 21 and 23. The cold exchangers of the refrigerator are within the vacuum and can be seen below the cold reference and shroud in Figure 22.

The refrigerator is shown in the photographs to be resting on a welded steel platform which is raised on jacks for mating to the chamber. This arrangement proved to be unstable during operation. A more rigid attachment of the space chamber and cryogenerator to the floor was needed along with a flexible flange coupling between the cryogenerator and chamber to prevent excessive loading on the cryogenerator. Figure 24 shows the mating arrangement; the chamber and cryogenerator are tied to the floor by steel beams, and the flexible coupling is provided by a stainless steel bellows with a spring rate of approximately 200 pounds per inch. The modified attachment and support permitted stable operation of the cryogenerator and proper cooling of the copper and aluminum (see Section 3.1). The equipment has been successfully operated for a total period of over 200 hours.

---

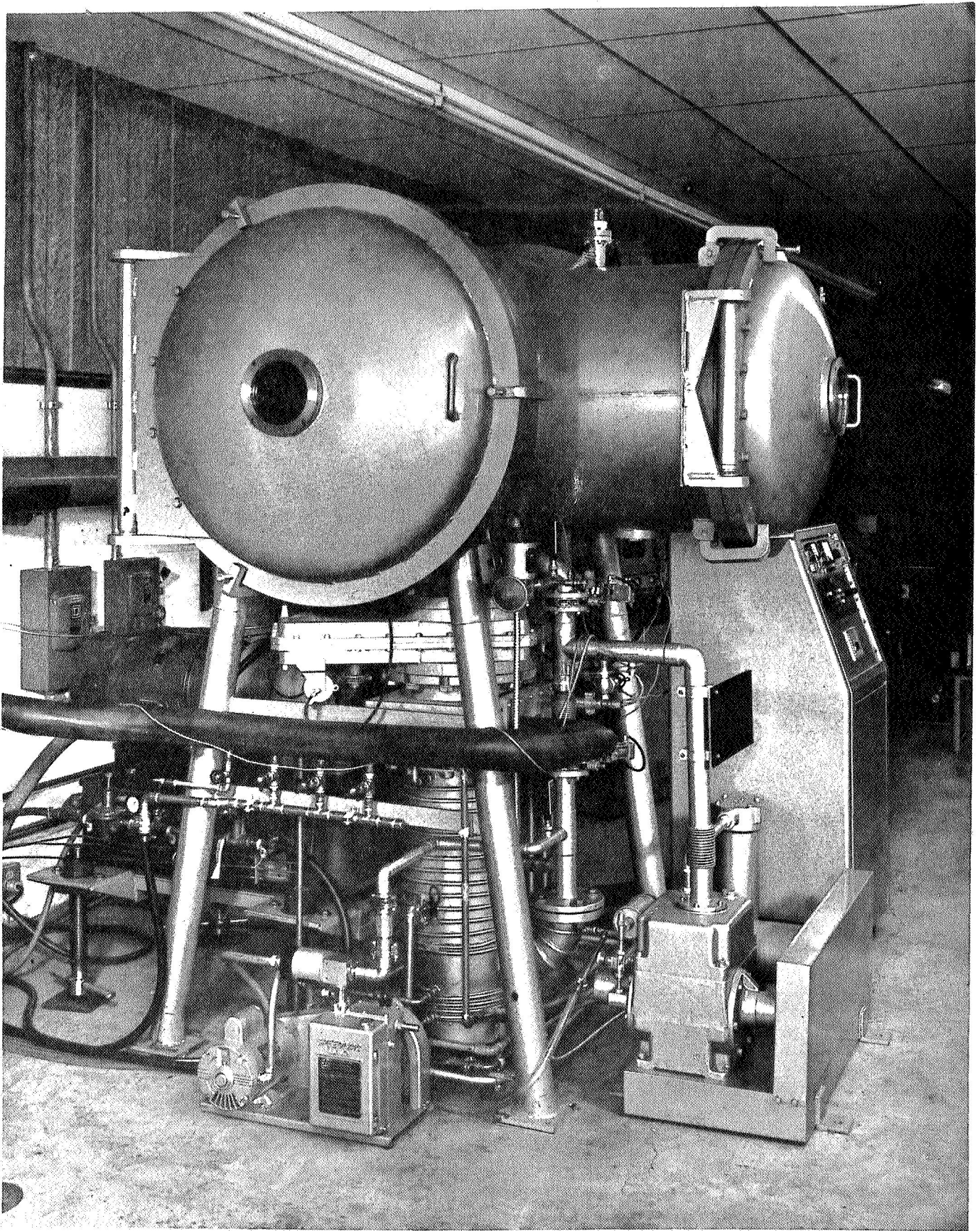6    Trademark of American Metal Climax, Inc.
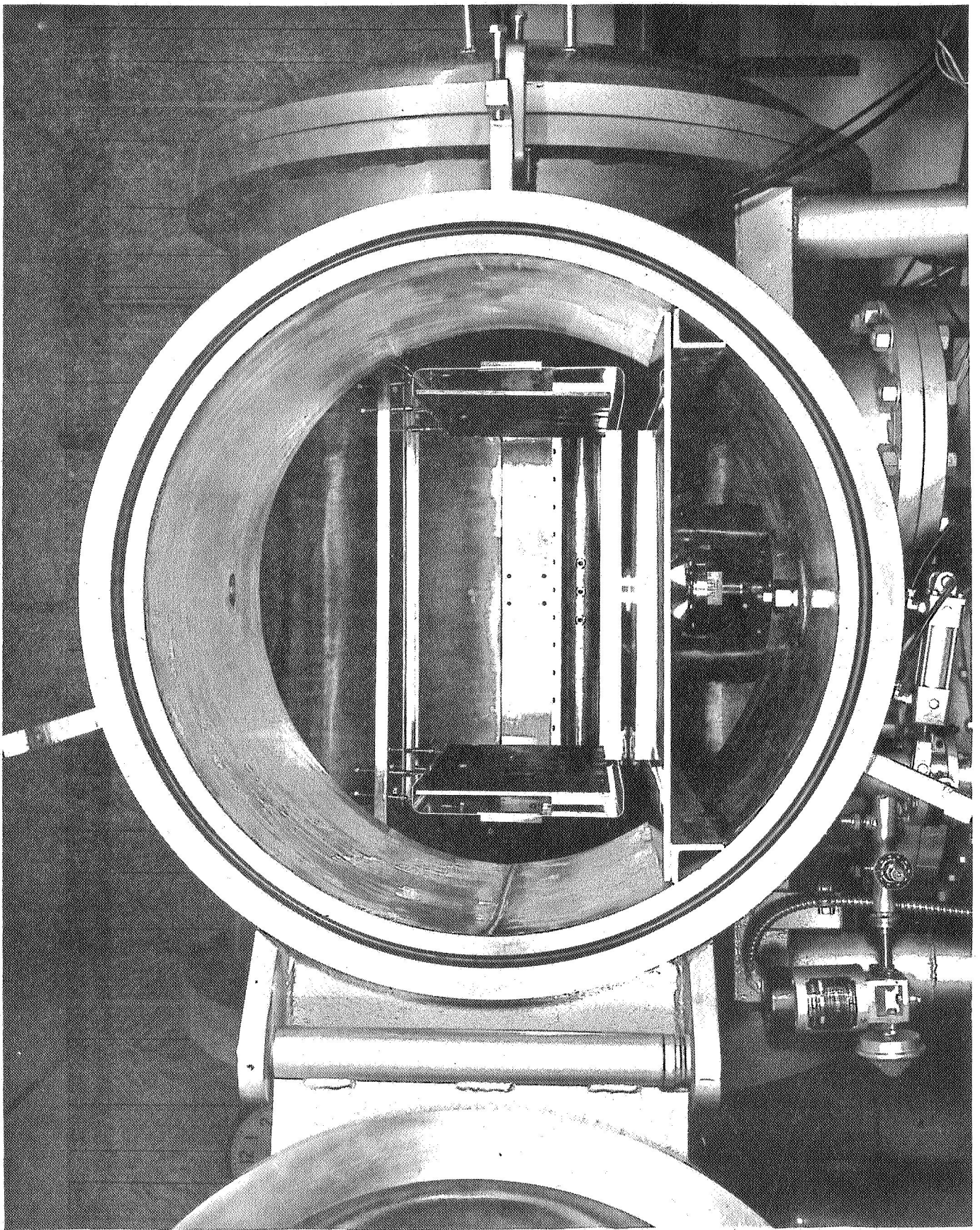
Figure 21    T-Shaped Space Chamber

95

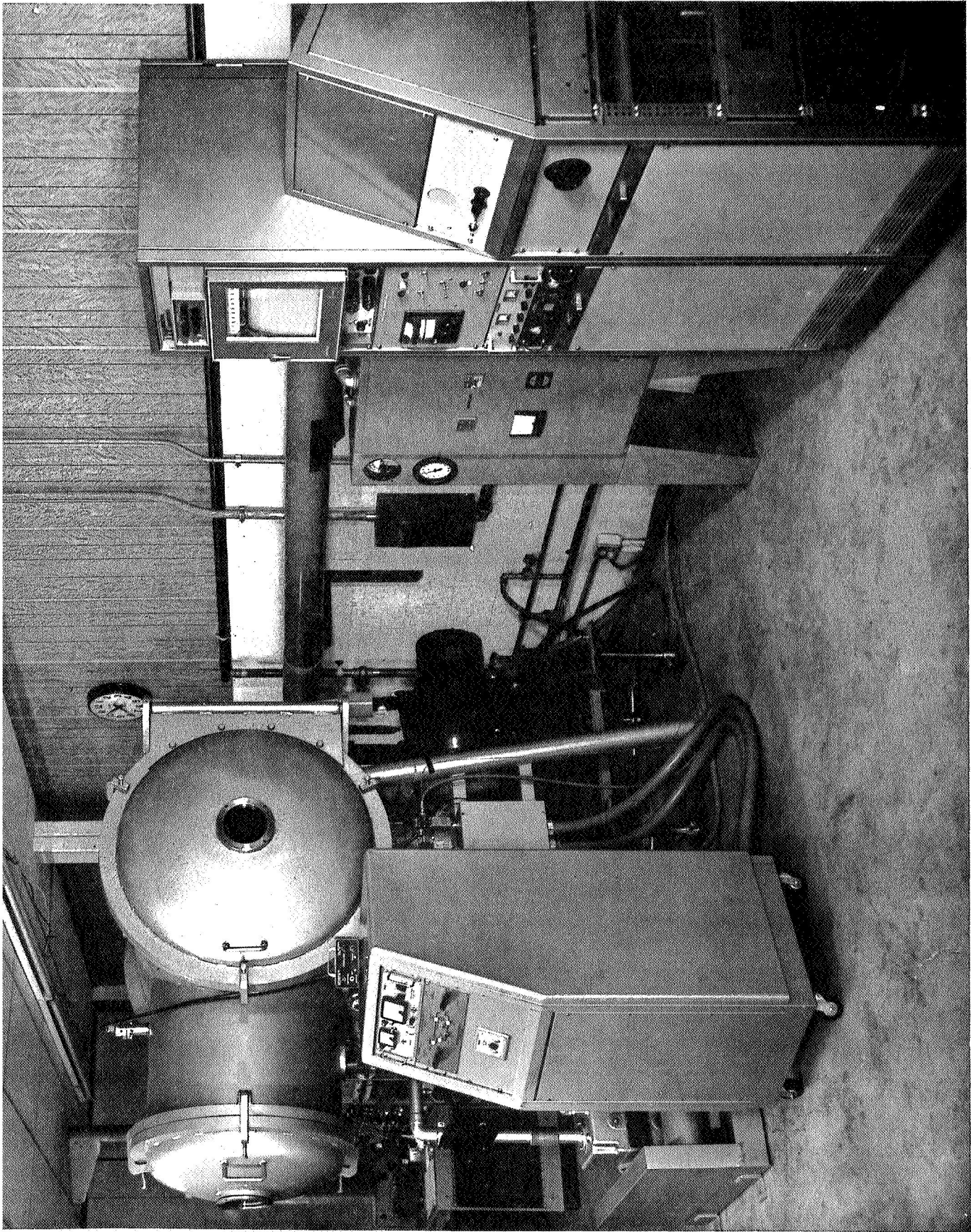Figure 22   Cold Reference and Shroud Mounted in Space Chamber

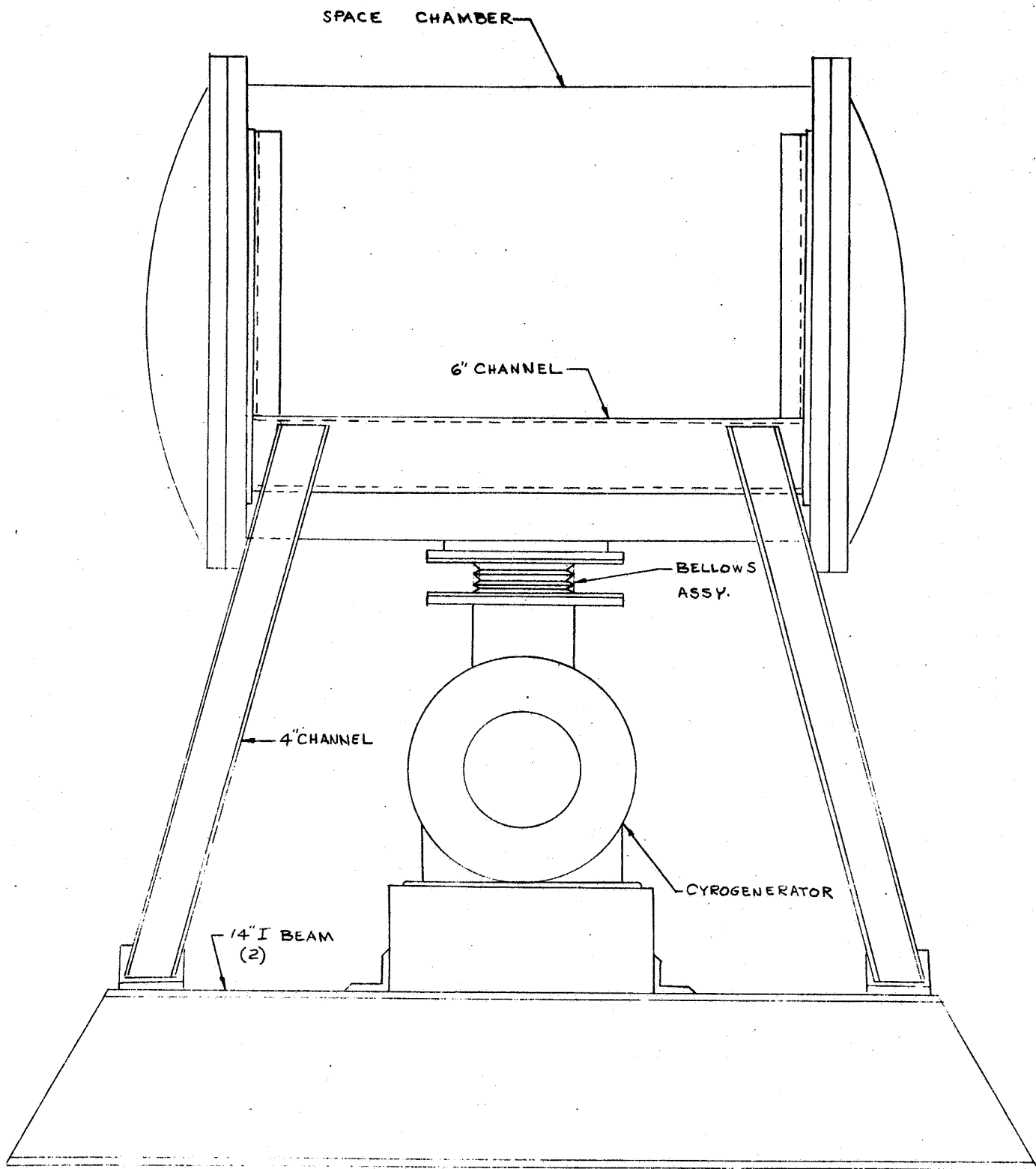Figure 23   Thermal-Vacuum Test Equipment

97

Figure 24 Space Chamber and Cryogenerator Support and Coupling

The controls and pressure gauges for the space chamber are housed in the free-standing cabinet with sloped front panel seen to the left in Figure 23. The two racks on the right (one with a sloping panel) contain the equipment for measuring and recording outputs from the temperature sensors. Thermocouples are used to measure temperatures in the radiant cooler and platinum resistance thermometers to measure the temperatures of the heat exchangers, cold reference, and shroud (Section 3.2). The signals from the thermocouples and resistance thermometer bridges are fed to a Honeywell Electronik 16 multipoint chart recorder. The console to the left of the rack holding the chart recorder contains controls and measuring instruments for the helium refrigerator.

### 3.1   Cold Space Reference

The second cold exchanger of a helium refrigerator (cryogenerator) cools a copper target used to simulate cold space. The copper target is shielded from ambient radiation by an aluminum shroud cooled by the intermediate cold exchanger of the helium refrigerator. Both the target and shroud are suspended in the space chamber as shown in Figure 25. The cable suspensions conduct a negligible amount of power from the space chamber to the copper target and aluminum shroud.

The copper reference has a volume of 482 cubic inches including connections to the second cold exchanger and weighs 155 pounds. It reaches thermal equilibrium in about 11 hours, as shown in Figure 26. The rapid drop in temperature below 80 degrees K is apparently due to the decrease in specific heat with decreasing temperature (see "Handbook of Chem. and Phys.", 44th Ed., Chemical Rubber Pub. Co., 1962, pp. 2352-2353). The cold reference temperatures given in Figure 26 were measured near the farthest point from the second cold exchanger.

The average cold reference equilibrium temperature for 5 tests was 29.5 degrees K and the average temperature drop to the second cold exchanger, 11.6 degrees K. The temperature drop corresponds to a thermal load on the copper of about 43 watts. This power was the equilibrium radiative loading from the chamber and the radiant cooler when the cooler was placed between the two copper reference plates. The thermal load from the aluminum shroud on the back side of the plates was negligible by comparison. The shroud attained an average thermal equilibrium temperature of 103 degrees K near the farthest point from the intermediate cold exchanger.

### 3.2   Temperature Measurements

The analysis (see Sections 1.0 and 2.0) of the radiative and conductive thermal transfer processes among the various components of the cooler, radiometer, and spacecraft shows the complexity of the problem due in large measure to the geometrical configuration of the radiating surfaces. Since certain assumptions have been made with respect to the temperature distribution (and other factors),

CRYOGENERATOR HEAD

COPPER COLD TARGET

ALUMINUM SHROUD

STAINLESS STEEL FRAME

COMPRESSION SPRING

STAINLESS STEEL CABLE

COLD FREEZER

INTERMEDIATE FREEZER
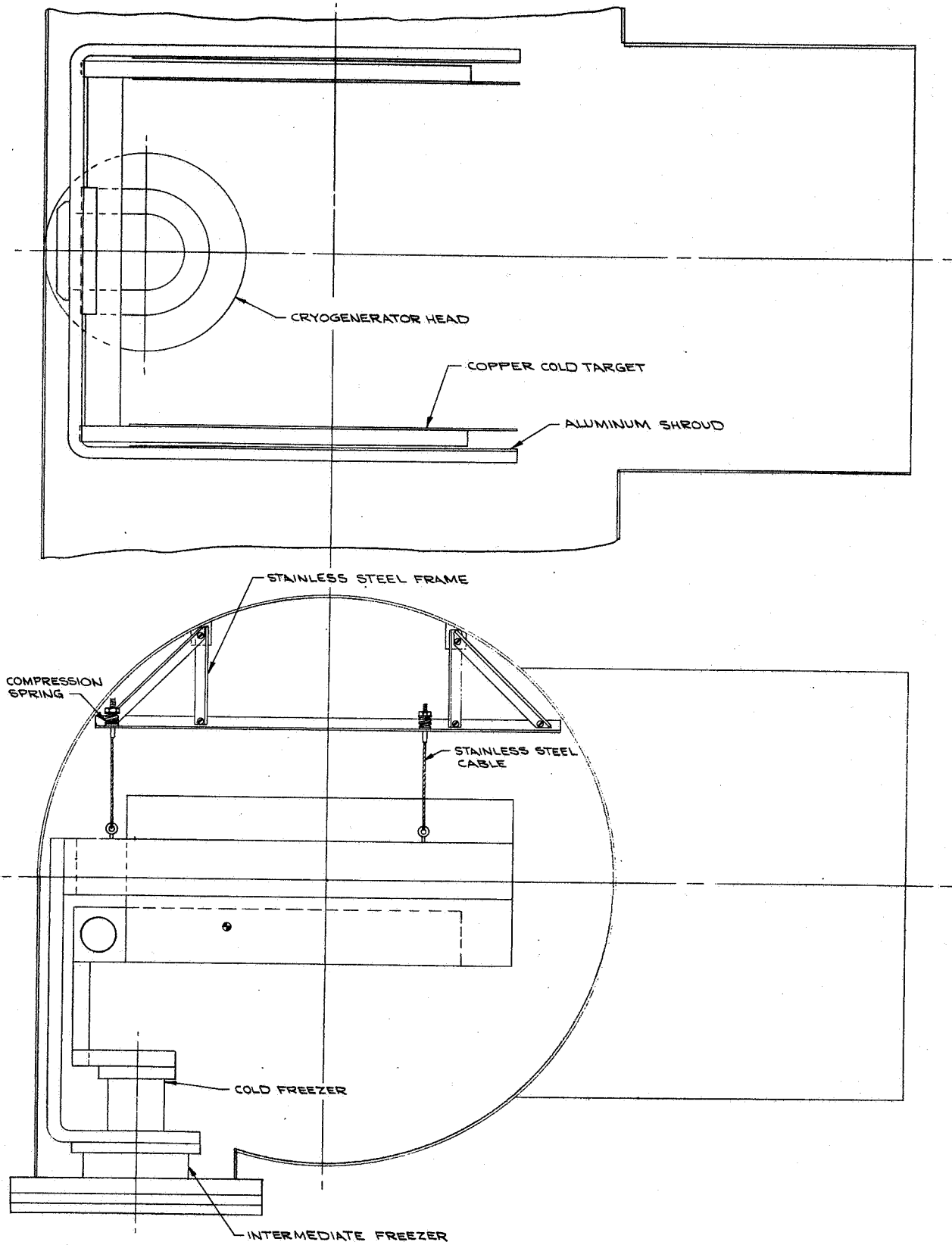
Figure 25 Suspension of Cold Target and Shroud in Space Chamber

100

°K

160
150
140
130
120
110
100
90

Aluminum
Shroud

Copper Cold
Reference

Second Cold
Exchanger

80
70
60
50
40
30
20
10

4  5  6  7  8  9  10  11  12  13  14  15  16  17  18  19  20  21  22  23  24

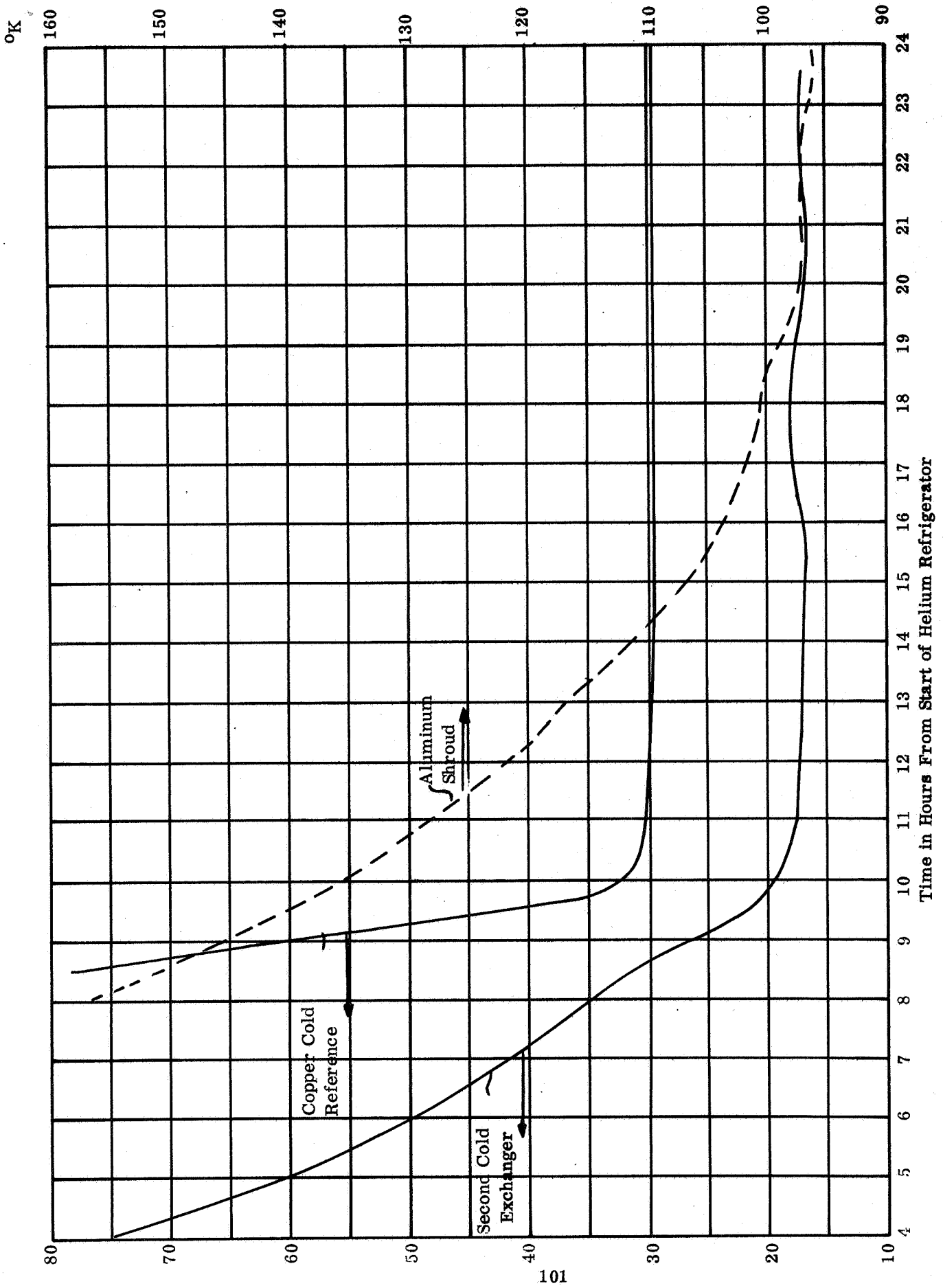Time in Hours From Start of Helium Refrigerator

Figure 26   Cool Down of Cold Space Simulator (Thermal Test 2)

101

the determination of this distribution under operating conditions which simulate as closely as possible the expected orbital flight condition is essential for the performance evaluation. Spot measurements of the temperatures at various points throughout the structure are made to determine the temperature distribution.

The measurements of spot temperatures are made using fine-wire thermocouples and a multipoint recorder to provide continuous recording of up to 24 channels. Since the range of temperatures (except for the helium refrigerator cold reference) is between 77 degrees K and 308 degrees K, the output voltage for a typical chromel P-alumel thermocouple is about -5.7 millivolts for 77 degrees K with 0 degrees C reference junction temperature. Operation with the reference temperature at or slightly above the highest expected temperature increases the output to about 7 millivolts (well suited for a 10 millivolt recorder span) and avoids the polarity reversal problems resulting from cross over of the reference junction temperature.

An important consideration here is the thermal conductance loading added by the thermocouple wires themselves. The Hoskins values for the thermal conductivity of chromel F and alumel are 0.199 and 0.297 watts per cm per degree C (at 100 degrees C) respectively. For a 0.003 inch diameter wire, the heat transfer along 1 cm of alumel with $\Delta T = 100$ degrees C is 1350 microwatts. Thus a couple 10 cm in length would provide about 270 microwatts thermal conductance load for a temperature difference of 100 degrees C or K. This magnitude of load has a negligible effect on the measured temperature, except in the case of the second-stage patch (Section 4.3.2).

The temperatures of the outer box, first-stage cone, and first-stage patch were measured with chromel-P-alumel thermocouples and that of the second-stage patch with a chromel-P-constantan thermocouple. The temperatures of the cold space reference, aluminum shroud, and helium refrigerator were measured with platinum resistance thermometers. In all cases the installations followed accepted low temperature practice. (See, for example: Baker, Ryder, and Baker, "Temperature Measurement in Engineering" Vol. I and II, John Wiley & Sons; or Scott, "Cryogenic Engineering", Van Nostrand).

Since the output of the chromel-P-alumel (and similar thermocouple combinations) is in the range of 0.02 to 0.04 millivolt per degree K down to the 77 degrees K temperature, the direct use of a 10 millivolt recording potentiometer instrument falls in the medium accuracy category. The normal (~10 inch) chart scale used on typical recorders (e.g. a Honeywell Electronik 16 recorder) is graduated to 0.1 millivolt and can be estimated fairly easily down to 0.02 millivolt. Thus without striving for high accuracy, the temperatures measured will be known to about 1 degree K. In view of the analysis of the radiative transfer processes, the uncertainties in the controlling surface parameters do not justify greater accuracy of the temperature determination.

## 3.3   Heat Transfer by Residual Gas

The residual gas pressure in the space chamber should be sufficiently low that the gas conducts a negligible amount of heat between surfaces. This is necessary for thermal simulation of in-orbit conditions. The following calculations show that the residual gas pressure should be no greater than about $2 \times 10^{-6}$ Torr. At this pressure the power conducted by the gas to a patch is about 1 percent of the power radiated by the patch.

The average pressure (over 6 tests) after evacuation of the radiant cooler but prior to starting the helium refrigerator was $1.6 \times 10^{-5}$ Torr. The cryo-pumping of the space simulator reduced this an average final value of $3.9 \times 10^{-7}$ Torr. The contribution of gas conduction to the thermal loads on the members of the cooler is entirely negligible at this pressure.

At low pressures (below $10^{-3}$ Torr), where the mean free path of the gas molecules is large compared to the dimensions of the structure, the power transported per unit area of the inner surface by free-molecule gas conduction is (R. H. Kropschot in "Applied Cryogenic Engineering", ed. by R. W. Vance and W. M. Duke, Wiley, 1962, p. 155)

$$H_g \quad = \quad K \, \alpha \, P \, (T_2 - T_1) \qquad\qquad (141)$$

where   K   =   a constant

   $\alpha$   =   over-all accommodation coefficient

   P   =   pressure

   $T_1$   =   absolute temperature of inner surface

   $T_2$   =   absolute temperature of outer surface

This equation is for concentric spheres, coaxial cylinders, and parallel plates. The constant K is given by

$$K \quad = \quad \frac{\gamma + 1}{\gamma - 1} \left( \frac{R}{8 \, \pi M T} \right)^{1/2}$$

where   $\gamma$   =   $C_p/C_v$, the specific heat ratio, assumed constant

   R   =   molar gas constant

   M   =   molecular weight of the gas

   T   =   absolute temperature at the point where P is measured

The over-all accommodation coefficient depends on the accommodation coefficients, $\alpha_1$ and $\alpha_2$, of the two surfaces according to

$$\alpha = \frac{\alpha_1 \ \alpha_2}{\alpha_2 + \alpha_1 (1 - \alpha_2) \dfrac{A_1}{A_2}}$$

where $A_1$ is the area of the inner surface and $A_2$ of the outer surface.

For $A_1/A_2$ equal to unity or less and for air at temperatures below 300 degrees K, $\alpha$ is approximately one, and

$$H_g = 1.5 \times 10^{-2} \ P \ (T_2 - T_1) \ \text{watts/cm}^2 \tag{142}$$

where P is in Torr and the temperatures are in degrees K. The temperature, T, at the pressure gauge is assumed to be 300 degrees K. Equation (142) will be used as an approximation to the geometries in the two-stage cooler.

In the space chamber the outer box is at about 290 degrees K and the first-stage cone at about 190 degrees K. The first-stage cone then emits about $1.5 \times 10^{-3}$ watts/cm$^2$. If the residual gas is to conduct 1 percent of this value, the pressure between the two surfaces must be no greater than

$$P = \frac{1.5 \times 10^{-5}}{1.5 \times 10^{-2} \times 10^2} = 1 \times 10^{-5} \ \text{Torr}$$

The addition of multilayer insulation would increase the maximum pressure.

Between the first-stage cone at 219 degrees K and the first-stage patch at 87 degrees, the maximum allowable pressure is

$$P = \frac{3.24 \times 10^{-6}}{1.5 \times 10^{-2} \times 132} = 1.6 \times 10^{-6} \ \text{Torr}$$

if the gas is to conduct 1 percent of the patch emittance of $3.24 \times 10^{-4}$ watts/cm$^2$.

Between the second-stage cone at 87 degrees K and the second-stage patch at 64 degrees K the maximum allowable pressure is

$$P = \frac{9.5 \times 10^{-7}}{1.5 \times 10^{-2} \times 23} = 2.7 \times 10^{-6} \ \text{Torr}$$

if the gas is to conduct 1 percent of the patch emittance of $9.5 \times 10^{-5}$ watts/cm$^2$.

## 4.0   EXPERIMENTAL RESULTS

The performance of the two-stage radiant cooler was determined experimentally using the double-ended model shown in Figures 27 through 30. The detailed design is given in Section 2.1.

The outer box and first-stage cone are constructed of 0.75 inch laminated panel with a foamthane core. The skins are 0.025 inch Alzak treated aluminum and 0.025 inch mill-finished aluminum. Three Alzak and one mill-finished surface form the outer surface of the box (Figure 27), with the latter on the side that would face the spacecraft. The Alzak surface facing the first-stage cone on the inside of the box is covered with 0.5 mil aluminized mylar.

The outer surface of the first-stage cone (Figure 28) is mill-finished aluminum. The cone is connected to the outer box by 8 fiberglas epoxy tubes, each of 1/2 inch OD, 1/4 inch ID and 1.5 inches length. The first-stage patch (Figures 29 and 30) is made of 0.025 inch aluminum shell and coated with 3 M Black Velvet. The patch is supported by two in-orbit fiberglas epoxy tubes of 1/4 inch diameter and 1/32 inch wall, each 4 inches long.

The second-stage cone (Figure 29) is molded rigid polyurethane foam; its surfaces are all covered with 0.5 mil aluminized mylar. The second-stage patch (Figure 30) is made of machined aluminum parts and coated with 3M Black Velvet. It is supported by a 1.42 inch long fiberglas epoxy tube of 1/8 inch OD and 3/32 inch ID.

Openings are provided in the cones and first-stage patch for the optical beam to the second-stage patch. The support tubes act as conduits for the electrical leads to the patches.

The feasibility of the two-stage radiant cooler was demonstrated during thermal test 7. The results of this test are covered in Sections 4.2 and 4.3. When corrected for the minimum cold reference reflectivity of 2 percent, the second-stage patch attained a temperature near 77 degrees K. The heat load conditions were made realistic by operating the first-stage cone near its expected in-orbit temperature. The orbital cone temperature had been estimated for a Nimbus-type orbit at an altitude of 600 nautical miles and an orbit normal to sun angle of 79 degrees (Section 4.4). Realistic mechanical conditions in critical cooler parts were insured by the successful vibration tests conducted on the patch assembly (Appendix II).

The accuracy of simulation of orbital operation is presently limited by the reflection of radiation from the first-stage cone to the first- and second-stage patches by way of the flat cold space reference (Section 4.5). For a nominal
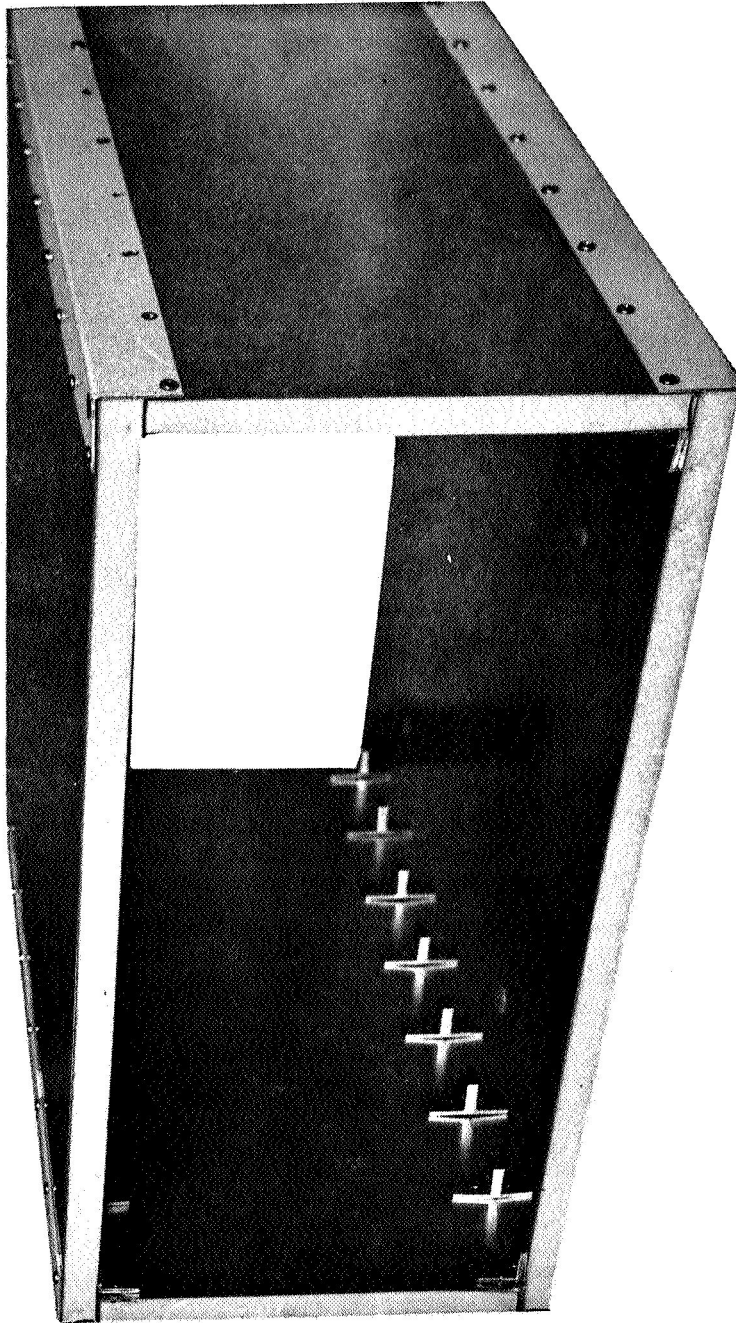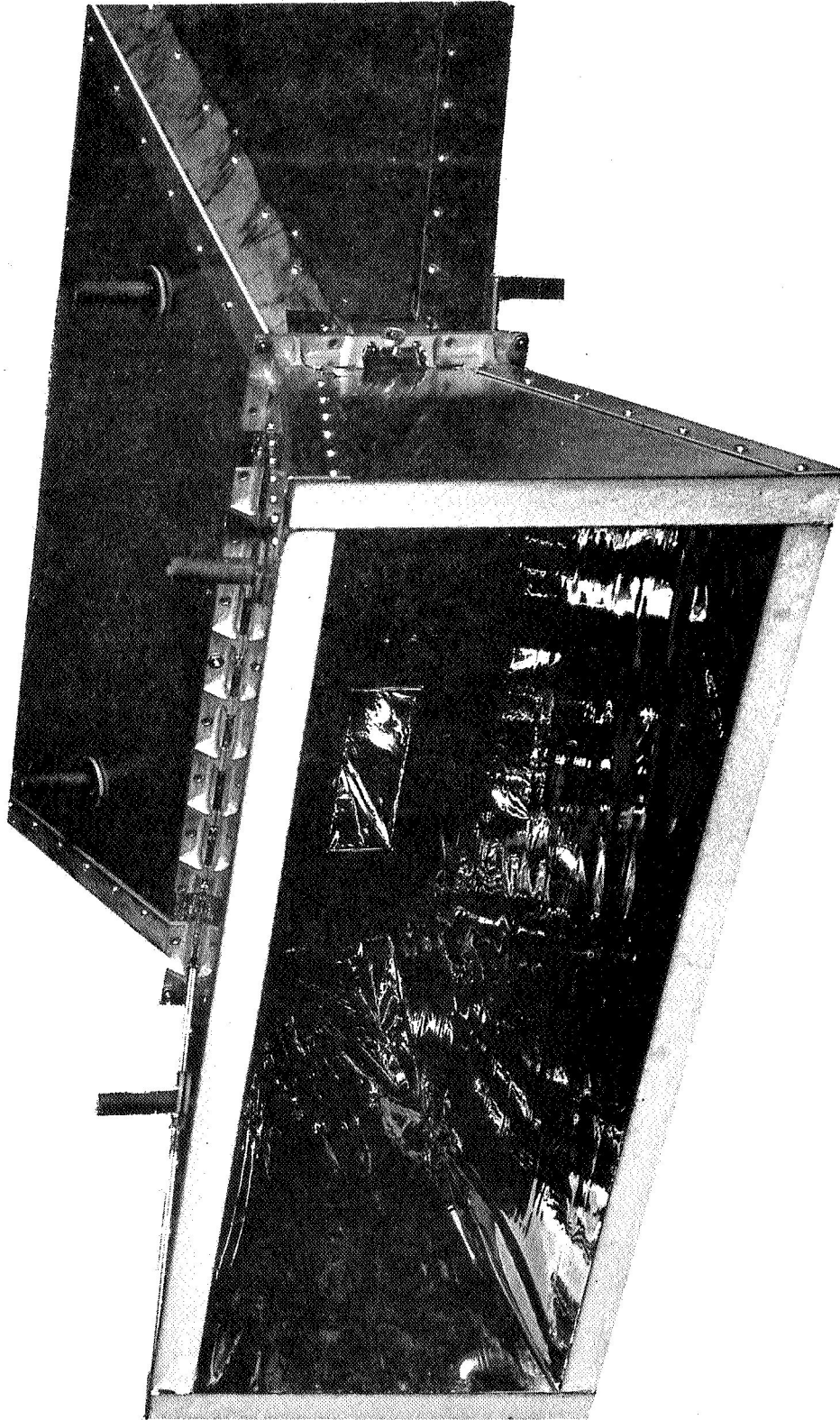
Figure 27  Outer Box

106

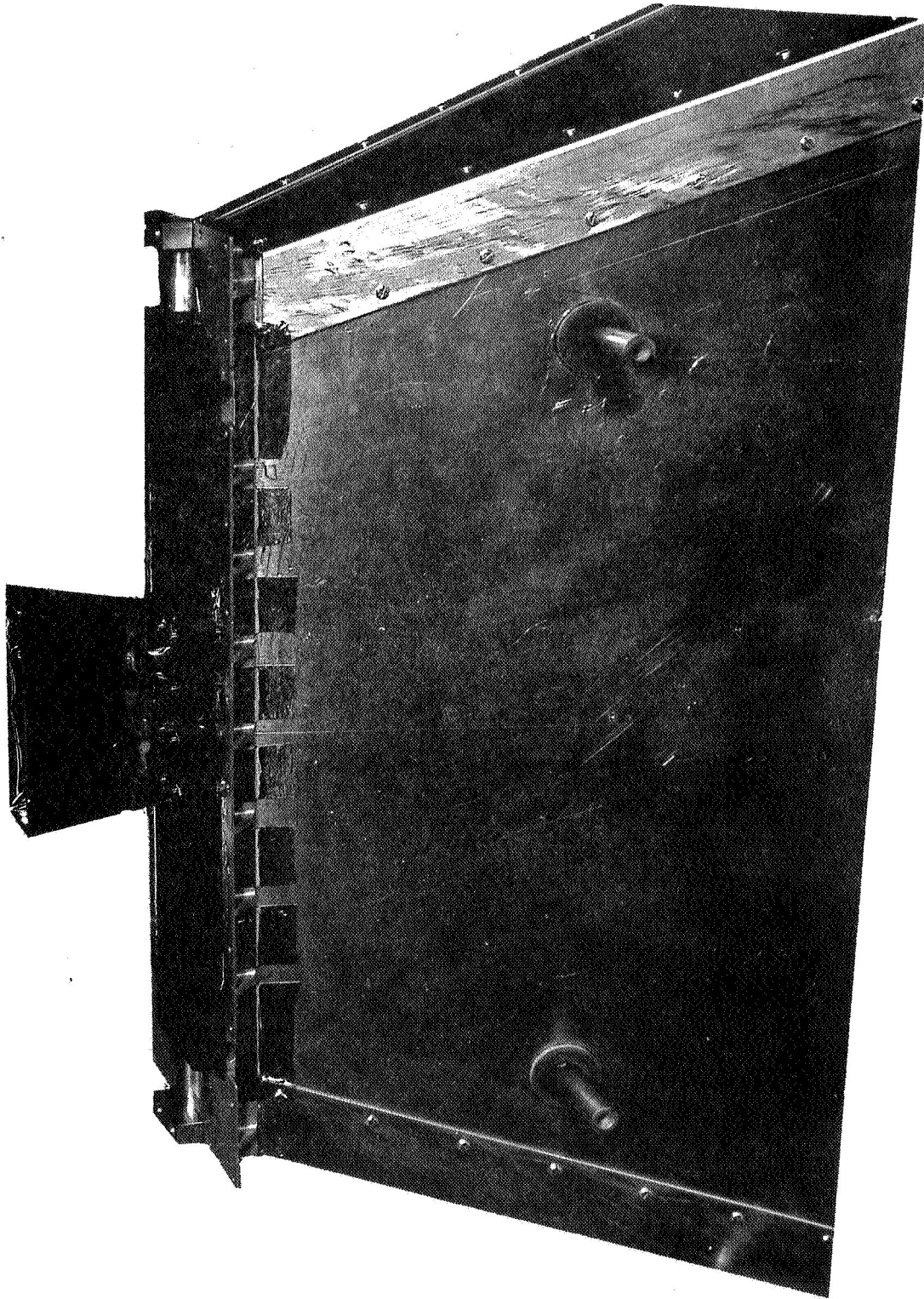Figure 28    First–Stage Cone

107
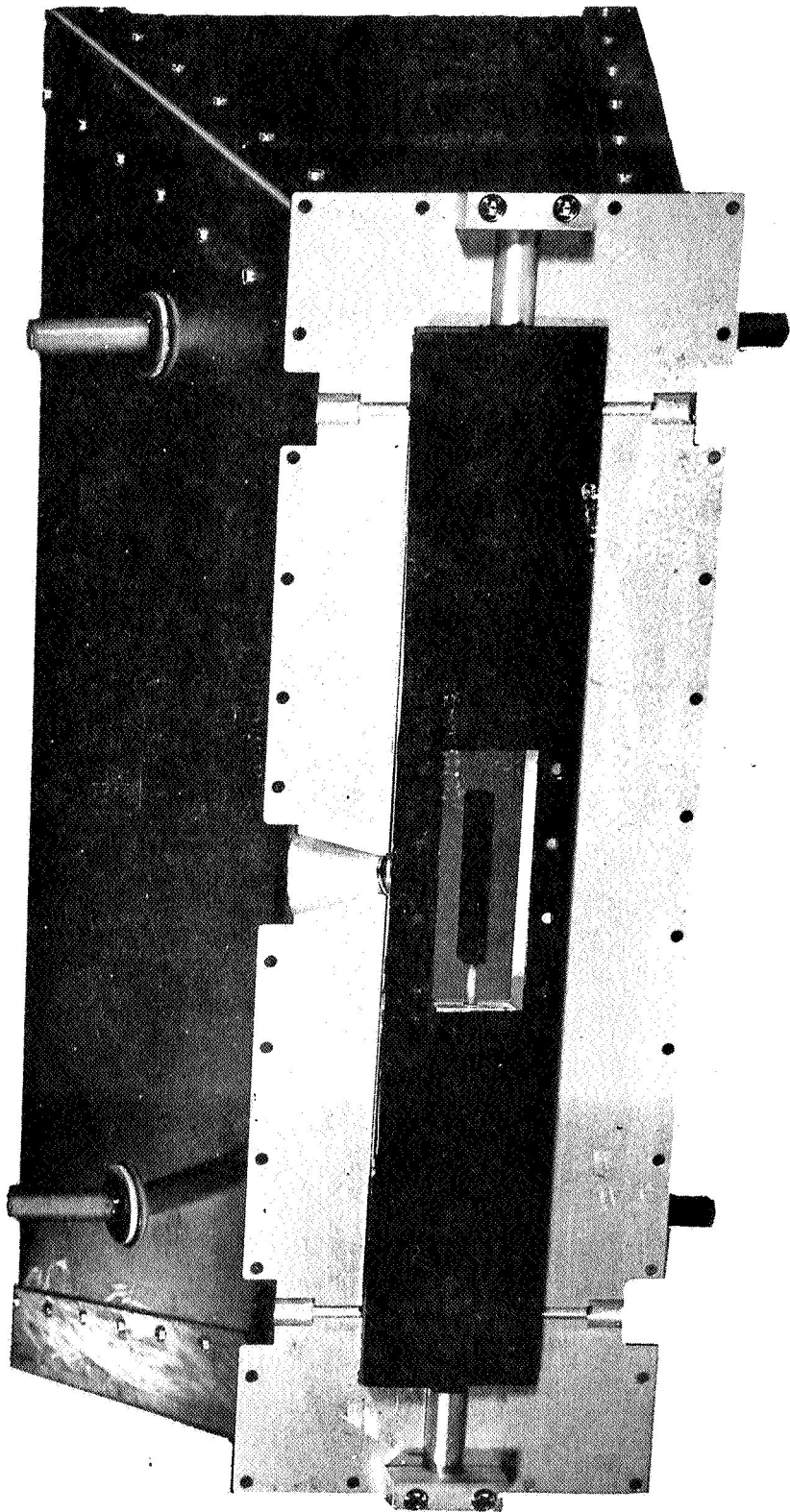
Figure 29   First-Stage Patch and Second-Stage Cone

Figure 30  First- and Second-Stage Patches

reference reflectivity of 5 percent, the total increase in the temperature of the second-stage patch is about 8 degrees K. The error produced by a reference temperature of 30 degrees K, which is above that of outer space (4 degrees K), is negligible by comparison. The reflectivity of the space reference can be reduced (absorptivity increased) by the use of the cavity effect, e. g. , by covering the surface with triangular grooves.

Analysis of thermal tests on a single-stage radiant cooler (Sections 4. 1 and 4. 3. 1) shows that the emissivity of the cone surface is 0. 070 ± 0. 007 when corrected for a space reference reflectivity of 0. 05 ± 0. 03. Analysis of thermal test 7 on a two-stage cooler (Section 4. 3. 1) shows that the performance of the first-stage patch in a two-stage cooler can be accurately predicted from data on a single-stage cooler.

Estimates of radiative transfer parameters are less accurate in the second-stage (Section 4. 3. 2). The error introduced by the imperfect cold space reference is larger, and the geometry of the patch-cone structure is more complex. For the nominal reference reflectivity of 0. 05, the estimated cone surface (aluminized mylar) emissivity in the second stage is 0. 066, which is close to the first-stage value. The measured temperature of the second-stage patch was about 5 percent below that predicted by the thin patch model (Section 2. 1. 5).

## 4. 1    Single-Stage Radiant Cooler

Four thermal tests were conducted on single-stage models of the two-stage radiant cooler. The first two tests were on a cooler with an Alzak cone surface covered with evaporated aluminum and gold. The second two were on a cooler with a cone surface covered with aluminized mylar. Patches in both coolers were painted with 3M Black Velvet and were supported at two ends by Synthane G-10 (in-orbit) support tubes of 1/4-inch outside diameter and 3/16-inch inside diameter. The support tubes were not covered with evaporated gold or wrapped with multilayer insulation (See Section 3. 1. 5). However, the radiative coupling to the surfaces of the tubes were reduced by concentric cylindrical inserts mounted to the patch and covered on their inner surfaces with evaporated gold (See Section 2. 1. 5, Figure 13). In addition to the openings through the cone wall for the support tubes, openings were provided for the optical beam and the four patch caging pins.

Temperature measurements during the first radiant cooler test are shown in Figure 31. Time is measured from the start of the A-20 helium refrigerator. The temperatures of the outer box, cone, and patch were measured by means of chromel-alumel thermocouples. The cone temperature was measured near its ends and at the frame in the center. There was a 3 to 4 degree K temperature difference from either end to the center of the cone. After about 12 or 13 hours the regular decrease in temperatures was interrupted, as shown by the break in the curves of temperature versus time. This was probably caused by the cracking and flaking of
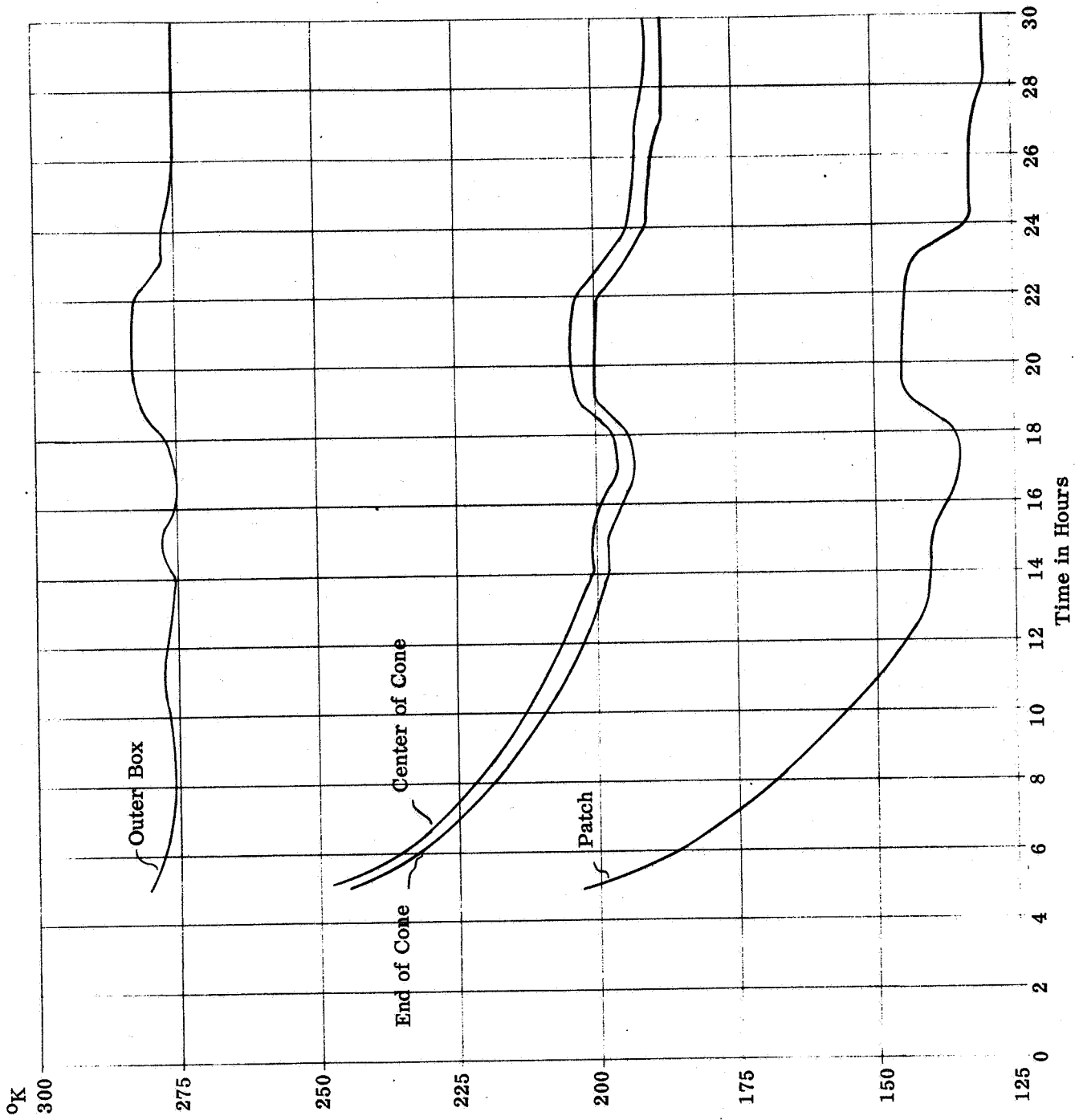
Figure 31 Radiant Cooler Test No. 1 (Au on Aℓ on Alzak Cone)

111

the paint (3M Black Velvet) on the copper space reference, which was evident on removal of the cooler. Toward the end of the test run, "frost" was evident on the cold exchanger of the A-20; this appears to have been produced by air leaking into the vacuum system. After the A-20 had been turned off to allow it to warm up, large volumes of gas were given off by the cold exchangers, copper reference, and aluminum shroud.

Following completion of the first thermal test and removal of the radiant cooler, the vacuum system was restarted (the helium refrigerator was not turned on). It was evident that a leak had developed; the pressure reached only $2 \times 10^{-4}$ Torr. A large leak was located in the O-ring seal of the front chamber door and a second, smaller leak in the O-ring seal of the air-release line. After repair of these leaks, the vacuum system operated satisfactorily, reaching pressure of 1.8 $\times 10^{-6}$ Torr after 5 hours of pumping.

The copper and plates used to simulate cold space were removed from the space chamber and cleaned of paint and primer. The plates were then sandblasted, repainted with 3M Black Velvet (no primer was used), and baked in an oven to set the paint. No cracking or flaking of the new paint surface was evident following temperature cycles from ambient to 30 degrees K and back during the remaining thermal tests (scraping and scratching were a problem, however, as discussed in Section 4.2).

Because of the problem with the space simulator and with vacuum leaks during the first run, a second thermal test was made on the Alzak cooler model. The results are shown in Figure 32. The patch reached a final (equilibrium) temperature of 113 degrees K with the cone at 177 degrees K (average over surface) and the outer box at 269 degrees K. Analysis of these results (Section 4.3.1) showed that they are not adequate; the cone surface has an emissivity about 2.3 times the maximum design value (0.086).

The second single-stage cooler to be tested has a cone surface of aluminized mylar. This surface was obtained by attaching sheets of 0.5-mil mylar covered with evaporated aluminum to the cone walls. The temperature measurements during the first test of this cooler (thermal test 3) are shown in Figure 33. The patch attained an equilibrium temperature of 88 degrees K with the cone at 183 degrees K and the outer box at 279 degrees K. The patch temperature is about 10 percent below the expected in-orbit value because the thermal load on the cone was too low (Section 4.4).

Relocation of the ambient sensor after thermal test 5 (Section 4.2) showed that a significant temperature difference could exist between the thermocouple reference junctions and the original position of the ambient sensor. This made the results of all previous thermal tests questionable. We therefore repeated the
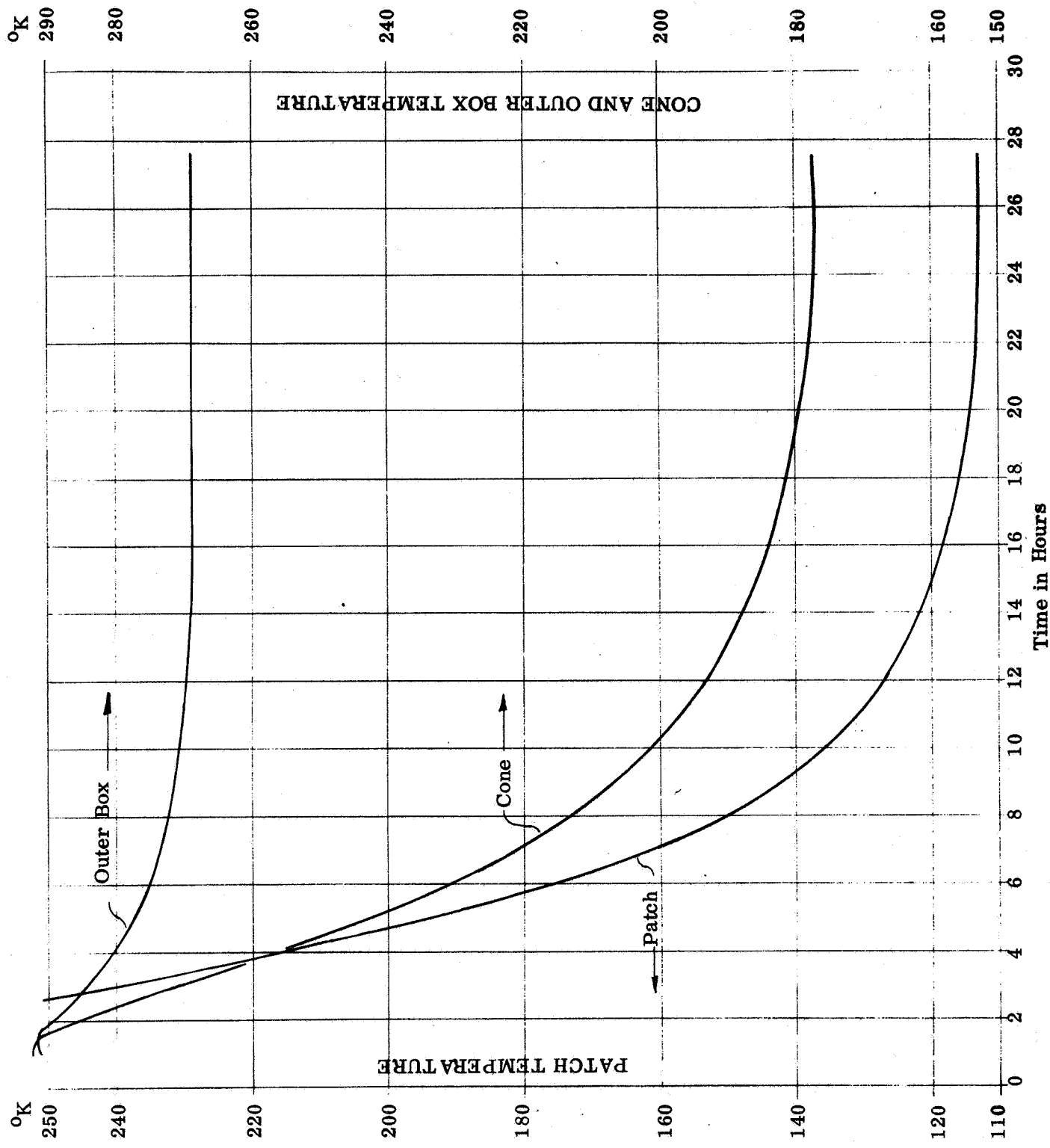
Figure 32 Radiant Cooler Test No. 2 (Au on Aℓ on Alzak Cone)

113
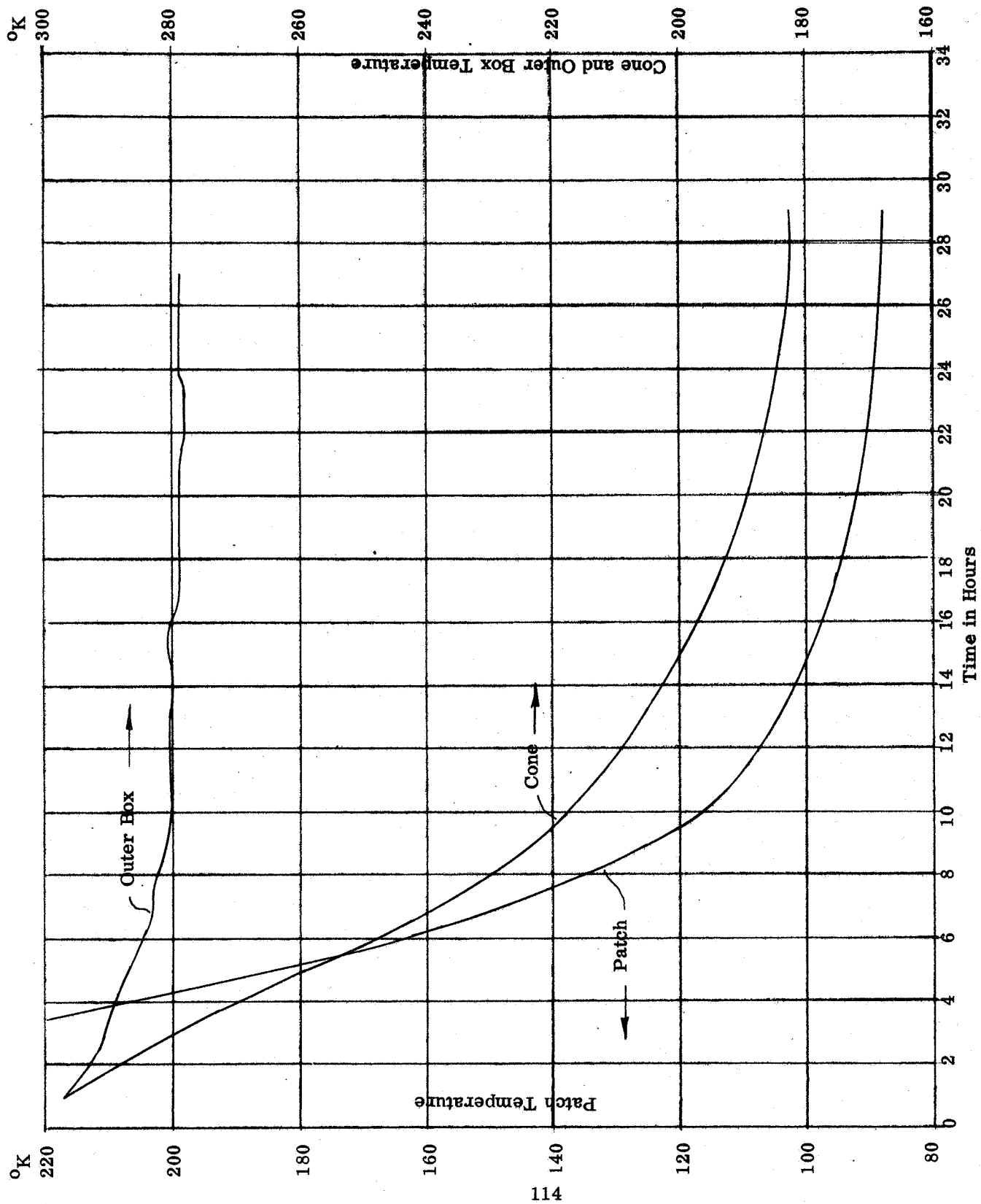
Figure 33 Radiant Cooler Test No. 3 (Aluminized Mylar Cone)

114

thermal test of the single-stage cooler with aluminized mylar attached to the cone walls (test 3). This time the ambient sensor was attached to the input board for the thermocouple wires. In addition, a blower was installed above the recorder to reduce temperature gradients in the test rack and to prevent high reference junction temperatures (and therefore large corrections when calculating thermocouple outputs referenced to 0 degrees C).

The temperature measurements during thermal test 6 (repeat of test 3) are shown in Figure 34. The cooler attained the following equilibrium temperatures (averages of 8 readings over a 5 hour period).

| | |
|---|---|
| Outer box | 288 degrees K |
| Cone | 204.4 degrees K |
| Patch | 105.1 degrees K |

The Alzak surface on the inside wall of the box was covered with aluminized mylar to attain better simulation of in-orbit thermal conditions. The other three box surfaces facing the cone (all mill-finished aluminum) were not covered. The result was a cone temperature within the expected orbital range (200 degrees K to 205 degrees K, Section 4.4).

The equilibrium patch temperature was corrected for the affect of a non-black space reference (Section 4.5.2.1). The results are shown in Table 23 for space reference reflectivities of 8, 5, and 2 percent. The 3M Black Velvet coating probably has a reflectivity of about 5 percent for greybody radiation at the cone temperature, $T_c$.

<div align="center">Table 23</div>

<div align="center">Single-Stage Measurements Corrected for Reference Reflectivity<br>(Test No. 6)</div>

| Space Reference Reflectivity | Correction to Patch Temperature % | $\Delta T_p$ | Corrected Patch Temperature ($T_p$) | $T_p/T_c$ |
|---|---|---|---|---|
| 0.08 | 6.6 | $-6.9^{\circ}K$ | $98.2^{\circ}K$ | 0.4804 |
| 0.05 | 4.2 | $-4.4^{\circ}K$ | $100.7^{\circ}K$ | 0.4926 |
| 0.02 | 1.7 | $-1.8^{\circ}K$ | $103.3^{\circ}K$ | 0.5053 |

The value of $T_p/T_c$ for test 3 was 0.481. Test 6 yielded a value of 2.4 percent higher for a reference reflectivity of 5 percent.

During test 6, a thermocouple was used to monitor the temperature difference between the reference junctions and the original positions of the ambient sensor. The difference was relatively stable at about 1 degree C and never exceeded this value.
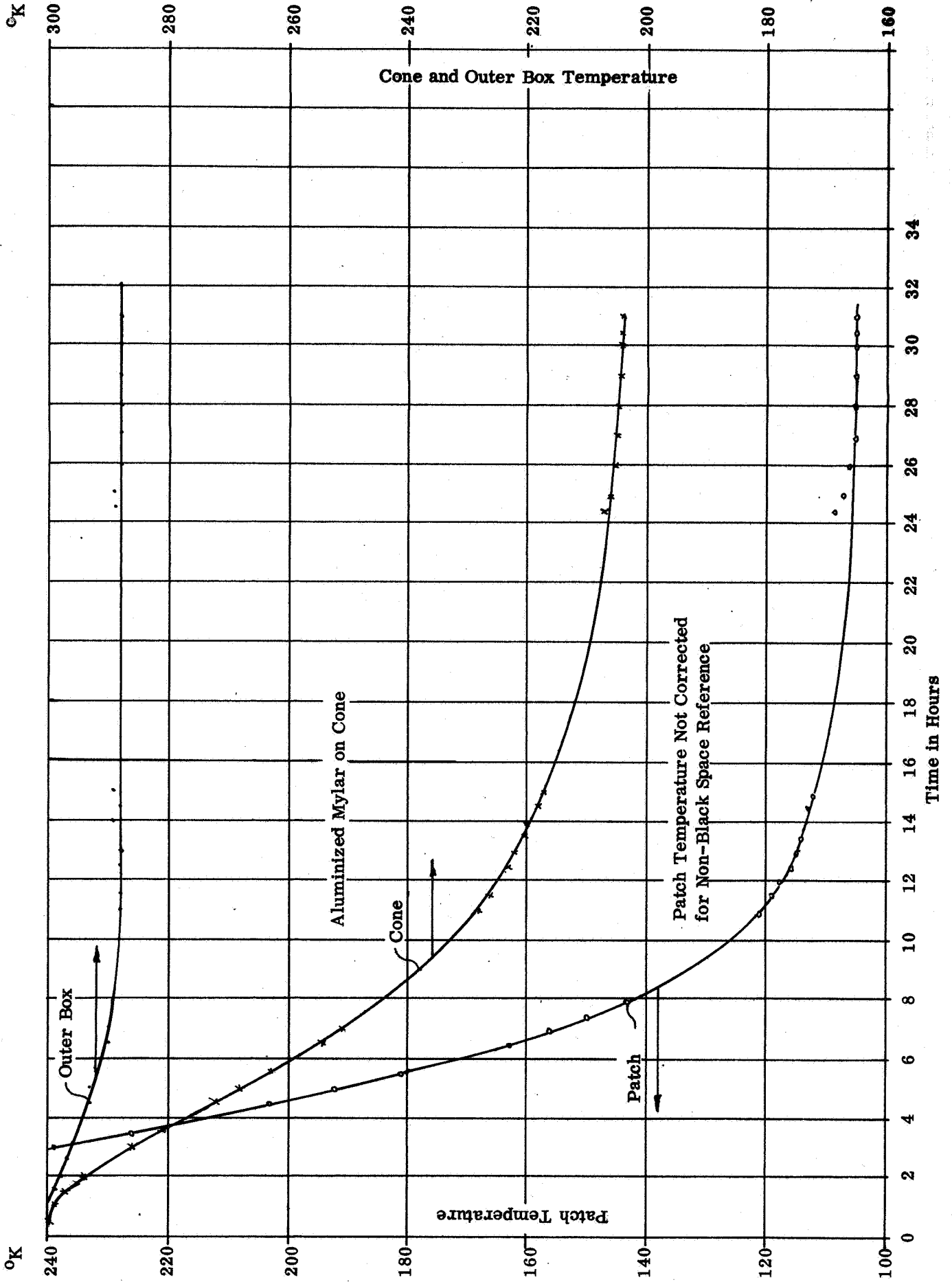
Figure 34   Radiant Cooler Test No. 6 (Aug. 21 & 22, 1967)

116

## 4.2    Two-Stage Radiant Cooler

Following the completion of thermal test 3 on the single-stage model of the radiant cooler (Section 4.1), a complete two-stage model was tested. Aluminized mylar was used to cover the inner surface of the first-stage cone and outer surface of the second-stage cone. The second-stage cone was molded of glass bead filled epoxy; its inner surface was covered directly with evaporated aluminum followed by evaporated gold.

The aluminized mylar was removed from the inner walls of the outer box to increase the thermal load on the first-stage cone and thereby more closely simulate in-orbit conditions (Section 4.4). However, this increased the cone temperature too much. Apparently the one Alzak surface on the inside of the box increased the radiative coupling more than expected.

The cooler temperatures at thermal equilibrium are listed below as measured and as corrected to an in-orbit cone temperature of 204 degrees K. These results should be considered approximate, however, because of the poor location of the ambient sensor during the test, as discussed below.

| | As Measured | Corrected to Orbital Conditions |
|---|---|---|
| Outer Box | $280^{\circ}$K | – |
| First-Stage Cone | $211^{\circ}$K | $204^{\circ}$K |
| First-Stage Patch | $117^{\circ}$K | $113^{\circ}$K |
| Second-Stage Patch | $90^{\circ}$K | $86^{\circ}$K |

Following the test, the ambient sensor (platinum resistance thermometer) in the test rack was mounted on the input board of the multi-channel recorder (where the thermocouple wires are attached). The sensor had previously been located about a foot below the input board. We found a significant temperature difference between these locations when the equipment was operating. The average difference was about 4 degrees C, but varied as thermal conditions in the room changed. The above results for the fourth test were corrected for a nominal difference of 4 degrees K. However, the results are not entirely reliable, especially at low temperatures.

A second test of a two-stage cooler model (thermal test 5) was then begun. The only change from test 4 was supposed to be that the inside surface of the second-stage cone had been lined with aluminized mylar. When it became apparent that the first-stage (which was unchanged) was not cooling as well as previously, the test was terminated. Examination of the cooler showed that it had not been properly assembled, i.e., changes had been made in addition to the attachment of

the aluminized mylar in the second-stage cone. In addition, the 3M Black Velvet coating on the copper space reference had been damaged. The bolt heads protruding from the copper had been scraped; other areas of the black coating had been scratched and wiped. The copper reference was repainted, and the bolts replaced with counter-sunk flat head screws. The test on the two-stage cooler was repeated following a re-test of the single-stage cooler (test 6, Section 4.1).

The single-stage radiant cooler from thermal test 6 was changed to a two-stage model and tested on August 28 and 29. The outer and inner surfaces of the second-stage cone were covered with 0.5 mil aluminized mylar. As in test 6, the ambient sensor was attached to the same board as the reference thermocouple junctions. All thermocouples were calibrated by immersion in liquid nitrogen; chromel-alumel couples were used on the first-stage cone and patch and a chromel-constantan couple on the second-stage patch.

Temperature measurements during test 7 are shown in Figure 35. The two-stage radiant cooler attained the following equilibrium temperatures (average of 13 readings over a 5-1/2 hour period).

| | |
|---|---|
| Outer box | $289.5^{O}K$ |
| First-stage cone | $201.6^{O}K$ |
| First-stage patch | $108.3^{O}K$ |
| Second-stage patch | $80.2^{O}K$ |

The Alzak surface on the inside wall of the outer box was covered with aluminized mylar, and the other inside surfaces were left uncovered. The result was, as in test 6, a cone temperature within the expected orbital range (Section 4.4).

The equilibrium patch temperatures were corrected for the effects of a non-black space reference. The temperature corrections are listed in Table 24 for reference (3M Black Velvet) reflectivities of 2, 5, and 8 percent. The detailed calculation of these corrections is given in Section 4.5.

Table 24

Two-Stage Corrections for Reference Reflectivity
(Test No. 7)

| Reference Reflectivity | Temperature Correction | |
|---|---|---|
| | First-Stage Patch | Second-Stage Patch |
| 0.02 | $-1.1^{O}K$ | $-2.5^{O}K$ |
| 0.05 | $-2.9^{O}K$ | $-6.7^{O}K$ |
| 0.08 | $-4.8^{O}K$ | $-11.8^{O}K$ |
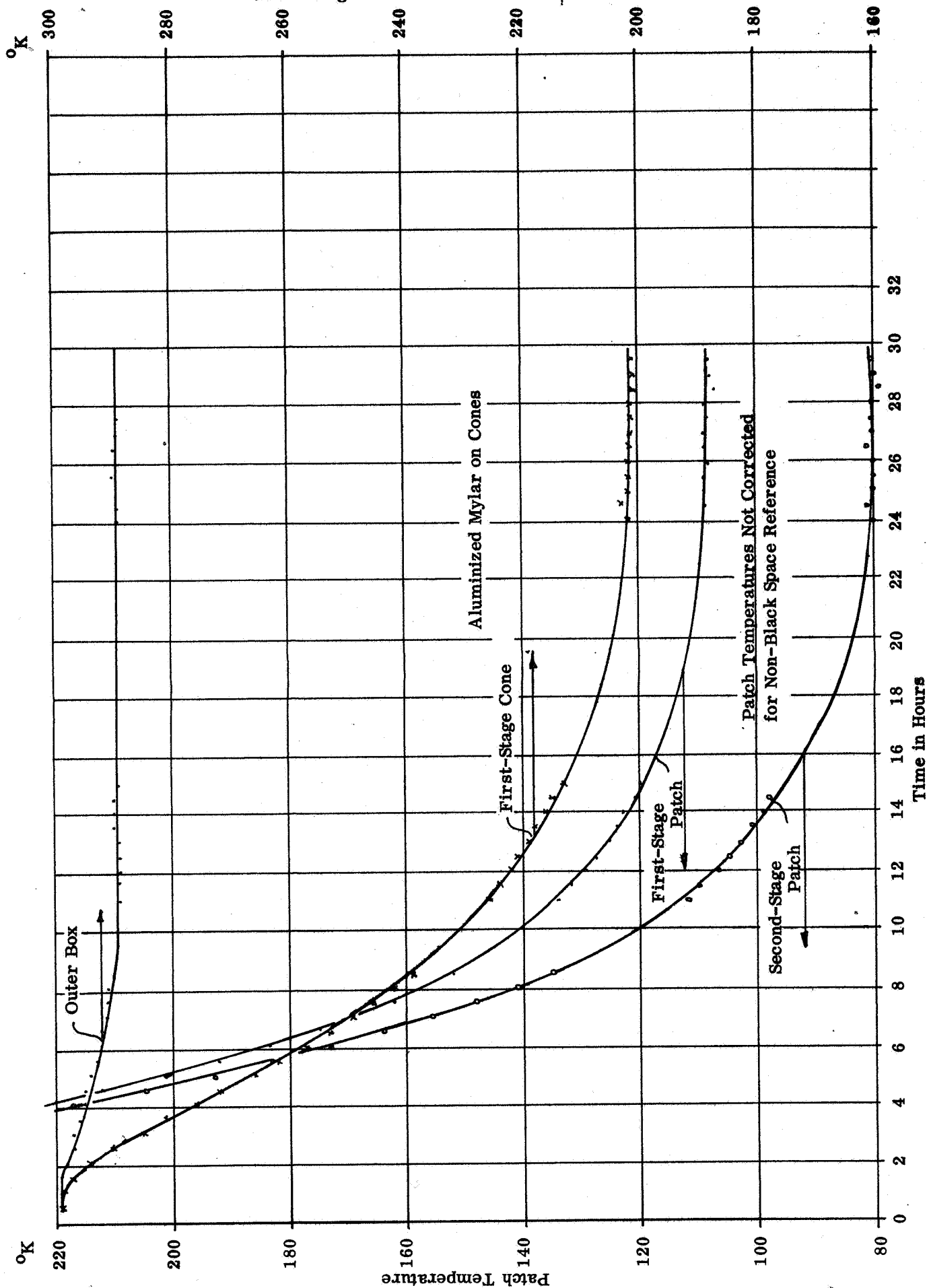
Figure 35  Radiant Cooler Test No. 7 (Aug. 28 & 29, 1967)

119

The temperature correction was first applied to the second-stage patch. The first-stage patch temperature was then corrected and the second-stage temperature ($T_{p2}$) adjusted for the corrected first-stage temperature ($T_{p1}$). Finally, the patch temperatures were determined for a first-stage cone temperature ($T_c$) of 204 degrees K to permit better comparison with previous results (test 6, Section 4.1). The results are shown in Table 25.

## Table 25

### Two-Stage Measurements Corrected for Reference Reflectivity
### (Test No. 7)

| Reference Reflectivity | Corrected Patch Temperatures | | | |
| --- | --- | --- | --- | --- |
| | $T_c = 201.6^OK$ | | $T_c = 204^OK$ | |
| | $T_{p1}$ | $T_{p2}$ | $T_{p1}$ | $T_{p2}$ |
| 0.02 | 107.2$^OK$ | 77.1$^OK$ | 108.5$^OK$ | 77.8$^OK$ |
| 0.05 | 105.4$^OK$ | 72.1$^OK$ | 106.7$^OK$ | 72.7$^OK$ |
| 0.08 | 103.5$^OK$ | 66.6$^OK$ | 104.7$^OK$ | 67.0$^OK$ |

The first-stage patch temperature was calculated for the change in cone temperature using the direct proportionality between the temperatures of the first-stage patch and first-stage cone (Section 1.5, equation 66). The second-stage temperature was adjusted for changes in the first-stage temperature using the thermal balance equation for the second stage (Section 1.6, equation 68).

The non-black space reference introduces a total error in the second-stage temperature in the range 3.1 to 13.6 degrees K. The joule heating in the infrared detector produces a much smaller temperature increase. For example, the detector to be used in the breadboard radiometer has a resistance of 171 ohms and an optimum bias current (i.e., the current which gives the maximum detectivity) of 0.9 ma. The joule heating is then 0.1385 milliwatts. This additional power would increase the temperature of a second-stage patch from 72.1 degrees K to 72.8 degrees K. This is an increase of only 0.7 degrees K, which is much smaller than that produced by reflections off the space reference. Moreover, this result is for a 1/2 mm square detector. The use of smaller detectors in higher resolution instruments will further reduce the influence of joule heating. Since detector dissipation is proportional to its area, a 1/4 mm square detector, for example, would dissipate only about 0.04 milliwatts.

## 4.3  Radiative Transfer Parameters

The emissivity, $\epsilon_g$, of the surface on the first-stage cone has a large influence on the design (Sections 1.4 and 1.7) and performance (Sections 2.1.3 to 2.1.5) of the two-stage radiant cooler. The effective emissivity, $\epsilon_{bc}$, between the outer box and first-stage cone plus the temperature of the box determine the thermal load on the first-stage cone during thermal tests. Adjustments in the box-cone emissivity can therefore be made to increase the accuracy of simulating in-orbit thermal conditions (Section 4.4). The value of $\epsilon_g$ was calculated from the measured temperatures of the first-stage patch and cone and the known geometry of the cooler. The value of $\epsilon_{bc}$ was calculated from the measured temperatures of the outer box and first-stage cone, the value of $\epsilon_g$, and the geometry of the cooler. The emissivity of the aluminized mylar was estimated from two $\epsilon_{bc}$ values and compared with the average cone surface emissivity, $\epsilon_g$.

The temperatures measured during thermal test 7 and corrected for space reference reflectivities of 2, 5, and 8 percent (Sections 4.2 and 4.5) were used to check the design equations of the first-stage patch and to estimate the radiative transfer parameters of the second stage. The radiative transfer parameters of the first stage determined from test 6 (Section 4.1) were used to predict the first-stage patch temperature in a two-stage cooler. The results were then compared with the measurements of test 7. The comparison was carried for space reference reflectivities of 2, 5 and 8 percent. The thermal balance equation for the second-stage patch was used to calculate the effective patch-to-cone emissivity and cone surface emissivity of the second stage. The surface emissivity was then used to check the thin patch model of the second-stage (Section 2.1.6).

### 4.3.1  First Stage

The average surface emissivity of the cone walls in a radiant cooler is the solution to the equation (Section 1.3.1).

$$1 - \epsilon_{pc} = \frac{1}{2} \underset{\text{Vertical}}{\Sigma f_n (1 - \epsilon_g)^n} + \frac{1}{2} \underset{\text{Horizontal}}{\Sigma f_n (1 - \epsilon_g)^n} \tag{143}$$

where $\epsilon_{pc}$ = effective patch-to-cone emissivity

$f_n$ = view factor from patch to space as seen by n reflections in the cone walls

The first sum uses the values of $f_n$ in the vertical plane and the second sum, in the horizontal plane. The value of $\epsilon_{pc}$ in a single-stage cooler is given by

$$\epsilon_{pc} = \left( \frac{T_p}{T_c} \right)^4 \tag{144}$$

121

where $T_p$ = patch temperature

$T_c$ = cone temperature

The values of $f_n$ are given in Table 4, Section 2.1.3. Substituting them into equation (143), we obtain

$$\epsilon_g = 1 + \frac{1.075 - [(1.075)^2 + 1.276\,(1.394 - 2\,\epsilon_{pc})]^{1/2}}{0.638} \qquad (145)$$

The values of $\epsilon_g$ were calculated from the measurements of thermal tests 2, 3, and 6. The patch temperatures in tests 2 and 3 were not corrected for the non-zero reflectivity of the space reference. The placement of the ambient sensor during these tests introduced errors opposite to those introduced by the space reference. The results are given in Table 26 for tests 2 and 3 and in Table 27 for test 6. The patch temperature of test 6 was corrected for space reference reflectivities of 2, 5, and 8 percent. The surface emissivity is an average value and assumes specular reflection at the cone walls and a black patch; it includes the openings for the in-orbit support tubes and optics as well as the small conductive coupling through the in-orbit support tubes.

### Table 26

#### Experimental Values of Cone Surface Emissivity
#### (Thermal Tests 2 and 3)

| Cone Wall Material | $T_p/T_c$ | $\epsilon_{pc}$ | $\epsilon_g$ |
|---|---|---|---|
| Au on Aℓ on Alzak | 0.630 | 0.166 | 0.202 |
| Aℓ on Mylar | 0.481 | 0.0535 | 0.0632 |

### Table 27

#### Emissivities Corrected for Reference Reflectivity
#### (Thermal Test 6)

| Space Reference Reflectivity | $\epsilon_{pc}$ | $\epsilon_g$ |
|---|---|---|
| 0.08 | 0.0533 | 0.0630 |
| 0.05 | 0.0589 | 0.0697 |
| 0.02 | 0.0652 | 0.0773 |

From test 6, the surface emissivity of an aluminized mylar cone is 0.070 ± 0.007. The emissivity for a space reference reflectivity of 5 percent is 10 percent higher than that from test 3. Because of the fourth power dependence, errors and uncertainties in temperature are amplified when expressed in terms of emissivity.

The value of box-cone emissivity for a single-stage cooler in the space chamber can be determined from the thermal balance equation of the cone

$$A_{ce} \sigma T_c^4 + A_c \sigma T_c^4 (\epsilon_{cx} + \epsilon_{cp}) = A_c \epsilon_{bc} \sigma(T_s^4 - T_c^4) \qquad (146)$$

where $T_s$ = temperature of outer box

$A_{ce}$ = area of cone ends

$A_c$ = area of cone walls

$\epsilon_{cx}$ = effective external emissivity of the cone

$\epsilon_{cp}$ = effective cone-to-patch emissivity

Solving for $\epsilon_{bc}$, we obtain

$$\epsilon_{bc} = \frac{\dfrac{A_{ce}}{A_c} + \epsilon_{cx} + \epsilon_{cp}}{\left(\dfrac{T_s}{T_c}\right)^4 - 1} \qquad (147)$$

The value of $A_{ce}/A_c$ is 0.118. Equation (146) assumes close-spaced or plane-parallel geometry, so there is no distinction between box-to-cone and cone-to-box emissivity.

The effective cone-to-patch emissivity is related to the effective patch-to-cone emissivity by the reciprocity relationship

$$\epsilon_{cp} = \frac{A_p}{A_c} \cdot \epsilon_{pc}$$

where $A_p$ is the radiating area of the patch. The value of $A_p/A_c$ is 0.065. The effective cone external emissivity is given by (Section 1.4.1.1).

$$\epsilon_{cx} = \frac{A_m}{A_c} \left[1 - \sum_{n=0} f_n' (1 - \epsilon_g)^n\right]$$

where $A_m$ = area of cone mouths

$f_n'$ = view factor from cone mouth to itself and patch as seen by n reflections in the cone walls

123

The values of $f_n'$ are listed in Table 5, Section 2.1.3. The value of $A_m/A_c$ is 0.316.

Values of $\epsilon_{cp}$, $\epsilon_{cx}$, and $\epsilon_{bc}$ were calculated for tests 2, 3, and 6. The results are listed in Table 28 and the types of surfaces given in Table 29.

Table 28

Experimental Values of Effective Emissivities

| Test No. | $\epsilon_{cx}$ | $\epsilon_{cp}$ | $\epsilon_{bc}$ |
|---|---|---|---|
| 2 | 0.105 | 0.0109 | 0.054 |
| 3 | 0.0375 | 0.00348 | 0.036 |
| 6 | 0.0412* | 0.00383* | 0.055 |

* For a reference reflectivity of 5 percent.

Table 29

Types of Surfaces

| Test No. | Inner Surface of Box | Outer Surface of Cone |
|---|---|---|
| 2 | A$\ell$ on mylar | Anodized aluminum |
| 3 | A$\ell$ on mylar | Mill-finished aluminum |
| 6 | 1 side, A$\ell$ on mylar 3 sides, mill-finished aluminum | Mill-finished aluminum |

The box-cone emissivity may be related to the surface emissivities of the box and cone by assuming plane-parallel or close-spaced geometry. For test 3, the relationship is

$$\epsilon_{bc} = \frac{1}{\dfrac{1}{\epsilon_1} + \dfrac{1}{\epsilon_2} - 1} = 0.036$$

where $\epsilon_1$ = emissivity of aluminized mylar (inner surface of box)

$\epsilon_2$ = emissivity of mill-finished aluminum (outer surface of cone)

During tests 6 and 7, 0.845 of the surface area was mill-finished aluminum facing mill-finished aluminum and 0.155 mill-finished aluminum facing aluminized mylar. The box-cone emissivity for this case is given by

$$\epsilon_{bc} = \frac{0.845}{\dfrac{2}{\epsilon_2} - 1} + \frac{0.155}{\dfrac{1}{\epsilon_1} + \dfrac{1}{\epsilon_2} - 1} = 0.055 \qquad (149)$$

Substituting (148) into (149) and solving for the emissivity of the mill-finished aluminum, we obtain

$$\epsilon_2 = 0.11$$

Substituting this result into (148) and solving for the emissivity of the aluminized mylar, we obtain

$$\epsilon_1 = 0.051$$

This result is in good agreement with the value (0.05) given by Hemmerdinger and Hembach ("Handbook of Military Infrared", Ed. by W. Wolfe, Office of Naval Research, 1965, p. 804) and by R. Sadler, et. al. (0.047; p. 219 of "Measurements of Thermal Radiation Properties of Solids", Ed. by J. C. Richmond, NASA SP-31, 1963).

When used on the first-stage cone surface facing the patch, aluminized mylar resulted in an average surface emissivity of about 0.070 (Table 27). This result assumes flat, specularly reflecting cone walls. The cone surface emissivity is increased above the value for aluminized mylar by the following factors

    a.     Waves and wrinkles in the mylar surface.

    b.     A diffuse component of reflection from the aluminized mylar.

    c.     Openings for the support tubes and optical beam.

    d.     Thermal inputs through the support tubes and electrical leads.

    e.     Contamination of the aluminum surface.

Factor d. accounts for about a 5 percent increase in the average surface emissivity.

The temperature of the first-stage patch in a two-stage radiant cooler is given by (Section 1.5)

$$T_{p1} = (\epsilon'_{pc})^{1/4} T_c \qquad\qquad (150)$$

where

$$\epsilon'_{pc} = \frac{\epsilon_{pc} \left(1 + \dfrac{1}{2} \dfrac{A_{c2}}{A_{p1}}\right)}{1 + \dfrac{A_{c2}}{A_{p1}} \left[\epsilon_g + \epsilon_{pc} (1/2 - \epsilon_g)\right]}$$

$\dfrac{A_{c2}}{A_{p1}}$ = outside surface area of second-stage cone to surface area of first-stage patch

The values of $\epsilon_{pc}$ and $\epsilon_g$ determined from thermal test 6 (single-stage cooler) are listed in Table 30 together with the calculated values of $\epsilon'_{pc}$ for $A_{c2}/A_{p1} = 0.810$.

Table 30

Parameters Used to Predict $T_{p1}$

| Space Reference Reflectivity | $\epsilon_g$ | $\epsilon_{pc}$ | $\epsilon'_{pc}$ |
|---|---|---|---|
| 0 | 0.0831 | 0.0699 | 0.0900 |
| 0.02 | 0.0773 | 0.0652 | 0.0844 |
| 0.05 | 0.0697 | 0.0589 | 0.0768 |
| 0.08 | 0.0630 | 0.0533 | 0.0700 |

The values of $\epsilon'_{pc}$ were used to calculate the first-stage patch temperature from equation (150) for a first-stage cone temperature of 201.6 degrees K (attained in test 7). The results are given in Table 31 together with measured temperatures corrected to the same values of reference reflectivity (Table 25).

Table 31

First-Stage Patch Temperatures

| Space Reference Reflectivity | Predicted ($^{O}$K) | Measured |
|---|---|---|
| 0.02 | 108.7 | 107.2 |
| 0.05 | 106.1 | 105.4 |
| 0.08 | 103.7 | 103.5 |

On the average, the predictions are less than 1 percent from the corrected measurements.

126

## 4.3.2   Second Stage

Estimates of radiative transfer parameters are much less accurate in the second stage than in the first.   The errors introduced by the imperfect cold space reference are larger in the second stage.   In addition, an estimate of the cone surface emissivity requires the removal of the geometrical effects (multiple reflections). The original design equations were based on thin patches (i. e. , they neglected the sides).   This is a reasonable assumption for the first-stage patch but quite inaccurate for the second.   Finally, the calculation of transfer parameters involves a temperature measurement raised to the fourth power.   Errors in temperature measurements are therefore amplified when the results are expressed as transfer parameters.

Reasonably accurate estimates of the radiative transfer parameters from experimental temperature measurements are possible only in the first stage.   A range of values can be calculated for the second stage, but the spread is somewhat larger.   Such a range of values was determined by use of a weighting factor to account for the greater patch-to-cone interaction of the side areas of the second-stage patch.

The thermal balance equation for the second-stage patch (Section 1.6) may be solved for the effective patch-to-cone emissivity of the second stage.

$$\epsilon_{pc}^{(2)} = \frac{\sigma A_{p2} T_{p2}^4 - K_c (T_{p1} - T_{p2})}{\sigma A_{p2} T_{p1}^4} \tag{151}$$

where $A_{p2}$ = surface area of second-stage patch = 2.62 $in^2$

$T_{p2}$ = temperature of second-stage patch

$K_c$ = conductive coupling coefficient between stages = 0.0366 $mw/^oK$

The measured patch temperatures for thermal test 7 corrected to reference reflectivities of 2, 5, and 8 percent are listed in Table 32 together with the values of $\epsilon_{pc}^{(2)}$ from equation (151)

### Table 32

Calculation of $\epsilon_{pc}^{(2)}$

| Space Reference Reflectivity | $T_{p1}$ ($^oK$) | $T_{p2}$ | $\epsilon_{pc}^{(2)}$ |
|---|---|---|---|
| 0 | | | 0.2227 |
| 0.02 | 107.2 | 77.1 | 0.1805 |
| 0.05 | 105.4 | 72.1 | 0.1159 |
| 0.08 | 103.5 | 66.6 | 0.0486 |

The calculation of $\epsilon_{pc}^{(2)}$ from the surface emissivity of the cone, $\epsilon_g^{(2)}$, is covered in Sections 1.3.1 and 2.1.6.2. The calculation is for a thin patch. For values of $\epsilon_g^{(2)}$ between 0.02 and 0.086, a linear approximation yields.

$$\epsilon_g^{(2)} \approx \frac{\epsilon_{pc}^{(2)}}{1.258} - 0.00067 \qquad (152)$$

However, the radiative coupling between the patch and cone is about twice as large for the side areas of the second-stage patch. The sides have a surface area of 1.527 $in^2$ out of a total of 2.62 $in^2$; their radiative coupling "weight" is therefore about

$$2 \times \frac{1.527}{1.093} = 2.794$$

The average weighting factor for the whole patch is then 1.397, and equation (152) becomes

$$\epsilon_g^{(2)} \approx \frac{1}{1.397} \left[ \frac{\epsilon_{pc}^{(2)}}{1.258} - 0.00067 \right] \qquad (153)$$

The calculated values of $\epsilon_g^{(2)}$ are given in Table 33 for the $\epsilon_{pc}^{(2)}$ values of Table 32.

Table 33

Estimate of Cone Surface Emissivity in Second Stage

| Space Reference Reflectivity | $\epsilon_g^{(2)}$ |
|---|---|
| 0 | 0.1262 |
| 0.02 | 0.1022 |
| 0.05 | 0.0655 |
| 0.08 | 0.0272 |

Note that the range of calculated surface emissivities (3.8 to 1) is nearly as great as the range of space reference reflectivities (4 to 1). The above model yields a value of $\epsilon_g^{(2)}$ within the range calculated for the first-stage cone (0.063 to 0.0773) only at a reference reflectivity of 5 percent.

According to the thin patch model, the temperature of the second-stage patch is the solution to (Sections 1.6 and 2.1.6.2)

$$4.79 \times 10^{-8} T_{p2}^4 + 0.0366 T_{p2} = 4.79 \times 10^{-8} \epsilon_{pc}^{(2)} T_{p1}^4 + 0.0366 T_{p1}$$

$$(154)$$

The area of the thin patch is 1.31 square inches, and $\epsilon_{pc}^{(2)}$ is determined by the procedure described in Section 1.3.1. The average value of $\epsilon_{pc}^{(2)}$ for the horizontal and vertical geometries of the second-stage cone is 0.0840 when $\epsilon_g^{(2)}$ equals 0.0655. For $T_{p1}$ equal to 105.4 degrees K (measured value corrected for a reference reflectivity of 5 percent), equation (154) becomes

$$4.79 \times 10^{-8} \, T_{p2}^{4} + 0.0366 \, T_{p2} = 4.354 \text{ milliwatts}$$

The solution is

$$T_{p2} = 75.8 \text{ degrees K} \tag{155}$$

This is 3.7 degrees K, or 5.1 percent, above the measured value corrected for a reference reflectivity of 5 percent (72.1 degrees K).

## 4.4 Thermal Simulation

If the temperature of the first-stage cone approximates its in-orbit value during thermal space chamber tests, the patch temperatures will also be close to their orbital values and the test will be realistic. The in-orbit cone temperature for a cone surface of aluminized mylar is calculated below for an orbit normal to sun angle of 79 degrees. The cone temperature during the thermal test 3 was about 10 percent below this temperature, so that the patch temperature was also 10 percent below its orbital value. Good simulation was obtained during tests 6 and 7 by increasing the radiative coupling from the outer box to the first-stage cone (Section 4.3.1). The cone temperatures during these two tests were within the orbital range calculated below.

The in-orbit temperature of the first-stage cone is calculated in Sections 2.1.3 and 2.1.4 at the extreme values of cone surface emissivity ($\epsilon_g$) and solar absorptivity ($\alpha_g$). The same procedure may be used to calculate the in-orbit cone temperature for an aluminized mylar surface. If we assume $\alpha_g$ equals 0.20[7] (L. H. Hemmerdinger and R. J. Hembach in "Handbook of Military Infrared", Ed. by W. Wolfe, Office of Naval Research, 1965, p. 804), the in-orbit cone temperature is the solution to

$$\sigma T_c^{4} \, [0.1356 \, \epsilon_d + \epsilon_{cx} + 1.405 \, \epsilon_{cp}] = 2.1 \times 10^{-2} \, \epsilon_{ce}^{s} + 2.168 \times 10^{-2} \, \epsilon_g \, \epsilon_{ct}$$

$$+ 7.1905 \times 10^{-4} + 0.1356 \, [1.53 \times 10^{-3} + 0.1157 \, (2.1 \times 10^{-2} \, \epsilon_d + 1.65 \times 10^{-2} \, \alpha_d)$$

$$+ 6.678 \times 10^{-3} \, \alpha_d + 1.463 \times 10^{-3} \, \epsilon_g \, \epsilon_d]$$

---

[7] On the other hand, W. B. Fusscell, et. al., in "Measurements of Thermal Radiation Properties of Solids", Ed. by J. C. Richmond, NASA SP-31, 1963, give $\alpha_g = 0.13$ for aluminized mylar (p. 100).

for an orbit normal to sun angle of 79 degrees and an earth shield attached to the outer box (Section 2.1.4). The side of the earth shield facing the cone is assumed to be covered with aluminized mylar of emissivity $\epsilon_g$. The cone temperature was determined for $\epsilon_g$ equal to 0.063 and 0.0697. The corresponding effective emissivities and absorptivities are listed in Table 34.

### Table 34

### Infrared Emissivities and Absorptivities

| $\epsilon_g$ | $\epsilon_{cx}$ | $\epsilon_{cp}$ | $\epsilon_{ce}^s$ | $\epsilon_{ct}$ |
|---|---|---|---|---|
| 0.063 | $3.75 \times 10^{-2}$ | $3.48 \times 10^{-3}$ | $6.64 \times 10^{-3}$ | $1.97 \times 10^{-3}$ |
| 0.0697 | $4.12 \times 10^{-2}$ | $3.83 \times 10^{-3}$ | $7.295 \times 10^{-3}$ | $2.18 \times 10^{-3}$ |

In Sections 2.1.3 and 2.1.4, the values used for the emissivity and solar absorptivity of the 1-1/16-inch wide cone ends were 0.9 and 0.18, respectively. If the ends are made of Alzak treated aluminum, better values are 0.8 and 0.15, respectively (Hemmerdinger and Hembach, op. cit.). The calculated cone temperatures are shown in Table 35 for all four combinations of $\epsilon_d$, $\alpha_d$, and $\epsilon_g$.

### Table 35

### In-Orbit Cone Temperature

| $\epsilon_g$ | $\epsilon_d$ | $\alpha_d$ | $T_c$ ($^\circ$K) |
|---|---|---|---|
| 0.063 | 0.9 | 0.18 | 203.1 |
| 0.063 | 0.8 | 0.15 | 205.3 |
| 0.0697 | 0.9 | 0.18 | 200.2 |
| 0.0697 | 0.8 | 0.15 | 204.4 |

As in Sections 2.1.3 and 2.1.4, the above calculations ignore the small decrease in equivalent earthshine emittance, $W_s$, produced by the decrease in orbit normal to sun angle from 90 to 79 degrees. From Appendix I, we see that this decreases $W_s$ by a factor of sin 79 degrees, or 0.982. Such a reduction produces a change in cone temperature much less than the variations shown in Table 35. For example, it reduces the bottom cone temperature by only 0.2 degrees K.

The cone and outer box temperatures during five thermal tests are listed in Table 36. Cone temperatures within the expected orbital range were obtained in tests 6 and 7. During these tests, the inner surface of the box consisted of three sides of mill-finished aluminum and one of aluminized mylar facing mill-finished aluminum on the outer cone surface. The outer box was cooled below room temperature by the foam core ends, which were partially exposed to the cold space reference. During test 2, we used a smaller box with greater exposure to the cold reference. Variations in the box temperature during the remaining tests were produced by variations in the room temperature and in the placement of the box with respect to the cold reference.

## Table 36

### In-Chamber Cone and Box Temperatures

| Test No. | $T_c$ ($^O$K) | $T_s$ ($^O$K) |
|---|---|---|
| 2 | 177 | 269 |
| 3 | 183 | 279 |
| 4 | 211 | 280 |
| 6 | 204 | 288 |
| 7 | 202 | 289.5 |

## 4.5 Corrections for Imperfect Space Reference

The cold reference used during chamber tests of the two-stage radiant cooler does not provide a complete simulation of outer space. It is not sufficiently cold and does not have an absorptivity of unity. The reference attains a temperature of about 30 degrees K (Section 3.1) rather than the 4 degrees K of space, and its absorptivity is that of 3M Black Velvet (0.92 to 0.98). The higher temperature produces very small errors for a patch at liquid nitrogen temperature or above, but the lower absorptivity produces significant errors even in the temperature of the first-stage patch. It therefore becomes necessary to correct the patch temperatures measured in the space chamber for a nominal range of space reference reflectivities. Equations for the corrections are derived below for single and two-stage radiant coolers and applied to the results of thermal test 7 (Section 4.2).

The absorptivity of the space reference can be increased by the use of cavities. For example, a reference covered with 30 degree triangular grooves decreases the reflectivity of the surface from the 2 to 8 percent range to 0.75 to 3.1 percent.

## 4.5.1 Space Reference Temperature

First we will show that a space reference temperature of 30 degrees K has only a very small influence on the temperature of the second-stage patch. The thermal-balance equation for the second-stage patch when viewing a black space reference at 0 degrees K is (Section 1.6, equation 68)

$$\sigma A_{p2} T_o^4 = \epsilon_{pc}^{(2)} \sigma A_{p2} T_{p1}^4 + K_c (T_{p1} - T_o) \qquad (156)$$

where $A_{p2}$ = radiating area of the second-stage patch

$T_o$ = temperature of the second-stage patch for a black space reference at 0 degrees K

$\epsilon_{pc}^{(2)}$ = effective patch-to-cone emissivity in the second stage

$T_{p1}$ = temperature of the first-stage patch

$K_c$ = conductive coupling coefficient between stages

If the same patch views a black space reference at a temperature $T_r$ above absolute zero, the patch temperature is increased to $T_{p2}$ and its thermal balance equation becomes

$$\sigma A_{p2} T_{p2}^4 = \epsilon_{pc}^{(2)} \sigma A_{p2} T_{p1}^4 + K_c (T_{p1} - T_{p2}) + (1 - \epsilon_{pc}^{(2)}) \sigma A_{p2} T_r^4 \qquad (156a)$$

This equation neglects the increase in first-stage temperature produced by the space reference. Subtracting equation (156) from equation (156a), we obtain

$$\sigma A_{p2} (T_{p2}^4 - T_o^4) = A_{p2} \sigma T_r^4 - K_c (T_{p2} - T_o)$$

for $\epsilon_{pc}^{(2)}$ much less than one (i. e., neglecting absorption of reference radiation in the second-stage cone). This may be rearranged to give

$$T_{p2}^4 + \frac{K_c}{\sigma A_{p2}} T_{p2} = T_o^4 + T_r^4 + \frac{K_c}{\sigma A_{p2}} T_o \qquad (157)$$

For $K_c$ = 0.0339 mw/$^o$K

$A_{p2}$ = 2.62 in$^2$

$T_o$ = 75$^o$K

$T_r$ = 30$^o$K

equation (157) becomes

$$T_{p2}^4 + 3.538 \times 10^5 \, T_{p2} = 0.5899 \times 10^8 \, {}^{\circ}K^4$$

The solution is

$$T_{p2} = 75.4 \, {}^{\circ}K \tag{158}$$

This is an increase of only 0.4 degrees K or about 1/2 percent.

### 4.5.2 Space Reference Reflectivity

The non-black space reference provides paths not present in outer space by which radiation from the first-stage cone and patch can reach the second-stage patch. Additional paths are also provided for radiative transfer from the first-stage cone and patch to the first-stage patch. The patch temperatures measured in the space chamber are therefore higher than those achieved in outer space and must be corrected to a condition of zero reference reflectivity. Procedures to determine these corrections are described below and applied to the results of thermal test 7. In Section 4.5.3, we consider the use of cavities to reduce the reflectivity of the space reference and therefore the magnitude of the corrections required to estimate the in-orbit performance.

The value of the reflectivity for the 3M Black Velvet coating on the space reference is not known. The reference is at about 30 degrees K and the incoming radiation from sources in the temperature range of 80 to 200 degrees K. D. L. Stierwalt (Applied Optics 5, 1914, 1966) shows that the emissivity (absorptivity) of 3M Black Velvet at 77 degrees K is about 0.95 over the wavelength range from 5 to 40 microns. Hemmerdinger and Hembach (chapter 20 in "Handbook of Military Infrared Technology", Ed. by W. L. Wolfe, Office of Naval Research, 1965) list an emissivity value of 3M Black Velvet over zinc chromate primer of 0.92 at 228 degrees K on an alodined aluminum substrate. Scott ("Cryogenic Engineering", D. Van Nostrand, 1959, p. 348) lists an emissivity of 0.97 for black matte lacquer at 373 degrees K. We have therefore selected three values of absorptivity for the space reference, 92, 95, and 98 percent; they correspond to reflectivities of 8, 5, and 2 percent.

A blackbody or graybody source at 200 degrees K has only about 14 percent of its energy at wavelengths above 40 microns. However, at 80 degrees K the percentage is 68. On the other hand, most of the increase in patch temperature is produced by the cone radiation at about 200 degrees K that is reflected off the space reference and absorbed in the patch. From the spectral data of Stierwalt, we may therefore conclude that center value of 5 percent reflectivity probably most nearly represents the actual case. (See also A. R. Karoli, et. al., Applied Optics 6, 1184, July 1967.) It is shown below that a 5 percent diffuse reflectivity increases the patch temperature by about 4 percent in a single-stage cooler and about 10 percent in the second-stage of a two-stage cooler.

## 4.5.2.1  Single-Stage Cooler

The fraction of patch radiation returned to the patch by reflection off the space reference is

$$F_{pp} = \rho_{pc} \rho_r (g_1 + g_2 \rho_r g_1 + g_2^2 \rho_r^2 g_1 + \cdots)$$

where  $\rho_{pc}$  =  fraction of radiant flux from patch that reaches cold reference by reflection in cone (Section 1.3.1)

$\rho_r$  =  diffuse reflectivity of cold space reference

$g_1$  =  fraction of diffuse radiation from space reference that reaches first-stage patch directly and by reflection in first-stage cone

$g_2$  =  fraction of diffuse radiation from reference that returns to reference by reflection in first-stage cone

This is a geometric progression and may be summed to yield

$$F_{pp} = \frac{\rho_{pc} \, \rho_r \, g_1}{1 - g_2 \, \rho_r} \qquad (159)$$

Similarly, the fraction of cone radiation which reaches the patch by reflection off the diffuse space reference is

$$\epsilon_{cx} (\rho_r \, g_1 + \rho_r^2 \, g_2 \, g_1 + \rho_r^3 \, g_2^2 \, g_1 + \cdots)$$

where $\epsilon_{cx}$ is the effective cone external emissivity (Section 1.4.1.1).  Summing this progression and adding it to the fraction that goes directly from the cone to the patch, $\epsilon_{cp}$ (Section 1.4.1), we obtain the total fraction of cone radiation absorbed in a black patch

$$F_{cp} = \epsilon_{cp} + \frac{\epsilon_{cx} \, \rho_r \, g_1}{1 - g_2 \, \rho_r} \qquad (160)$$

The net power emitted by the black patch at a temperature $T_p$ is $(1 - F_{pp}) \cdot \sigma T_p^4 A_p$, where $A_p$ is the area of the patch.  The power absorbed from the cone at a temperature $T_c$ is $F_{cp} \, \sigma T_c^4 A_c$, where $A_c$ is the surface area of the cone walls.  Equating these two powers, we obtain the thermal balance equation for the patch and the equation

$$\left(\frac{T_p}{T_c}\right)^4 = \frac{F_{cp}}{\dfrac{A_p}{A_c} (1 - F_{pp})} \qquad (161)$$

134

In the derivation of the equation for the effective cone external emissivity (Section 1.4.1.1 and 2.1.3), we obtained the values of $f_n'$, the fraction of diffuse radiation entering the mouth of a perfectly reflecting cone that requires n cone wall reflections to return to the mouth or to go to the patch. The fraction $f_n'$ may be divided into two parts

$$f_n' = f_{np}' + f_{nm}'$$

where $f_{np}'$ = fraction going to patch

$f_{nm}'$ = fraction returning to mouth

The fraction of diffuse radiation from the space reference reaching the black patch by reflection in the cone (but without reflection off the reference) is then

$$g_1 = \Sigma f_{np}' \rho_g^n \qquad (162)$$

for a cone surface of reflectivity $\rho_g$. And the fraction returned to the space reference (cone mouth) by reflection in the cone (but without reflection off the reference) is

$$g_2 = \Sigma f_{nm}' \rho_g^n \qquad (163)$$

Values of $f_{np}'$ and $f_{nm}'$ are given in Table 37 for diffuse reflection from the center of the cone mouth in the vertical and horizontal planes of the first-stage. In the vertical plane, about 10 percent of the diffuse emission entering the mouth of a perfect cone goes to the patch and 90 percent goes back out the mouth. In the horizontal plane, about 50 percent goes to the patch and 50 percent back to the mouth.

Table 37

Distribution of Radiation Entering Mouth of Perfect Cone

| n | Vertical Plane $f_{np}'$ | $f_{nm}'$ | Horizontal Plane $f_{np}'$ | $f_{nm}'$ |
|---|---|---|---|---|
| 0 | 0.0116 | 0 | 0.306 | 0 |
| 1 | 0.0587 | 0.101 | 0.182 | 0.166 |
| 2 | 0.0319 | 0.187 | 0 | 0.308 |
| 3 | 0 | 0.238 | 0 | 0.038 |
| 4 | 0 | 0.229 | | |
| 5 | 0 | 0.1428 | | |
| | 0.1022 | 0.8978 | 0.488 | 0.512 |

For a cone wall emissivity ($\epsilon_g$) of 0.063, $\rho_g$ equals 0.937. Using the average of the horizontal and vertical plane values from equations (162) and (163) and the data of Table 37, we then obtain

$$g_1 = 0.2856$$

$$g_2 = 0.5958$$

The remaining fraction of reflected radiation, $1 - (g_1 + g_2) = 0.1186$, is absorbed in the cone walls and therefore equals the absorptivity of the conical cavity (Section 1.4.1.1). Multiplying 0.1186 by the ratio of cone mouth to cone wall area, we obtain the effective cone external emissivity of 0.0375 (Table 28). The value of $\epsilon_{cp}$ for $\epsilon_g$ equal to 0.063 is also given in Table 28. The magnitudes of $g_1$ and $g_2$ are relatively insensitive to the exact value of $\epsilon_g$. For example, if the cone wall emissivity in 0.070 rather than 0.063, $g_1$ is reduced by only 0.0011 (0.4 percent) and $g_2$ by 0.0013 (0.2 percent).

The values of $F_{pp}$ and $F_{cp}$ were calculated according to equations (159) and (160) for reference reflectivities of 0.08, 0.05, and 0.02. The results are listed in Table 38.

Table 38

Fraction of Radiation Reaching Patch

$$\rho_g = 0.937$$

| $\rho_r$ | From Patch $F_{pp}$ | From Cone $F_{cp}$ |
|---|---|---|
| 0.08 | 0.02271 | 0.00438 |
| 0.05 | 0.01393 | 0.00403 |
| 0.02 | 0.00547 | 0.00370 |
| 0 | 0 | 0.00348 |

The ratio of patch temperature to cone temperature was then determined by equation (161). The results are given in Table 39 for $A_p/A_c$ equal to 0.065.

Table 39

Ratio of Patch to Cone Temperature
$$\rho_g = 0.937$$

| $\rho_r$ | $T_p/T_c$ |
|---|---|
| 0. 08 | 0. 5124 |
| 0. 05 | 0. 50075 |
| 0. 02 | 0. 4891 |
| 0 | 0. 4809 |

We divided the temperature ratio for a non-zero reference reflectivity by the ratio for zero reflectivity and subtracted unity from the result to obtain the fractional increase in patch temperature produced by a non-black reference. The results are shown in Table 40 as percentage increases.

Table 40

Increase in Patch Temperature Produced by Non-Black Space Reference
$$\rho_g = 0.937$$

| $\rho_r$ | % Increase |
|---|---|
| 0. 08 | 6. 6 |
| 0. 05 | 4. 2 |
| 0. 02 | 1. 7 |

4.5.2.2   Two-Stage Cooler

The radiant power from the first-stage patch diffusely reflected off the space reference is given by

$$\Phi_{p-r} = \sigma A_{p1} T_{p1}^4 \rho_{pc} \rho_r (1 + \rho_r g_2 + \rho_r^2 g_2^2 + \cdots )$$

$$\Phi_{p-r} = \sigma A_{p1} T_{p1}^4 \frac{\rho_{pc} \rho_r}{1 - g_2 \rho_r} \tag{164}$$

where $A_{p1}$ =     radiating area of the first-stage patch

$T_{p1}$ =     temperature of the first-stage patch

Similarly, the power from the first-stage cone reflected off the space reference is given by

$$\Phi_{c-r} = A_c \; \sigma T_c^4 \; \frac{\epsilon_{cx} \, \rho_r}{1 - g_2 \, \rho_r} \tag{165}$$

where $A_c$ = inner surface area of first-stage cone

$T_c$ = temperature of first-stage cone

The total radiant power reaching the second-stage patch from the first stage by way of the space reference is then

$$\Phi_{s1 - p2} = g_0 \, (\Phi_{p-r} + \Phi_{c-r}) \tag{166}$$

where $g_0$ = fraction of diffuse radiation from space reference that reaches second-stage patch directly and by reflection in second-stage cone

At the edge of the first-stage mouth, $g_0$ is essentially zero. The cooler is designed so that the second-stage patch sees little or none of the first-stage cone either directly or by reflection in the second-stage cone. At the center of the first-stage mouth, $g_0$ was calculated as the average for right-circular cones having the geometries of the vertical and horizontal planes of the cooler according to

$$g_{oc} = \sum_n \; F^n_{r-p2} \; \rho_g^n \tag{167}$$

where $F^n_{r-p2}$ = view factor from center of first-stage mouth (space reference) to second-stage patch as seen by n reflections in second-stage cone

$\rho_g$ = reflectivity of second-stage cone wall

We also have for the right-circular geometry

$$F^n_{r-p2} = \sin^2 \gamma_n - \sin^2 \gamma_{n-1}$$

where $\gamma_n$ = angle from cooler axis to intersection of the n-1 and n reflections of second-stage patch in second-stage cone

Values of $\sin^2 \gamma_n$ were determined by means of scale drawings. The results are listed in Table 41.

138

Table 41

View Factor to First n-1 Reflections of Second-Stage Patch

| n | $\sin^2 \gamma_n$ Vertical | Horizontal |
|---|---|---|
| 1 | 0. 00024 | 0. 0118 |
| 2 | 0. 00228 | 0. 0598 |
| 3 | 0. 00470 | 0. 0657 |
| 4 | 0.. 00582 | – |

The values of $g_0$ at the center of the first-stage mouth were calculated for the vertical and horizontal geometries using $\rho_g = 0.93$. The results are listed in Table 42.

Table 42

Calculation of $g_{oc}$ for $\rho_g = 0.93$

| n | $F^n_{r-p2}$ Vertical | Horizontal | $\rho_g^n F^n_{r-p2}$ Vertical | Horizontal |
|---|---|---|---|---|
| 0 | 0. 00024 | 0. 0118 | 0. 00024 | 0. 0118 |
| 1 | 0. 00204 | 0. 0480 | 0. 00190 | 0. 0446 |
| 2 | 0. 00242 | 0, 0059 | 0. 00209 | 0. 0051 |
| 3 | 0.. 00112 | – | 0. 00090 | – |
| $g_{oc}$: | | | 0. 00513 | 0. 0615 |

Using the average of the vertical and horizontal values, we obtain

$$g_{oc} = 0.0333$$

In keeping with the geometry used to calculate the view factors, we assumed that $g_0$ varies linearly along a radius of the mouth of a right-circular cone and goes to zero at the edge. The average value of $g_0$ over the mouth (space reference) is then

$$g_O = \frac{1}{\pi r_o^2} \int_0^{2\pi} \int_0^{r_c} g_O (1 - \frac{r}{r_o}) \, r \, dr \, d\theta$$

where $r_o$ is the radius of the cone mouth and $r$, $\theta$ are polar coordinates in the plane of the mouth. Integrating, we obtain

$$g_O = \frac{1}{3} g_{oc} = 0.0111$$

In thermal test 7, the cooler attained the equilibrium temperatures shown in Table 43.

### Table 43

### Results of Thermal Test 7

| Member | Equilibrium Temperature ($^O$K) |
|---|---|
| Outer Box | 298.5 |
| First-Stage Cone | 201.6 |
| First-Stage Patch | 108.3 |
| Second-Stage Patch | 80.2 |

For an average surface emissivity, $\epsilon_g$, of 0.063 on the first-stage cone, we also have (Tables 26 and 28)

$$\rho_{pc} = 1 - \epsilon_{pc} = 0.9465$$

$$\epsilon_{cx} = 0.0375$$

In addition,

$$A_{p1} = 70.23 \text{ in}^2$$

$$A_{c1} = 933 \text{ in}^2$$

$$g_2 = 0.5958$$

The radiant power from the first-stage reflected off the space reference was then (equations 164 and 165)

$$\Phi_{p-r} + \Phi_{c-r} = \frac{2448\,\rho_r}{1-0.5958\,\rho_r}$$

during thermal test 7. Values of this power are listed in Table 44 together with the power absorbed in the second-stage patch for $g_o = 0.0111$.

<div align="center">Table 44</div>

<div align="center">Radiant Power Reflected from Space Reference</div>

| $\rho_r$ | Total $(\Phi_{p-r} + \Phi_{c-r})$, mw | To second-stage patch $g_o\,(\Phi_{p-r} + \Phi_{c-r})$, mw |
|---|---|---|
| 0.02 | 49.5 | 0.55 |
| 0.05 | 126.1 | 1.40 |
| 0.08 | 205.6 | 2.28 |

The power radiated by a black second-stage patch at 80.2 degrees K is

$$\Phi_{p2} = \sigma A_{p2}\, T_{p2}^4 = 3.96 \text{ milliwatts}$$

This power is balanced by radiative inputs from the second-stage cone and space reference and by a conductive input from the first-stage patch. The thermal-balance equation is therefore

$$3.96 \text{ mw} = \Phi_r + K_c\,(T_{p1} - T_{p2}) \tag{168}$$

where $\Phi_r$ is the radiative input. The value of the conductive coupling coefficient, $K_c$, may be calculated from

$$K_c = \frac{1}{\ell}\,\Sigma A_i K_i$$

where  $\ell$  =  length of conductive path between stages

$A_i$  =  cross-sectional area of conductive member i

$K_i$  =  thermal conductivity of conductive member i

The conductive members are listed in Table 45; all have a length, $\ell$ , of 1.42 inches.

<div align="center">141</div>

Table 45

Conductive Members Between Stages in Test 7

| Material | Cross-sectional dimensions, inch | Thermal Conductivity watt/cm$^{\circ}$C |
|---|---|---|
| chromel | 2 x 10$^{-3}$ dia. | 0.200 @ 100$^{\circ}$K |
| constantan | 2 x 10$^{-3}$ dia. | 0.192 @ 373$^{\circ}$K |
| nylon sleeve (2) | 3.1 x 10$^{-2}$ O.D. 7.5 x 10$^{-3}$ wall | 3.1 x 10$^{-3}$, average 20$^{\circ}$K -300$^{\circ}$K |
| Synthane G-10 | 1/8 O.D., 3/32 I.D. | 2.94 x 10$^{-3}$ @ 293$^{\circ}$K |

We will assume the chromel and constantan have a conductivity of 0.200 watt/cm degrees C at the average temperature between stages and that the Synthane G-10 has a conductivity of 2.94 x 10$^{-3}$ watt/cm degrees C at the same temperature. We then have

$$K_c \quad = \quad 0.0366 \text{ milliwatt/}^{\circ}K$$

For this value of conductive coupling, coefficient, $T_{p1} = 108.3^{\circ}K$, and $T_{p2} = 80.2^{\circ}K$, equation (168) yields

$$\Phi_r \quad = \quad 2.93 \text{ milliwatts}$$

By subtracting the radiant power from the space reference, we obtain the radiant power to the second-stage patch for outer-space operation (space reference reflectivity of zero). The results are shown in Table 46 for reference reflectivities of 2, 5, and 8 percent.

Table 46

Thermal Load on Second-Stage Patch for Reference Reflections to First Stage Only

| $\rho_r$ | Radiant Power from Second-Stage Cone to Second-Stage Patch (mw) |
|---|---|
| 0.02 | 2.38 |
| 0 05 | 1.53 |
| 0.08 | 0.65 |

For the power levels of Table 46, a first-stage temperature of 108.3 degrees K, and $K_c$ equal to 0.0366 mw/degrees K, equation (88) of Section 1.6 yields

$$0.0366\ T_{p2} + 9.581 \times 10^{-8}\ T_{p2}^{4} = \left\{ \begin{array}{c} 6.344 \\ 5.494 \\ 4.614 \end{array} \right\}\ \text{milliwatts} \qquad (169)$$

The values of power on the right-hand side of the equation are for reference reflectivities of 2, 5, and 8 percent, top to bottom.

Equation (169) was solved for the temperature $(T_{p2})$ of the second-stage patch when no power is reflected off the space reference. The results are given in Table 47.

Table 47

Temperature of Second-Stage Patch for Reference Reflections to First-Stage Only

| $\rho_r$ | Temperature of Second-Stage Patch For No Interstage Coupling Via Space Reference ($^{\circ}$K) |
|---|---|
| 0.02 | 77.7 |
| 0.05 | 73.5 |
| 0.08 | 68.5 |

The radiant power from the first stage reflected from the space reference and absorbed in a black first-stage patch is given by

$$\Phi_{s1\text{-}p1} = g_1 (\Phi_{p\text{-}r} + \Phi_{c\text{-}r}) \qquad (170)$$

where $g_1$ is equal to 0.2856.

Values of $\Phi_{s1\text{-}p1}$ are listed in Table 48 for reference reflectivities of 2, 5, and 8 percent and the values of $(\Phi_{p\text{-}r} + \Phi_{c\text{-}r})$ given in Table 44.

Table 48

Thermal Load on First-Stage Patch Reflected from Space Reference

| $\rho_r$ | Radiant Power from Space Reference to First-Stage Patch, mw |
|---|---|
| 0.02 | 14.1 |
| 0.05 | 36.0 |
| 0.08 | 58.7 |

143

The power radiated by a black first-stage patch at 108.3 degrees K is

$$\Phi_{p1} = \sigma A_{p1} T_{p1}^4 = 353.3 \text{ milliwatts}$$

By subtracting the value of $\Phi_{s1-p1}$ from $\Phi_{p1}$, we obtain the power to the first-stage patch for zero reflectivity. Equating the result to $A_{p1}\,\sigma T_{p1}^4$ and solving for the new value of $T_{p1}$, we obtain the patch temperature for zero reference reflectivity (this procedure assumes only radiative coupling in the first stage). The results are shown in Table 49.

Table 49

Outer Space Temperature of First-Stage Patch

| $\rho_r$ | Temperature of First-Stage Patch for No Coupling Via Space Reference ($^O$K) |
|---|---|
| 0.02 | 107.2 |
| 0.05 | 105.4 |
| 0.08 | 103.5 |

Finally, the corrected second-stage temperatures (Table 47) were adjusted for the corrected first-stage temperatures (Table 49). This was done in the same manner as the original corrections to the temperature of the second-stage patch. In this case, the thermal-balance equation yields

$$0.0366\, T_{p2} + 9.581 \times 10^{-8}\, T_{p2}^4 = \left\{ \begin{array}{c} 6.208 \\ 5.230 \\ 4.330 \end{array} \right\} \quad \text{milliwatts}$$

The solutions to this equation are listed in Table 50.

Table 50

Outer Space Temperature of Second-Stage Patch

| $\rho_r$ | Temperature of Second-Stage Patch For No Coupling Via Space Reference ($^O$K) |
|---|---|
| 0.02 | 77.1 |
| 0.05 | 72.1 |
| 0.08 | 66.6 |

## 4.5.3 Reduction of Temperature Corrections

The reflectivity of the space reference can be reduced by providing cavities in its surface. The cavities should cover most or all of the surface area so that little or no flat area is left. In addition, the cavities should be reasonably easy to make and designed so their shape is not significantly changed when painted. A surface covered with 30 degree (total angle) V-grooves is a good choice. Essentially all the surface area can be covered with cavities and the angle is not so narrow that paint filling is a problem. In addition, the absorptivity of a V-groove is essentially the same as that of a conical cavity of the same angle (See E. M. Sparrow and R. C. Cess, "Radiation Heat Transfer," Brooks/Cole Div. of Wadsworth, 1966, pp. 168-169).

According to E. W. Treuenfels (JOSA 53, 1162, 1963), the absorptivity of a V-groove of total angle $\omega$ and surface absorptivity $\epsilon_0$ is given by

$$\epsilon_c = \frac{\epsilon_0}{\epsilon_0 + f_1 (1 - \epsilon_0)} \qquad (171)$$

where

$$f_1 = 1 - \frac{\pi - \omega}{4} \cos \frac{\omega}{2} \qquad (172)$$

These equations are for a diffusely reflecting surface. Values of $\epsilon_c$ are given in Table 51 for $\omega$ equal to 30 degrees and $\epsilon_0$ values of 0.98, 0.95, and 0.92 (reflectivities of 0.02, 0.05, and 0.08). Also shown are values of the cavity reflectivity, $\rho_c = 1 - \epsilon_c$.

### Table 51

### Properties of a 30° V-Groove Cavity

| $\epsilon_0$ | $\epsilon_c$ | $\rho_c$ |
|---|---|---|
| 0.98 | 0.9925 | 0.0075 |
| 0.95 | 0.9810 | 0.0190 |
| 0.92 | 0.9690 | 0.0310 |

The values given in Table 51 are in good agreement (within ~ 0.001) of the results shown in Figure 6-6 of Sparrow and Cess (op. cit.) and in Figure 9 of Sparrow and Lin ("Absorption of Thermal Radiation in V-Groove Cavities," U. of Minn. for NASA-Lewis, N62 10682, July 1962).

The use of a 30 degree groove therefore reduces the nominal 5 percent reflectivity of 3M Black Velvet to 1.9 percent. This reduces the nominal total temperature correction for the second-stage patch from 8.1 degrees K to about 3.1 degrees K.

145

## 5.0 <u>NEW TECHNOLOGY</u>

The two-stage radiant cooler is considered new technology according to the NASA new technology clause of September 1964. The general design of a cooler (Section 1.0) and specific designs for a Nimbus-type spacecraft (Section 2.0) are covered in this part of the final project report. The cooler attained a second-stage temperature below 80 degrees K under realistic thermal and mechanical conditions (Section 4.0). The low temperatures are achieved by radiation to cold space without power consumption or stored coolants.

Specific components of the two-stage radiant cooler which are considered new technology are the radiant patch supports, the relay optic design, and the earth shield.

The patch supports are covered in Sections 2.1.5 and 2.1.6. They provide low thermal conductivity support for the black radiant patches and are in the form of tubes. The centers of the supports act as conduits for electrical leads to and from the patches.

The design of the relay optic is covered in Sections 2.1.7. This portion of the optics transfers radiant energy from the plane of the chopper to the infrared detector. The design minimizes thermal loading of the cooler by radiative exchange through the optical opening. This is accomplished by reducing the speed of the optical beam as it passes through the outside of the cooler (first-stage cone) and increasing the speed of the beam to the detector by means of a lens mounted on the first-stage patch. In addition, the spectral filter is cooled by mounting it on the first-stage patch.

The earth shield is covered in Sections 1.7, 2.1.4, and 2.2.2. It substitutes low emissivity infrared radiation for earth infrared and earthshine, thus reducing the thermal load on the interior (first-stage cone) of the radiant cooler. It is especially useful for low altitude orbits and higher values of cone wall emissivity.

APPENDIX I

EARTHSHINE AND EARTH INFRARED EMITTANCES

The sunlight reflected from the earth (earthshine) will be expressed as an average equivalent source emittance for a sun-synchronous, polar orbiting earth-oriented spacecraft. Because the thermal time constants of the cooler members are very long, at least the order of the time it takes the spacecraft to orbit the earth, only the earthshine value averaged over a spacecraft period is needed.

The average earth solar reflection factor is assumed to be independent of the angle of incidence at the earth and the angle of view from the cooler to the earth's surface. In addition, it is assumed that the amount of reflected sunlight is directly proportional to the cosine of the incidence angle at the earth's surface (i. e. , to the illuminated area projected in the sun's direction). With the subpoint of the spacecraft at the point where the sun is perpendicular to the earth's surface, (high-noon orbiting) the average value of this cosine over the area seen from the spacecraft is given by (See Figure I-1).

$$\cos \theta' = \frac{\int_{-\varphi_0}^{\varphi_0} \int_{0}^{\vartheta_0} \sin \vartheta \cos \vartheta \, d\vartheta \, d\varphi}{\int_{-\varphi_0}^{\varphi_0} \int_{0}^{\vartheta_0} \sin \vartheta \, d\vartheta \, d\varphi}$$

$$\cos \theta' = \frac{2 \varphi_0 \frac{1}{2} \sin^2 \vartheta_0}{2 \varphi_0 (1 - \cos \vartheta_0)} = \frac{\sin^2 \vartheta_0}{2 (1 - \cos \vartheta_0)} \qquad (I-1)$$

The angle $\vartheta_0$ is the complement of the angle from the spacecraft nadir to the tangent line to the earth. The bottom integral is the solid angle subtended at the earth's center by the earth's surface seen from the satellite. The top integral is the same solid angle weighted by the cosine of the angle between surface element normals and the direction to the sun. Note that the result is independent of $\varphi_0$ so that it can be used for both vertical and horizontal spacecraft surfaces. For near earth orbit, $\vartheta_0$ is such that $\cos \theta'$ is near unity.

We now make the approximation that the solar illumination is reduced uniformly over the earth area seen from the spacecraft as the subpoint varies in earth latitude over an angular range of 90 degrees. The average cosine of the angle between the normal to an element at the subpoint and the sun is, for a high-noon orbit

$$\frac{2}{\pi} \int_0^{\pi/2} \cos \theta \cdot d\theta = \frac{2}{\pi}$$

I-1
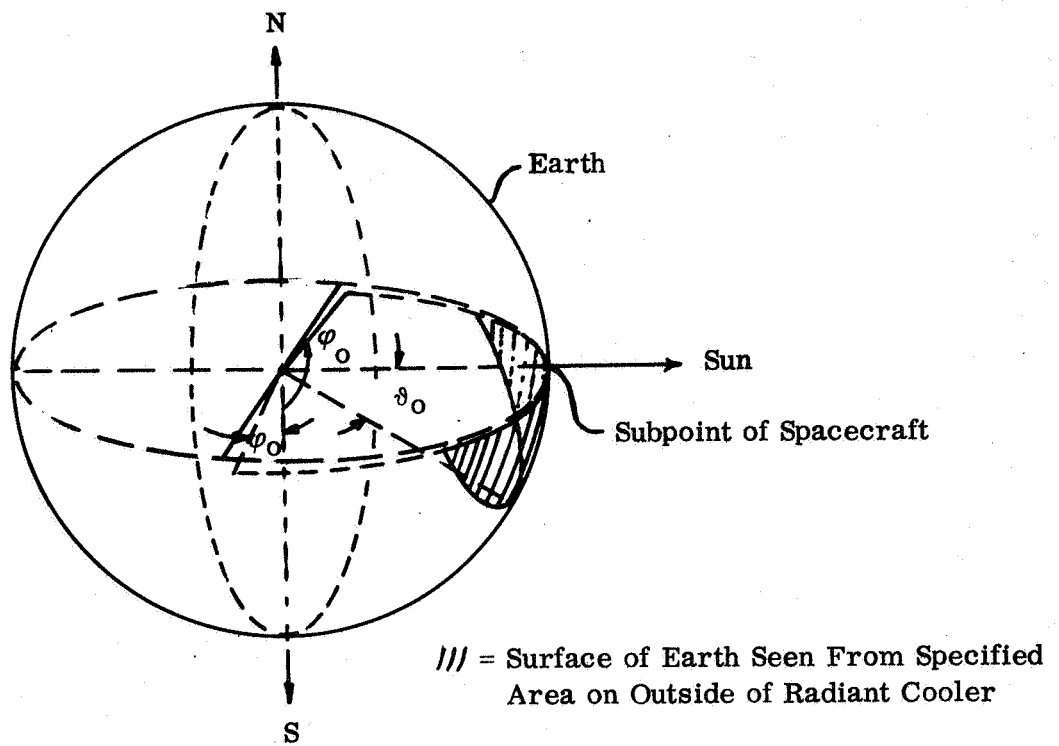
$\vartheta, \varphi$ = spherical coordinate angles at center of earth, with pole in direction of sun (through subpoint)

cos $\vartheta$ = cosine of angle between normal to surface element and direction to sun

Figure I-1  Calculation of Cosine of Incidence Angle for Sun Vector Normal to Subpoint Area

The cosine of the angle between the normal to an element on the earth's surface and the vector to the sun is then

$$\frac{1}{2\pi} \frac{\sin^2 \vartheta_0}{(1 - \cos \vartheta_0)}$$

when averaged over the surface seen from the spacecraft and over an orbit. A factor of 1/2 has been included since half the earth is sun illuminated.

From a sun-synchronous polar orbit with an orbit normal to sun angle of $\phi_s$, the solar illumination of the visible earth area is reduced by $\sin \phi_s$. The average equivalent earthshine emittance is then

$$W_s = \frac{1}{2\pi} S_0 A \frac{\sin^2 \vartheta_0}{(1 - \cos \vartheta_0)} \sin \phi_s \qquad \text{(I-2)}$$

for a nadir to earth tangent line angle of $(\pi/2 - \vartheta_0)$. $S_0$ is the solar constant (0.14 watts/cm$^2$) and A the average solar reflection factor for the earth (0.4).

The solar radiation not reflected by the earth is absorbed by it and radiated to space at infrared wavelengths. The average infrared emittance of the earth, $W_e$, is therefore determined by

$$4\pi R'^2 W_e = \pi R'^2 S_0 (1 - A)$$

$$W_e = (1/4) S_0 (1 - A) = 2.1 \times 10^{-2} \text{ watts/cm}^2 \qquad \text{(I-3)}$$

where R' is the earth's radius. If the earth were a uniform blackbody in the infrared as seen from space (which it is not), its temperature would be 247 degrees K.

# APPENDIX II

## VIBRATION TESTS

A patch assembly for the two-stage radiant cooler (Figure 29, Section 4. 0) was subjected to a sinusoidal vibration test on May 8 and 9, 1967. The purpose of this test was to determine if the support mechanisms of an integrated patch assembly could sustain the same vibration levels as those imposed on Nimbus prototype instruments. The first-stage patch was held by a caging mechanism consisting of four removable pins mechanically interchangeable with retractable piston actuators (Atlas Chemical Industries, Inc. , Type 1 MT-18A) and by two in-orbit Synthane G-10 support tubes (1/4 inch O. D. , 3/16 inch I. D. ).

The assembly was first vibrated with the smaller, second-stage patch removed. After vibrating in all three planes from 0 to 2000 cps at 10 g and then at 20 g, the patch and supports were found to be free of any damage. During the 20 g vibration some small deflection waves were observed at the end of the second stage cones through the 80 to 170 cps range.

The patch was then reassembled with the smaller, or second-stage patch in place and aligned with respect to the optical axis. This integrated patch was then vibrated as above, first at 10 g and then at 20 g. Through the frequency range of 75 to 135 cps the small patch became unstable and the deflection reached approximately 1/8 inch at 20 g when vibrated in the plane perpendicular to the throat of the cone (i. e. along the cone axis). After the tests were completed the patch assembly was inspected and no parts were found to be damaged or to have shifted from their initial positions. The test report is reproduced on the next page.

ITT Federal Laboratories
Fort Wayne, Indiana
Test Laboratory

No. 1197                     Procedure Report                  May 10, 1967

## 1. 0 Description

1. 1   One (1) patch assembly, manufactured by ITT Industrial Laboratories, was submitted for test.   The patch assembly part number is D-4710251.

## 2. 0 Procedure

2. 0   The patch assembly was mounted on the vibration machine in an ITT Industrial Laboratories supplied fixture and subjected to a harmonic motion along each of three mutually perpendicular axes.   One sweep in each of the three mutually perpendicular planes was at an acceleration level of 1/4 inch DA or 10 g's whichever is less.   One sweep in each of the three mutually perpendicular planes was at an acceleration level of 1/4 inch DA or 20 g's whichever is less except in the frequency range of 40 to 500 cps where the level was 17 g's.   The total frequency range of 5 cps to 2000 cps was swept at rates so that the ranges 5 to 100 cps, 100 cps to 500 cps and 500 cps to 2000 cps were traversed in approximately 3. 25 minutes, 2. 75 minutes and 2. 56 minutes respectively for a total sweep time of approximately 8. 56 minutes.

2. 1. 1   The above procedure was repeated after the installation of the secondary patch or otherwise known as the small patch.

## 3. 0 Results

3. 1   The patch assembly was mounted in the vibration fixture and observed during the vibration tests by Mr. J. Lodder of ITT Industrial Laboratories.

3. 2   No visible damage was noted during the vibration tests.

## 4. 0 Notes

4. 1   The test was requested by Mr. J. Lodder.

4. 2   The test was completed on May 9, 1967.

4. 3   The vibration test was performed by _____